People`s Democratic Republic of Algeria
Ministry of Higher Education and Scientific Research
University of Echahid Hamma Lakhdar - El Oued
Faculty of Technology
Department of Process Engineering & Petrochemistry

Dissertation

ACADEMIC MASTER

Domain: Science and Technology

Specialty: Chemical Engineering

Presented by:

1. **Asma Habita**

Entitled:

Influence of Film Thickness on Optical Band Gap of CuO Thin Films

In order to obtain a diploma of an Academic Master's degree

Publicly defended in: 24 /05 /2026

Board of Examiners:

Dr. Mohrem Abdelkrim	**Chairman**
Dr. Lakhdar Sek	**Supervisor**
Dr. Segueni Leila	**Examiner**

Academic Year: 2025/2026

Abstract

This master's dissertation investigates the influence of film thickness on the optical band gap of copper oxide (CuO) thin films prepared by the sol-gel spin coating technique. Three sets of CuO thin films were fabricated on glass substrates by varying the number of deposited layers (6, 9, and 12 layers), corresponding to thicknesses of approximately 201 nm, 422 nm, and 943 nm, respectively. Copper acetate monohydrate was used as the precursor, ethanol as the solvent, and monoethanolamine as the stabilizing agent. The films were annealed at 500°C for 2 hours in air. The structural, optical, and electrical properties were characterized using X-ray diffraction (XRD), UV-Visible spectroscopy, and the four-point probe technique.

XRD analysis confirmed the formation of pure polycrystalline monoclinic CuO (tenorite phase) in all samples, with no secondary phases detected. The crystallite size exhibited a non-monotonic variation with thickness, reaching a maximum of 15.12 nm at the intermediate thickness of 422 nm, accompanied by minimum lattice strain and dislocation density, indicating optimal crystallographic quality at this thickness.

The central finding of this work is the systematic decrease of the optical band gap from 2.79 eV to 2.11 eV as the film thickness increases from 201 nm to 943 nm. This band gap narrowing of approximately 0.68 eV is attributed to the relaxation of quantum confinement effects, the increase in structural disorder (reflected by the increase of Urbach energy from 328.8 meV to 564.0 meV), and the reduction of grain boundary effects in thicker films. An inverse correlation between the optical band gap and the Urbach energy was established, confirming the dominant role of structural disorder in controlling the optical absorption properties.

The electrical measurements revealed that the resistivity reaches a minimum of 74 Ω·cm at the intermediate thickness of 422 nm, correlating with the best structural quality. This result confirms that grain boundary scattering is the primary mechanism governing charge transport in polycrystalline CuO films.

These results demonstrate that film thickness is a simple and effective parameter for tuning the optical band gap of CuO thin films over a significant energy range, enabling their optimization for specific applications in solar cells, photodetectors, photocatalysis, and other optoelectronic devices.

Keywords: Copper oxide, CuO, thin films, sol-gel, spin coating, film thickness, optical band gap, Tauc plot, Urbach energy, crystallite size, XRD, UV-Visible spectroscopy, four-point probe.

Résumé

Ce mémoire de master étudie l'influence de l'épaisseur du film sur la bande interdite optique des couches minces d'oxyde de cuivre (CuO) préparées par la technique sol-gel spin coating. Trois séries de couches minces de CuO ont été déposées sur des substrats en verre en faisant varier le nombre de couches déposées (6, 9 et 12 couches), correspondant à des épaisseurs d'environ 201 nm, 422 nm et 943 nm, respectivement. L'acétate de cuivre monohydraté a été utilisé comme précurseur, l'éthanol comme solvant et la monoéthanolamine comme agent stabilisant. Les films ont été recuits à 500°C pendant 2 heures sous air. Les propriétés structurales, optiques et électriques ont été caractérisées par diffraction des rayons X (DRX), spectroscopie UV-Visible et la méthode des quatre pointes.

L'analyse DRX a confirmé la formation d'une phase CuO monoclinique polycristalline pure (phase ténorite) dans tous les échantillons, sans phases secondaires détectées. La taille des cristallites a montré une variation non monotone avec l'épaisseur, atteignant un maximum de 15,12 nm pour l'épaisseur intermédiaire de 422 nm, accompagnée d'une contrainte résiduelle et d'une densité de dislocations minimales, indiquant une qualité cristallographique optimale à cette épaisseur.

Le résultat central de ce travail est la diminution systématique de la bande interdite optique de 2,79 eV à 2,11 eV lorsque l'épaisseur du film augmente de 201 nm à 943 nm. Ce rétrécissement de la bande interdite d'environ 0,68 eV est attribué à la relaxation des effets de confinement quantique, à l'augmentation du désordre structural (reflétée par l'augmentation de l'énergie d'Urbach de 328,8 meV à 564,0 meV) et à la réduction des effets des joints de grains dans les films plus épais. Une corrélation inverse entre la bande interdite optique et l'énergie d'Urbach a été établie, confirmant le rôle dominant du désordre structural dans le contrôle des propriétés d'absorption optique.

Les mesures électriques ont révélé que la résistivité atteint un minimum de 74 Ω·cm pour l'épaisseur intermédiaire de 422 nm, en corrélation avec la meilleure qualité structurale. Ce résultat confirme que la diffusion aux joints de grains est le mécanisme principal régissant le transport de charges dans les films polycristallins de CuO.

Ces résultats démontrent que l'épaisseur du film est un paramètre simple et efficace pour ajuster la bande interdite optique des couches minces de CuO sur une gamme d'énergie significative, permettant leur optimisation pour des applications spécifiques dans les cellules solaires, les photodétecteurs, la photocatalyse et d'autres dispositifs optoélectroniques.

Mots-clés : Oxyde de cuivre, CuO, couches minces, sol-gel, spin coating, épaisseur du film, bande interdite optique, diagramme de Tauc, énergie d'Urbach, taille des cristallites, DRX, spectroscopie UV-Visible, méthode quatre pointes.

ملخص

تتناول مذكرة الماستر هذه دراسة تأثير سمك الطبقة الرقيقة على فجوة الطاقة البصرية لأغشية أكسيد النحاس (CuO) الرقيقة المحضرة بتقنية الطلاء بالدوران (spin coating) باستخدام طريقة السول-جل. تم تحضير ثلاث مجموعات من أغشية أكسيد النحاس الرقيقة على ركائز زجاجية بتغيير عدد الطبقات المرسبة (6 و9 و12 طبقة)، وهو ما يقابل سماكات تقريبية تبلغ 201 نانومتر و422 نانومتر و943 نانومتر على التوالي. استُخدم أسيتات النحاس أحادي الماء كمادة أولية، والإيثانول كمذيب، وأحادي إيثانول أمين كعامل استقرار. تم تلدين الأغشية عند درجة حرارة 500 درجة مئوية لمدة ساعتين في الهواء. تمت دراسة الخصائص البنيوية والبصرية والكهربائية باستخدام حيود الأشعة السينية (XRD) والتحليل الطيفي فوق البنفسجي-المرئي (UV-Vis) وتقنية المسبار رباعي النقاط.

أكد تحليل حيود الأشعة السينية تكوّن طور أكسيد النحاس أحادي الميل (طور التينوريت) النقي متعدد البلورات في جميع العينات، دون اكتشاف أي أطوار ثانوية. أظهر حجم البلورات تغيراً غير رتيب مع السمك، حيث بلغ أقصى قيمة له 15.12 نانومتر عند السمك المتوسط 422 نانومتر، مصحوباً بأقل قيم للإجهاد الشبكي وكثافة الانخلاعات، مما يدل على أفضل جودة بلورية عند هذا السمك.

النتيجة الرئيسية لهذا العمل هي الانخفاض المنتظم لفجوة الطاقة البصرية من 2.79 إلكترون فولت إلى 2.11 إلكترون فولت مع زيادة سمك الطبقة الرقيقة من 201 نانومتر إلى 943 نانومتر. يُعزى هذا التضييق في فجوة الطاقة بمقدار 0.68 إلكترون فولت تقريباً إلى عدة عوامل: تراجع تأثيرات الحصر الكمي، وزيادة الاضطراب البنيوي (الذي ينعكس في ارتفاع طاقة أورباخ من 328.8 ميلي إلكترون فولت إلى 564.0 ميلي إلكترون فولت)، وتقلص تأثيرات الحدود الحبيبية في الأغشية الأكثر سمكاً. تم إثبات وجود علاقة عكسية بين فجوة الطاقة البصرية وطاقة أورباخ، مما يؤكد الدور المهيمن للاضطراب البنيوي في التحكم بخصائص الامتصاص البصري.

كشفت القياسات الكهربائية أن المقاومة النوعية تصل إلى حدها الأدنى البالغ 74 أوم·سم عند السمك المتوسط 422 نانومتر، بما يتوافق مع أفضل جودة بنيوية. تؤكد هذه النتيجة أن التشتت عند الحدود الحبيبية هو الآلية الرئيسية المتحكمة في نقل حاملات الشحنة في أغشية أكسيد النحاس متعددة البلورات.

تُبرهن هذه النتائج أن سمك الطبقة الرقيقة يمثل معلمة بسيطة وفعالة لضبط فجوة الطاقة البصرية لأغشية أكسيد النحاس الرقيقة عبر نطاق واسع من الطاقة، مما يتيح تحسينها لتطبيقات محددة في الخلايا الشمسية وكواشف الضوء والتحفيز الضوئي وأجهزة الإلكترونيات الضوئية الأخرى.

الكلمات المفتاحية: أكسيد النحاس، CuO، أغشية رقيقة، سول-جل، الطلاء بالدوران، سمك الطبقة الرقيقة، فجوة الطاقة البصرية، مخطط تاوك، طاقة أورباخ، حجم البلورات، حيود الأشعة السينية، التحليل الطيفي فوق البنفسجي-المرئي، المسبار رباعي النقاط.

DEDICATION

أهدي هذا العمل أولًا إلى نفسي...

إلى تلك التي صبرت، وثابرت، وعادت بعد انقطاع دام عشر سنوات لتواصل الطريق من جديد،

إلى من آمنت بأن الأحلام لا تموت، وأن البدايات المتأخرة لا تقل جمالًا عن غيرها،

إلى روحي التي قاومت كل الصعاب بصمت، ولم تستسلم رغم التعب، حتى بلغت هذا اليوم.

إلى أبي الراحل...

رحمك الله يا من كنت السند والأمان، يا من غبت عن عيني ولم تغب عن قلبي،

أهديك هذا النجاح، لعلّه يصل إليك دعاءً ووفاءً لا ينقطع.

إلى أمي الحبيبة، حفظها الله وأطال في عمرها،

يا من كانت دعواتها سر قوتي، وحنانها ملجأي في كل ضعف،

لكِ مني كل الحب والامتنان، فهذا الإنجاز ثمرة من صبرك قبلي.

إلى فلذتي كبدي، نصر وزين،

أنتما النور الذي يضيء دربي، والفرحة التي تسكن قلبي،

من أجلكما كان التعب يهون، وكان الأمل يكبر.

إلى زوجي الغالي،

شكرًا لدعمك اللامحدود، لصبرك، لتفهمك، ولمساندتك في كل لحظة،

كنت خير السند في هذه الرحلة.

إلى إخوتي وأخواتي: سارة، بشيرة، إكرام، إشراق، اعتدال، أمينة، وعلي وطاهر،

أنتم السند بعد الله، ورفقة العمر التي لا تُعوّض،

بكم تكتمل فرحتي، ولكم مني كل المحبة والتقدير.

وإلى أستاذي الكريم،

تقديرًا لجهودك، وصبرك، وتوجيهاتك التي أنارت لي الطريق،

لك مني كل الاحترام والعرفان.

إليكم جميعًا... أهدي ثمرة جهدي وتعبي،

محفوفة بالحب، ومكللة

ACKNOWLEDGEMENTS

First and foremost, I would like to express my deepest gratitude to Almighty Allah for granting me the strength, health, and patience to complete this research work.

I would like to extend my sincere appreciation and profound gratitude to my supervisor, ***Dr. Sek Lakhdar****, for his invaluable guidance, continuous support, and constructive feedback throughout all stages of this thesis. His academic expertise and encouragement were fundamental to the completion of this work.*

I am also deeply honored and grateful to the esteemed members of the examining committee for their valuable time, careful reading, and constructive suggestions that helped improve this thesis.

My heartfelt thanks also go to the faculty and staff of the ***Department of Process Engineering and Petrochemistry, Faculty of Technology, Echahid Hamma Lakhdar University of El-Oued****, for their academic support throughout my years of study.*

Finally, I owe my deepest gratitude to my beloved parents and family for their endless love, prayers, sacrifices, and unwavering support. To my friends and colleagues who supported me in any way, I extend my sincere thanks.

TABLE OF CONTENTS

Tables Of Contents

LIST OF FIGURES

LIST OF TABLES

GENERAL INTRODUCTION

The rapid advancement of modern technology has created an ever-growing demand for semiconductor materials with precisely controlled properties. In fields ranging from renewable energy and environmental monitoring to optoelectronics and flexible electronics, the ability to tailor the physical characteristics of thin film materials has become essential for achieving optimal device performance [1, 2]. Among the many classes of materials being explored for these applications, transition metal oxide thin films have attracted particularly intense research interest due to their remarkable combination of functional properties, earth abundance, chemical stability, and environmental compatibility [3].

Copper oxide (CuO), also known as cupric oxide or tenorite, occupies a special position among transition metal oxides. It is a naturally occurring p-type semiconductor with a monoclinic crystal structure belonging to the space group C2/c. CuO possesses a narrow direct band gap, typically reported in the range of 1.2 to 2.1 eV depending on the preparation conditions, which makes it an excellent absorber of visible light [4, 5]. Combined with its high absorption coefficient (of the order of 10^5 cm^{-1}), non-toxicity, earth abundance, and low production cost, CuO stands out as a highly promising material for a diverse range of technological applications, including thin film solar cells, photodetectors, gas sensors, photocatalytic degradation of organic pollutants, lithium-ion batteries, supercapacitors, and thermoelectric devices [6, 7, 8].

Despite these attractive characteristics, the widespread deployment of CuO in commercial devices requires a thorough understanding and precise control of its physical properties. It is well established that the properties of thin film materials differ significantly from those of their bulk counterparts, and that these properties are highly sensitive to the conditions under which the films are prepared [9]. Numerous studies have investigated the effects of various deposition parameters on the characteristics of CuO thin films, including the choice of precursor and solvent, the substrate temperature, the annealing temperature and duration, the doping with foreign elements, and the deposition technique itself [10, 11, 12].

Among all the parameters that influence thin film properties, film thickness is one of the most fundamental and practically important. The thickness of a thin film directly affects its crystallite

size, grain boundary density, defect concentration, surface morphology, optical absorption, light transmission, and electrical transport behavior [13, 14]. Of particular significance is the influence of thickness on the optical band gap (Eg), which is the minimum photon energy required to excite an electron from the valence band to the conduction band. The band gap is a critical parameter that determines the spectral range of light absorption by the material and, consequently, its suitability for specific optoelectronic applications [15].

Several physical mechanisms are responsible for the thickness dependence of the optical band gap in nanocrystalline thin films. Quantum confinement effects arise when the crystallite size is comparable to or smaller than the exciton Bohr radius, leading to a widening of the band gap in very thin films with small crystallites [16]. Structural disorder, quantified by the Urbach energy, creates localized states (band tails) near the edges of the valence and conduction bands that effectively narrow the apparent band gap [17]. Grain boundary effects introduce potential barriers that modify the electronic structure and influence the absorption edge [18]. The interplay between these mechanisms makes the relationship between thickness and band gap complex and material-dependent, necessitating systematic experimental studies for each specific material system and deposition technique.

Various techniques have been employed for the deposition of CuO thin films, including reactive sputtering, pulsed laser deposition, chemical vapor deposition, spray pyrolysis, successive ionic layer adsorption and reaction (SILAR), chemical bath deposition, and sol-gel methods [19, 20, 21]. Among these, the sol-gel method combined with spin coating has emerged as one of the most attractive approaches for laboratory-scale research and prototyping. This technique offers several compelling advantages: it requires only simple and inexpensive equipment, operates at relatively low temperatures, provides excellent control over film composition and thickness through the adjustment of solution concentration and number of deposited layers, produces highly homogeneous films with good adhesion to the substrate, and is compatible with a wide range of substrate materials [22, 23].

In the sol-gel spin coating process, the film thickness can be conveniently controlled by varying the number of coating cycles (layers). Each cycle involves dispensing the precursor solution onto the rotating substrate, spinning to form a uniform wet layer, and preheating to evaporate the solvent. By repeating this cycle multiple times, films of progressively greater thickness can be

obtained while maintaining the same solution chemistry and processing conditions for each individual layer [24].

Despite the extensive body of research on CuO thin films, there remains a need for systematic studies that clearly establish the quantitative relationship between film thickness and the optical band gap under well-controlled deposition conditions. Much of the existing literature examines thickness as one of many variables, making it difficult to isolate its specific influence from those of other parameters that may change simultaneously. Furthermore, the mechanisms responsible for the observed band gap variations are not always clearly identified or distinguished.

Objective of this Work

The primary objective of this master's dissertation is to systematically investigate the influence of film thickness on the optical band gap of CuO thin films prepared by the sol-gel spin coating technique. Specifically, this work aims to :

1. Fabricate CuO thin films of different thicknesses by varying the number of deposited layers (6, 9, and 12 layers) while keeping all other deposition parameters constant.
2. Characterize the structural properties of the films using X-ray diffraction (XRD) to determine the crystalline phase, crystallite size, lattice strain, and dislocation density as a function of thickness.
3. Determine the optical properties using UV-Visible spectroscopy, including the transmittance, absorption coefficient, optical band gap (using the Tauc plot method), and Urbach energy.
4. Measure the electrical properties using the four-point probe technique to evaluate the resistivity and conductivity as a function of thickness.
5. Establish correlations between the structural, optical, and electrical properties and identify the physical mechanisms responsible for the observed thickness dependence of the band gap.
6. Determine the optimal thickness that provides the best combination of properties for potential optoelectronic applications.

Organization of the Dissertation

This dissertation is organized into three chapters, preceded by this general introduction and followed by a general conclusion:

Chapter 1: Copper Oxide Thin Films — Fundamentals, Structural and Optical Properties

This chapter provides a comprehensive literature review of CuO thin films. It begins with general concepts related to thin films and their deposition techniques, then presents the chemistry, crystal structure, and fundamental properties of CuO. The structural, optical, and electrical properties of CuO thin films are reviewed in detail, with particular attention to the influence of various deposition parameters. The effect of film thickness on these properties is discussed based on previous studies, and the main applications of CuO thin films are presented. This chapter establishes the theoretical and bibliographic foundation for the experimental work.

Chapter 2: Experimental Procedure and Characterization Methods

This chapter describes in detail the experimental methodology employed in this work. It begins with a thorough description of the sol-gel process and its underlying chemistry, followed by the principles and parameters of the spin coating technique. The complete experimental procedure for CuO thin film preparation is presented step by step, including solution preparation, substrate cleaning, film deposition, and thermal treatment. The chapter then describes the characterization techniques used: X-ray diffraction (XRD) for structural analysis, UV-Visible spectroscopy for optical characterization, and the four-point probe method for electrical measurements. For each technique, the underlying principles, the equations used for data analysis, and the equipment specifications are presented.

Chapter 3: Results and Discussion — Influence of Film Thickness on the Optical Band Gap

This chapter presents and discusses all the experimental results obtained in this work. The results are organized into four sections: thickness measurement, structural characterization (XRD), optical characterization (UV-Visible spectroscopy), and electrical characterization (four-point probe). Each section includes a detailed analysis of the observed trends and their physical interpretation, supported by comparisons with literature data. The central finding — the systematic decrease of the optical band gap with increasing film thickness — is discussed in

depth, with identification of the responsible physical mechanisms. Correlations between all measured properties are established, and the implications for potential applications are discussed.

Finally, the **General Conclusion** summarizes the principal findings, discusses their significance, acknowledges the limitations of the study, and proposes directions for future research.

References

[1] G. J. Snyder and E. S. Toberer, "Complex thermoelectric materials," Nature materials, vol. 7, pp. 105-114, 2008.

[2] I. Petsagkourakis, K. Tybrandt, X. Crispin, I. Ohkubo, N. Satoh, and T. Mori, "Thermoelectric materials and applications for energy harvesting power generation," Science and technology of advanced materials, vol. 19, pp. 836-862, 2018.

[3] N. Silva, S. Ramírez, I. Díaz, A. Garcia, and N. Hassan, "Easy, quick, and reproducible sonochemical synthesis of CuO nanoparticles," Materials, vol. 12, p. 804, 2019.

[4] B. Balamurugan and B. Mehta, "Optical and structural properties of nanocrystalline copper oxide thin films prepared by activated reactive evaporation," Thin solid films, vol. 396, pp. 90-96, 2001.

[5] M. Dhaouadi, M. Jlassi, I. Sta, I. B. Miled, G. Mousdis, M. Kompitsas, and W. Dimassi, "Physical properties of copper oxide thin films prepared by sol–gel spin–coating method," Am. J. Phys. Appl, vol. 6, pp. 43-50, 2018.

[6] G. Filipič and U. Cvelbar, "Copper oxide nanowires: a review of growth," Nanotechnology, vol. 23, p. 194001, 2012.

[7] A. Rydosz, "The use of copper oxide thin films in gas-sensing applications," Coatings, vol. 8, p. 425, 2018.

[8] T. V. Thi, A. K. Rai, J. Gim, and J. Kim, "Potassium-doped copper oxide nanoparticles synthesized by a solvothermal method as an anode material for high-performance lithium ion secondary battery," Applied surface science, vol. 305, pp. 617-625, 2014.

[9] F. A. Akgul, G. Akgul, N. Yildirim, H. E. Unalan, and R. Turan, "Influence of thermal annealing on microstructural, morphological, optical properties and surface electronic structure of copper oxide thin films," Materials Chemistry and Physics, vol. 147, pp. 987-995, 2014.

[10] N. Touka, D. Tabli, and K. Badari, "Effect of annealing temperature on structural and optical properties of copper oxide thin films deposited by sol-gel spin coating method," Journal of Optoelectronics and Advanced Materials, vol. 21, pp. 698-701, 2019.

[11] M. L. Zeggar, M. Aida, and N. Attaf, "Copper oxide thin films deposition by spray pyrolysis," Journal of New Technology and Materials, vol. 277, pp. 1-3, 2014.

[12] H. Siddiqui, M. R. Parra, M. Qureshi, M. Malik, and F. Z. Haque, "Studies of structural, optical, and electrical properties associated with defects in sodium-doped copper oxide (CuO/Na) nanostructures," Journal of materials science, vol. 53, pp. 8826-8843, 2018.

[13] H. B. Saâd, M. Ajili, S. Dabbabi, and N. T. Kamoun, "Investigation on thickness and annealing effects on physical properties and electrical circuit model of CuO sprayed thin films," Superlattices and Microstructures, vol. 142, p. 106508, 2020.

[14] Y. Akaltun, "Effect of thickness on the structural and optical properties of CuO thin films grown by successive ionic layer adsorption and reaction," Thin Solid Films, vol. 594, pp. 30-34, 2015.

[15] R. Shabu, A. M. E. Raj, C. Sanjeeviraja, and C. Ravidhas, "Assessment of CuO thin films for its suitablity as window absorbing layer in solar cell fabrications," Materials Research Bulletin, vol. 68, pp. 1-8, 2015.

[16] S. Saleem, A. H. Jabbar, M. H. Jameel, A. Rehman, Z. H. Kareem, A. H. Abbas, Z. Ghaffar, S. A. Razzaq, R. A. Pashameah, and E. Alzahrani, "Enhancement in structural, morphological, and optical properties of copper oxide for optoelectronic device applications," Nanotechnology Reviews, vol. 11, pp. 2827-2838, 2022.

[17] N. Sharma, K. Prabakar, S. Ilango, S. Dash, and A. Tyagi, "Optical band-gap and associated Urbach energy tails in defected AlN thin films grown by ion beam sputter deposition: Effect of assisted ion energy," Advanced Materials Proceedings, vol. 2, pp. 342-346, 2017.

[18] B. Meyer, A. Polity, D. Reppin, M. Becker, P. Hering, P. Klar, T. Sander, C. Reindl, J. Benz, and M. Eickhoff, "Binary copper oxide semiconductors: From materials towards devices," physica status solidi (b), vol. 249, pp. 1487-1509, 2012.

[19] X. Zhang, Z. Li, and J. Fan, "An effect of rapid post-annealing temperature on the properties of cupric oxide thin films deposited by a remote plasma sputtering technique," Materials Science in Semiconductor Processing, vol. 137, p. 106227, 2022.

[20] T. Çayir Taşdemirci, "Copper oxide thin films synthesized by SILAR: role of varying annealing temperature," Electronic Materials Letters, vol. 16, pp. 239-246, 2020.

[21] P. Ooi, S. Ng, M. Abdullah, H. A. Hassan, and Z. Hassan, "Effects of oxygen percentage on the growth of copper oxide thin films by reactive radio frequency sputtering," Materials Chemistry and Physics, vol. 140, pp. 243-248, 2013.

[22] D. Bokov, A. Turki Jalil, S. Chupradit, W. Suksatan, M. Javed Ansari, I. H. Shewael, G. H. Valiev, and E. Kianfar, "Nanomaterial by sol-gel method: synthesis and application," Advances in Materials Science and Engineering, vol. 2021, pp. 1-21, 2021.

[23] L. Znaidi, "Sol–gel-deposited ZnO thin films: A review," Materials Science and Engineering: B, vol. 174, pp. 18-30, 2010.

[24] K. Kamli, Z. Hadef, B. Chouial, and B. Hadjoudja, "Thickness effect on electrical properties of copper oxide thin films," Surface Engineering, vol. 35, pp. 86-90, 2019.

CHAPTER 1: Copper Oxide Thin Films — Fundamentals, Structural and Optical Properties

1.1 Introduction

The growing interest in semiconductor materials has revolutionized many fields of modern technology, particularly in electronics, optoelectronics, photovoltaics, sensors, and energy conversion devices [1]. Among the various classes of semiconductors, transition metal oxides have attracted considerable attention due to their unique combination of optical, electrical, magnetic, and catalytic properties [2]. These materials offer numerous advantages such as low cost, abundance, environmental friendliness, and chemical stability, making them attractive candidates for many advanced technological applications [3].

Among transition metal oxides, copper oxide (CuO) stands out as one of the most extensively studied compounds. CuO is a p-type semiconductor with a narrow direct band gap typically ranging from 1.2 to 2.1 eV, depending on the deposition conditions [4]. Its strong absorption in the visible region of the electromagnetic spectrum, combined with its abundance, low production cost, and non-toxicity, makes it a promising candidate for solar cells, photocatalysis, gas sensors, lithium-ion batteries, and thermoelectric devices [5, 6, 7].

The properties of CuO thin films depend strongly on the deposition method, deposition conditions, and post-deposition treatments. Many parameters influence the structural, optical, and electrical properties of these films, including the precursor concentration, the choice of solvent, the substrate temperature, the annealing temperature, the doping concentration, and most importantly, the film thickness [8, 9].

Film thickness is a fundamental parameter that affects:

- The crystallite size and grain boundary density,
- The defect concentration (dislocations, vacancies, microstrain),
- The surface roughness,
- The optical absorption and transmission,
- The optical band gap (through quantum confinement effects),

- The electrical conductivity and carrier mobility [10, 11].

The objective of this chapter is to provide a comprehensive review of the fundamental properties of CuO thin films, with particular emphasis on the structural and optical characteristics. The chapter is organized as follows: Section 1.2 introduces the general concepts of thin films. Section 1.3 presents the chemistry and properties of copper oxide. Section 1.4 describes the crystal structure of CuO. Section 1.5 details the structural, optical, and electrical properties of CuO thin films. Section 1.6 discusses the influence of film thickness on these properties. Finally, Section 1.7 presents the main applications of CuO thin films.

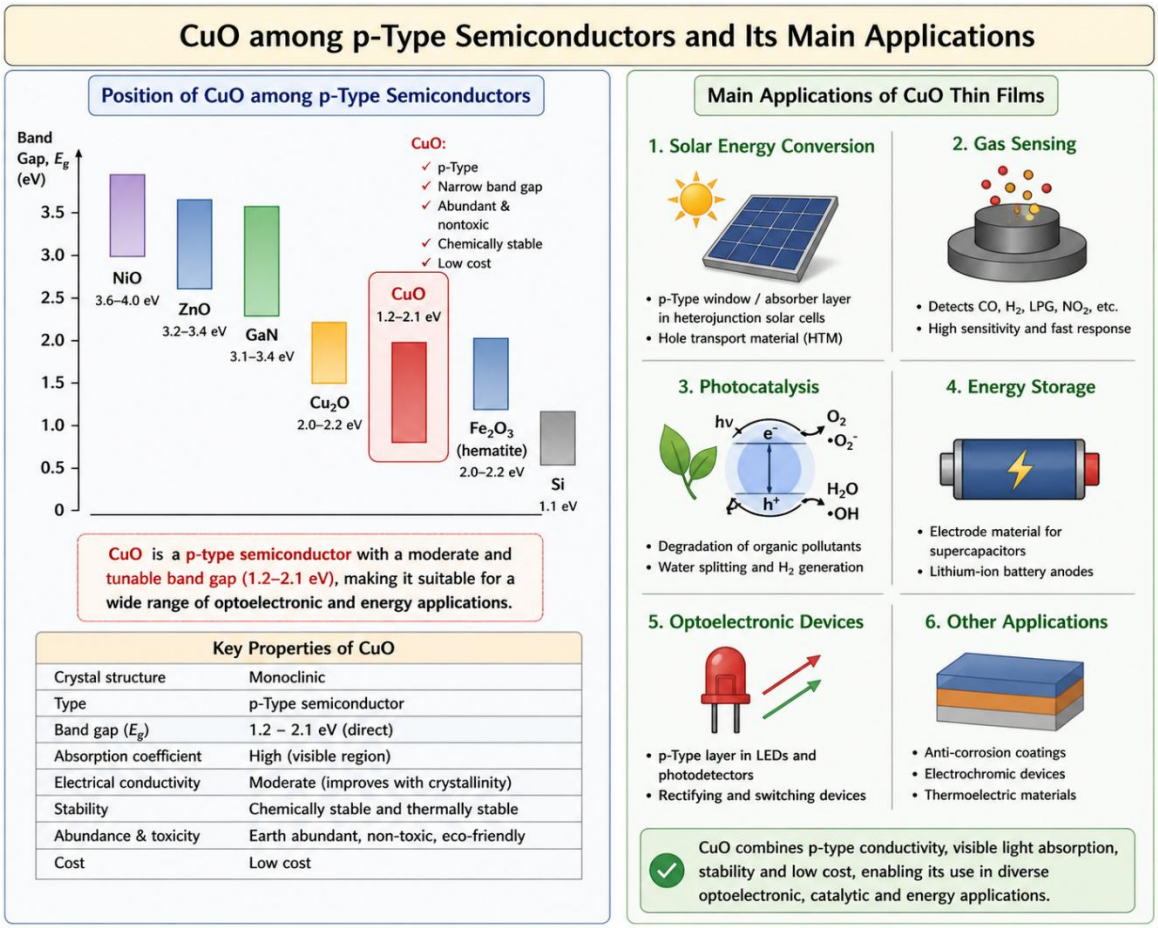

Figure 1. 1 Schematic diagram showing the position of CuO among p-type semiconductors and a summary of its main applications.

1.2 Generalities on Thin Films

1.2.1 Definition

A thin film is a layer of material with a thickness ranging from a few nanometers to several micrometers, deposited on a substrate to provide specific functional properties [12]. Thin films are characterized by a high surface-to-volume ratio, which gives them physical and chemical properties that often differ significantly from those of the corresponding bulk material [13].

1.2.2 Importance of Thin Films

Thin film technology has become indispensable in many fields:

- **Microelectronics:** transistors, integrated circuits, memories.
- **Optoelectronics:** light-emitting diodes (LEDs), photodetectors, lasers.
- **Photovoltaics:** thin film solar cells (CdTe, CIGS, perovskites).
- **Optical coatings:** antireflection coatings, mirrors, optical filters.
- **Sensors:** gas sensors, biosensors, pressure sensors.
- **Decorative coatings and protection against corrosion** [14].

1.2.3 Stages of Thin Film Growth

The growth of a thin film generally proceeds in several stages [15]:

1. **Adsorption:** Atoms or molecules from the gas or liquid phase adhere to the substrate surface.
2. **Surface diffusion:** The adsorbed species move on the surface to find energetically favorable sites.
3. **Nucleation:** The species form small stable nuclei.
4. **Growth of nuclei:** The nuclei grow by accumulation of additional atoms.
5. **Coalescence:** The nuclei merge to form a continuous film.
6. **Continued growth:** The film thickens with continued deposition.

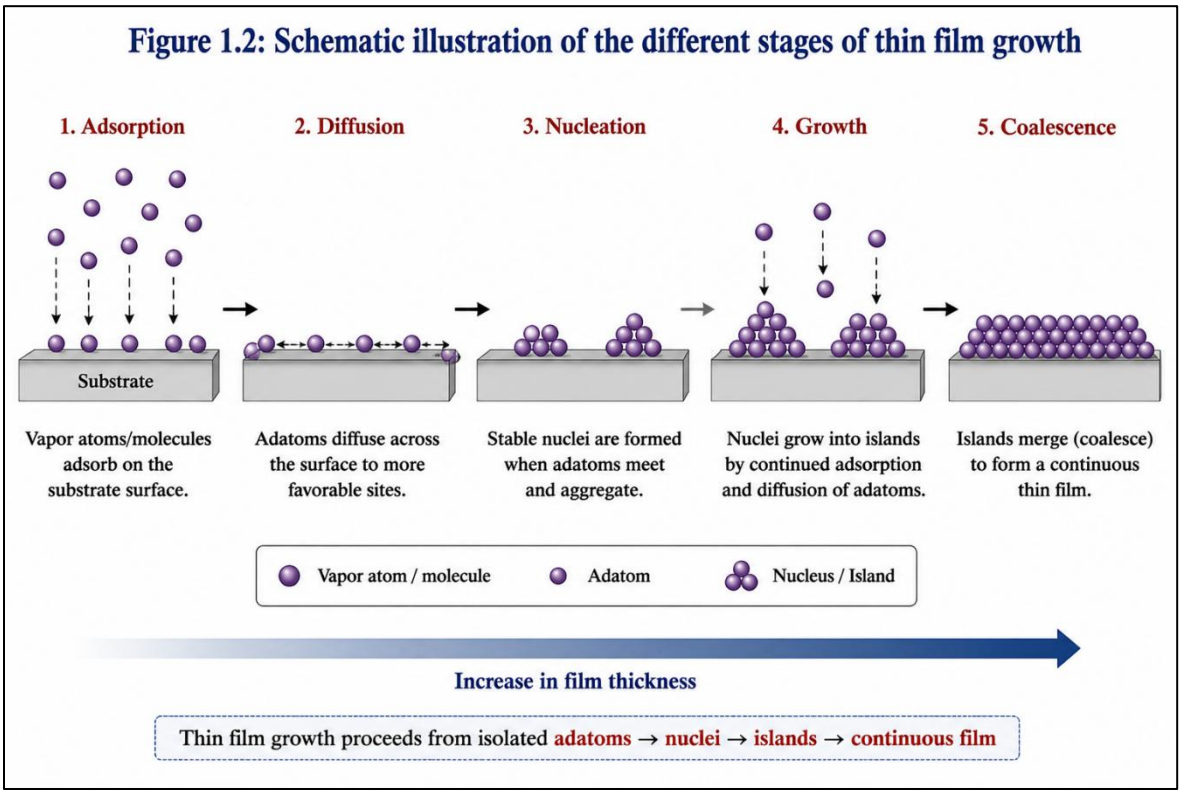

Figure 1. 2 Schematic illustration of the different stages of thin film growth: adsorption, diffusion, nucleation, growth, and coalescence.

1.2.4 Thin Film Deposition Techniques

Many techniques exist for depositing thin films, which can be classified into two main categories:

a) Physical Vapor Deposition (PVD)

- **Thermal evaporation:** the source material is heated until evaporation, then condenses on the substrate.
- **Sputtering:** atoms are extracted from a target by bombardment with energetic ions.
- **Pulsed laser deposition (PLD):** a high-energy laser pulse vaporizes the target [16].

b) Chemical Methods

- **Chemical vapor deposition (CVD):** chemical reactions in the gas phase produce a solid film on the substrate.

- **Spray pyrolysis:** a solution is sprayed onto a hot substrate where it decomposes to form the film.
- **Sol-gel:** a colloidal solution is transformed into a gel and then a solid film through hydrolysis and condensation reactions.
- **Chemical bath deposition (CBD):** the substrate is immersed in a chemical bath where the deposition takes place [17].

Each technique has its own advantages and disadvantages in terms of cost, simplicity, control of thickness and composition, and quality of the deposited films. The sol-gel method, used in this work, is particularly attractive due to its simplicity, low cost, excellent thickness control, and the high homogeneity of the films produced [18].

1.3 Copper Oxide: Generalities

1.3.1 Copper Oxide Phases

Copper naturally forms two stable oxides:

- **Cuprous oxide (Cu_2O)** also known as cuprite, in which copper is in the +1-oxidation state. Cu_2O has a cubic crystal structure and a band gap of approximately 2.0 eV [19].
- **Cupric oxide (CuO)** also known as tenorite, in which copper is in the +2-oxidation state. CuO has a monoclinic crystal structure and a narrower band gap of about 1.2–2.1 eV [20].

A third less stable phase, paramelaconite (Cu_4O_3), is sometimes mentioned in the literature, but it remains rare and difficult to obtain in pure form [21].

The transition between these phases depends on the synthesis conditions, particularly the temperature and oxygen partial pressure. At low temperatures and reducing atmospheres, the formation of Cu_2O is favored, while at high temperatures and oxidizing atmospheres, the formation of CuO is preferred [22]:

$$4Cu + O_2 \rightarrow 2Cu_2O$$
$$2Cu_2O + O_2 \rightarrow 4CuO$$

1.3.2 Physical Properties of CuO

The main physical properties of CuO are summarized in Table 1.1.

Table 1. 1 Main physical and chemical properties of CuO [4, 7].

Property	Value
Chemical formula	CuO
Other names	Cupric oxide, tenorite, copper monoxide
Molecular mass	79.55 g/mol
Color	Black or dark brown
Crystal system	Monoclinic
Space group	C2/c
Density	6.32 g/cm³
Melting point	1134 °C
Boiling point	2000 °C
Solubility in water	Insoluble
Relative permittivity	12
Type of conductivity	p-type
Band gap	1.2 – 2.1 eV
Refractive index	2.0 – 2.5

CuO is chemically stable at room temperature and does not react significantly with water or atmospheric oxygen. It is reduced to metallic copper or Cu_2O by reducing agents such as hydrogen at high temperatures [23].

1.3.3 Why Copper Oxide?

CuO has several intrinsic advantages that make it a particularly attractive material for many applications:

1. **Abundance and low cost:** Copper is the 25th most abundant element in the Earth's crust and is available at low cost compared to other elements used in semiconductors [24].

2. **Non-toxicity:** Unlike materials such as cadmium or lead, copper is non-toxic and environmentally friendly [25].
3. **Direct band gap suitable for solar cells:** A band gap close to the optimum value for absorbing solar radiation [26].
4. **High absorption coefficient:** of the order of 10^5 cm^{-1} in the visible region [27].
5. **Native p-type conductivity:** which avoids the need for doping to obtain p-type behavior [28].
6. **Theoretical energy conversion efficiency** of about 31%, comparable to that of silicon [29].

1.4 Crystal Structure of CuO

1.4.1 Description of the Monoclinic Structure

CuO crystallizes in a monoclinic structure belonging to the space group C2/c (n° 15). The unit cell contains four CuO formula units (Z = 4) and is characterized by the following lattice parameters [30]:

- a = 4.6837 Å
- b = 3.4226 Å
- c = 5.1288 Å
- $\alpha = \gamma = 90°$
- $\beta = 99.54°$

In this structure :

- Each copper atom is coordinated with four oxygen atoms located at the corners of an approximately rectangular parallelogram.
- Each oxygen atom is coordinated with four copper atoms located at the corners of a distorted tetrahedron.

The Cu–O–Cu chains form an interconnected network, giving CuO its particular electronic and magnetic properties [31].

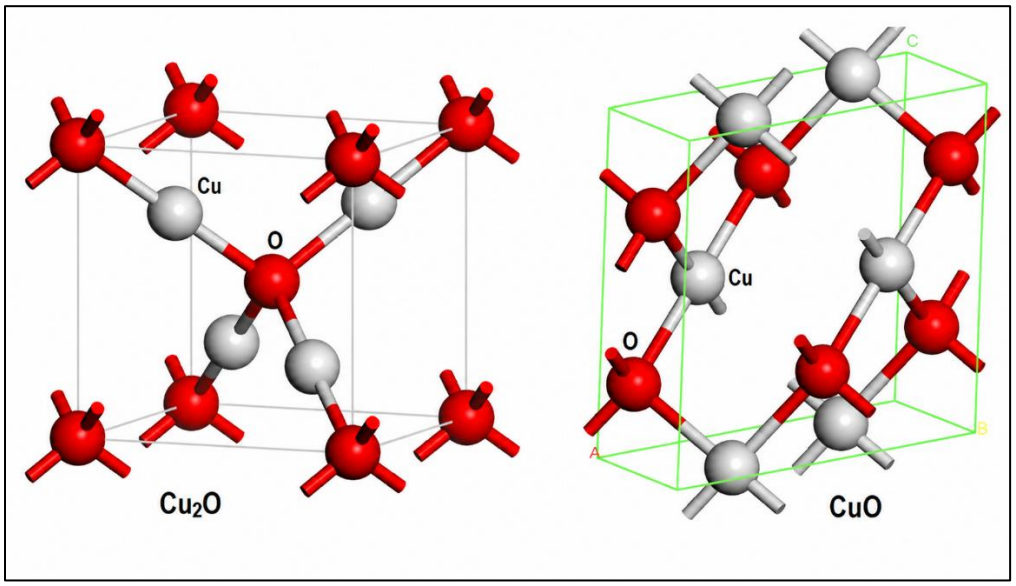

Figure 1. 3 Crystal structure of CuO (monoclinic, tenorite) and Cu_2O (cubic, cuprite) showing the arrangement of copper and oxygen atoms.

Table 1. 2 Crystallographic properties of CuO [30].

Parameter	Value
Crystal system	Monoclinic
Space group	C2/c
A	4.6837 Å
B	3.4226 Å
C	5.1288 Å
B	99.54°
Cu–O distance	1.95 Å
O–O distance	2.62 Å
Cu–Cu distance	2.90 Å
Cell volume	81.08 $Å^3$
Number of formula units (Z)	4

1.4.2 Main Diffraction Peaks of CuO

The X-ray diffraction (XRD) pattern of CuO is characterized by several diffraction peaks corresponding to different crystallographic planes. The most intense peaks of CuO appear at the following 2θ angles (for Cu-Kα radiation, λ = 1.5406 Å) [32]:

2θ (°)	(hkl)	d (Å)
32.48	(110)	2.751
35.56	(-111)	2.522
38.71	(111)	2.323
48.82	(-202)	1.864
53.45	(020)	1.713
58.30	(202)	1.581
61.60	(-113)	1.504
66.30	(-311)	1.408
68.10	(220)	1.376

These peaks are referenced in JCPDS card No. 98-004-3179 (or JCPDS 48-1548) and serve as a reference for identifying the CuO phase in the prepared films [33].

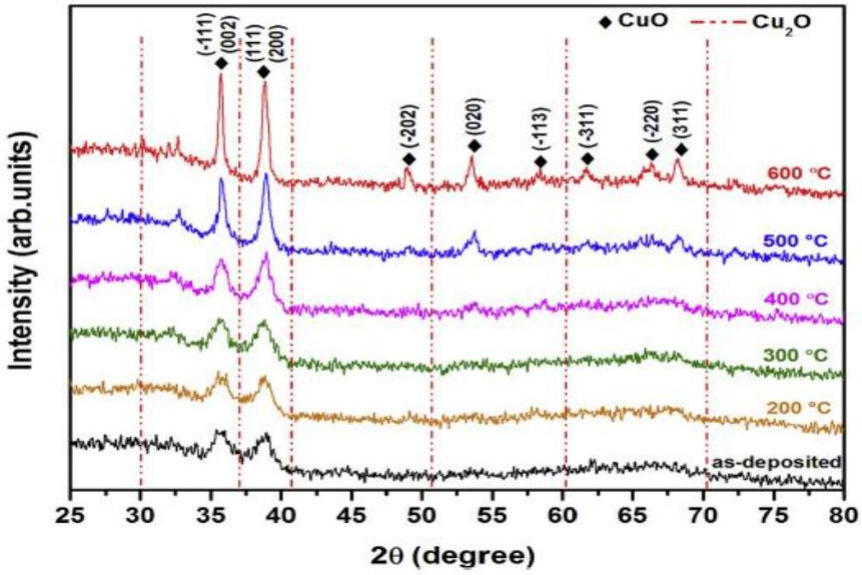

Figure 1. 4 Reference XRD pattern of CuO with the main peaks indexed.

1.4.3 Raman Spectroscopy of CuO

Raman spectroscopy is a powerful complementary technique for confirming the CuO phase. The CuO crystal has 12 degrees of freedom with the following irreducible representation [34]:

- 4Au + 5Bu + Ag + 2Bg

This decomposes into:

- 3 acoustic modes (Au + 2Bu)
- 3 Raman-active modes (Ag + 2Bg)
- 6 IR-active modes (3Au + 3Bu)

The three characteristic Raman peaks of CuO are observed at approximately 296, 346, and 632 cm^{-1}, attributed to the Ag and 2Bg phonon modes [35].

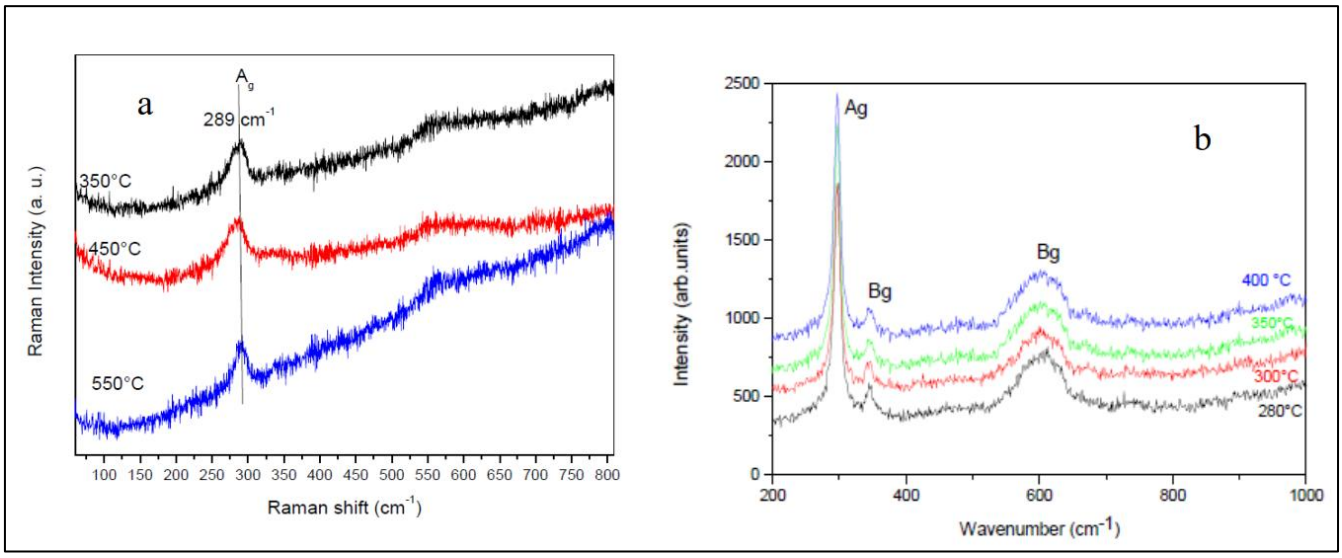

Figure 1. 5 Typical Raman spectrum of CuO showing the three characteristic peaks.

1.5 Properties of CuO Thin Films

1.5.1 Structural Properties

1.5.1.1. Influence of the Deposition Method

The structural properties of CuO thin films depend strongly on the deposition method used. Table 1.3 summarizes some studies on CuO films deposited by different techniques.

Table 1. 3 Influence of the deposition technique on the structural properties of CuO films [36-40].

Technique	Crystal structure	Crystallite size (nm)	Reference
Sol-gel spin coating	Monoclinic	19.99 – 31.47	[36]
Spray pyrolysis	Monoclinic	22 – 33	[37]
Reactive sputtering	Monoclinic	13 – 14.8	[38]
SILAR	Monoclinic	11.09 – 14.88	[39]
Heat treatment	Monoclinic	9 – 23	[40]

1.5.1.2. Influence of Annealing Temperature

The annealing temperature has a major influence on the structural properties of CuO films. As the temperature increases:

- The **$Cu_2O \rightarrow CuO$ phase transition** occurs around 250–300 °C [41].
- The **crystallite size increases** due to grain coalescence at high temperatures [42].
- The **microstrain decreases** due to defect relaxation [43].
- The **dislocation density decreases**, indicating an improvement in crystalline quality [44].

1.5.1.3. Calculation of Structural Parameters

The structural parameters of CuO films are calculated from the XRD data using the following equations:

a) Crystallite size (Scherrer's formula):

$$D = \frac{K \cdot \lambda}{\beta \cos \theta}$$

where K = 0.9 is the Scherrer constant, λ is the X-ray wavelength, β is the full width at half maximum (FWHM) of the peak in radians, and θ is the Bragg angle [45].

b) Lattice parameters (for monoclinic structure):

$$\frac{1}{d^2} = \frac{1}{\sin^2\beta}\left(\frac{h^2}{a^2} + \frac{k^2\sin^2\beta}{b^2} + \frac{l^2}{c^2}\right) - \frac{2hl\cos\beta}{ac\sin^2\beta}$$

c) Lattice strain:

$$\varepsilon = \frac{\beta}{4\tan\theta}$$

d) Dislocation density:

$$\delta = \frac{1}{D^2}$$

These parameters provide important information on the crystalline quality and defect density of the films [46].

1.5.2 Electrical Properties

1.5.2.1. p-type Conductivity

CuO is intrinsically a p-type semiconductor due to the presence of copper vacancies (V_Cu) in its lattice. These vacancies act as shallow acceptors that introduce holes into the valence band [47]. Copper vacancies are particularly common in CuO due to the volatility of copper during synthesis [48].

The conductivity mechanism of CuO can be described as follows:

1. Each copper vacancy creates two holes in the valence band (since Cu^{2+} contributes 2 electrons).
2. These holes serve as charge carriers, giving CuO its p-type behavior.
3. Interstitial oxygen (O_i) can also contribute to acceptor states [49].

1.5.2.2. Resistivity and Mobility

The electrical resistivity of CuO thin films depends strongly on the deposition conditions. Typical values are :

- **Resistivity:** $10^2 – 10^6$ Ω·cm
- **Hole mobility:** 10 – 100 $cm^2/V·s$
- **Carrier concentration :** $10^{10} – 10^{16}$ cm^{-3} [50, 51].

1.5.2.3. Influence of Various Factors

Several factors influence the electrical properties of CuO films:

- **Annealing temperature:** Increasing temperature reduces resistivity by improving crystallinity and reducing grain boundaries [52].
- **Film thickness:** Thicker films generally exhibit lower resistivity due to larger crystallites and fewer defects [53].
- **Doping:** Doping with impurities such as Li, Na, K, or transition metals can significantly modify the conductivity [54].
- **Oxygen partial pressure:** Affects the concentration of copper vacancies and consequently the conductivity [55].

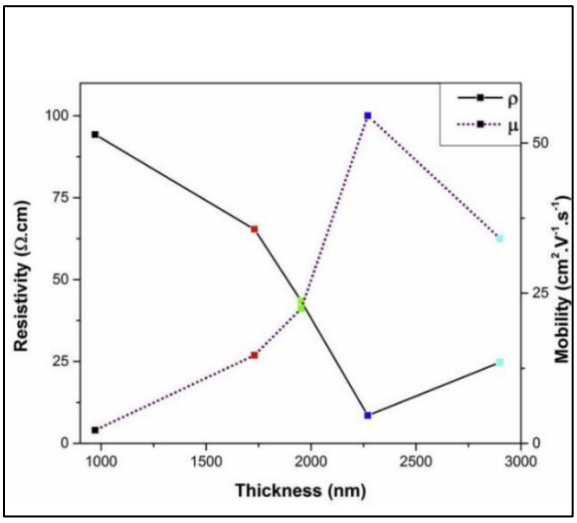

Figure 1. 6 Variation of resistivity and Hall mobility of CuO films as a function of thickness.

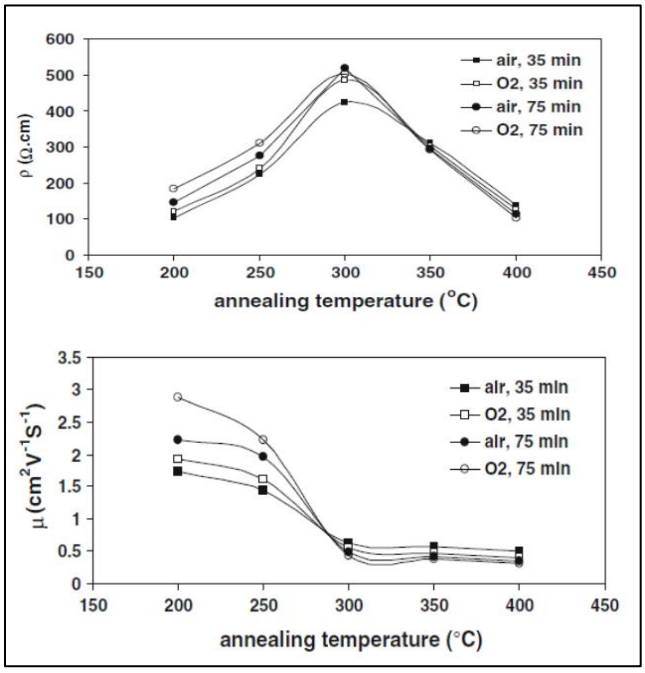

Figure 1. 7 Variation of resistivity and Hall mobility of CuO films as a function of annealing temperature.

1.5.3 Optical Properties

The optical properties of CuO thin films are essential for their use in optoelectronic applications. The main optical characteristics include the transmittance, absorption coefficient, refractive index, optical band gap, and Urbach energy [56].

1.5.3.1. Optical Transmittance

The optical transmittance T(λ) is the ratio of the intensity of light transmitted through the film to the intensity of incident light. CuO films generally exhibit low transmittance in the visible region (typically 10–30%) and increased transmittance in the near-infrared region [57]. This behavior gives CuO films their characteristic black or dark brown color.

The transmittance is governed by the Beer–Lambert law:

$$T = e^{-\alpha d}$$

where α is the absorption coefficient and *d* are the film thickness.

1.5.3.2. Absorption Coefficient

The absorption coefficient α is calculated from the transmittance using:

$$\alpha = \frac{1}{d} \ln \left(\frac{1}{T}\right)$$

For CuO, α typically reaches values of the order of 10^5 cm^{-1} in the visible region, indicating strong absorption [58]. This high value makes it possible to use very thin layers (a few hundred nanometers) to absorb a large fraction of incident light, which is particularly advantageous for solar cell applications.

1.5.3.3. Optical Band Gap (Eg)

The optical band gap is one of the most important parameters of a semiconductor, as it determines the threshold for optical absorption. For CuO, which is a direct band

gap semiconductor, the absorption coefficient near the absorption edge is given by Tauc's relation [59]:

$$(\alpha h\nu)^2 = A(h\nu - E_g)$$

where A is a constant, hν is the photon energy, and Eg is the optical band gap.

The band gap is determined by plotting $(\alpha h\nu)^2$ as a function of hν and extrapolating the linear part of the curve to the energy axis [60].

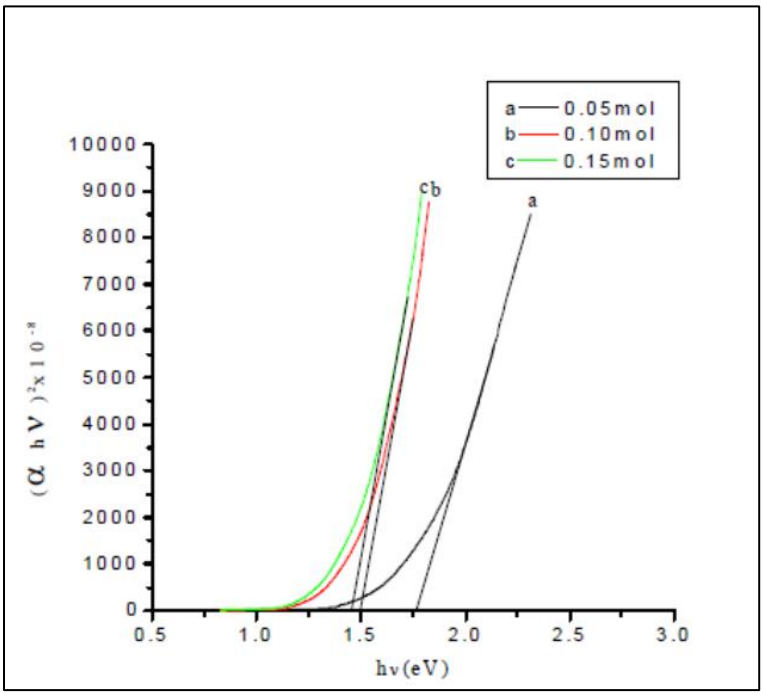

Figure 1. 8 Typical Tauc plot used to determine the optical band gap of CuO.

The band gap value of CuO reported in the literature varies between 1.2 and 2.1 eV depending on the deposition conditions, crystallite size, and defects [61, 62].

1.5.3.4. Urbach Energy (Eu)

The Urbach energy characterizes the disorder present in the material. It corresponds to the formation of localized states in tails near the edges of the valence and conduction bands. The Urbach energy is defined by Urbach's law [63] :

$$\alpha = \alpha_0 \exp\left(\frac{h\nu}{E_u}\right)$$

It is determined from the slope of the curve ln(α) vs. hν:

$$E_u = \left[\frac{d(\ln\ \alpha)}{d(h\nu)}\right]^{-1}$$

A higher Urbach energy indicates a higher density of disorder and defects in the film [64].

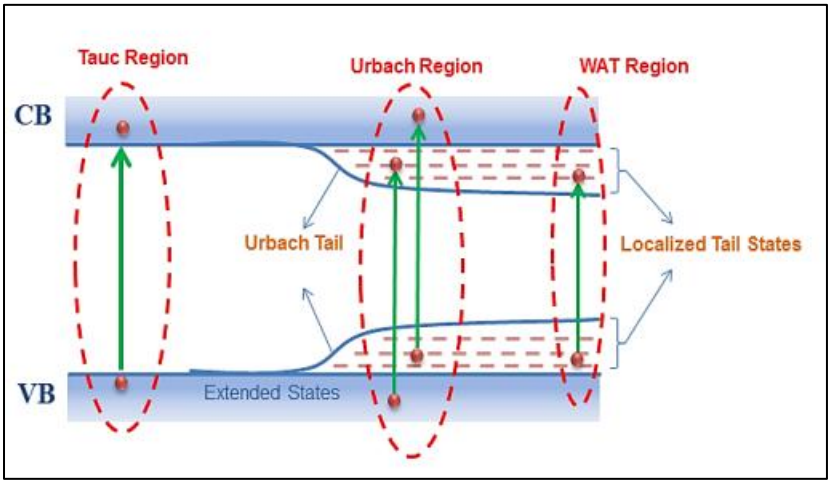

Figure 1. 9 Schematic representation of optical transitions between the valence band and the conduction band, showing the Tauc, Urbach, and weak absorption regions.

1.5.3.5. Influence of Different Factors on Optical Properties

The optical properties of CuO films are influenced by several factors:

a) **Influence of precursor concentration:** A higher concentration leads to thicker films with lower transmittance and a smaller band gap [65].
b) **Influence of substrate temperature:** Higher temperatures generally lead to a decrease in the band gap due to improved crystallinity [66].

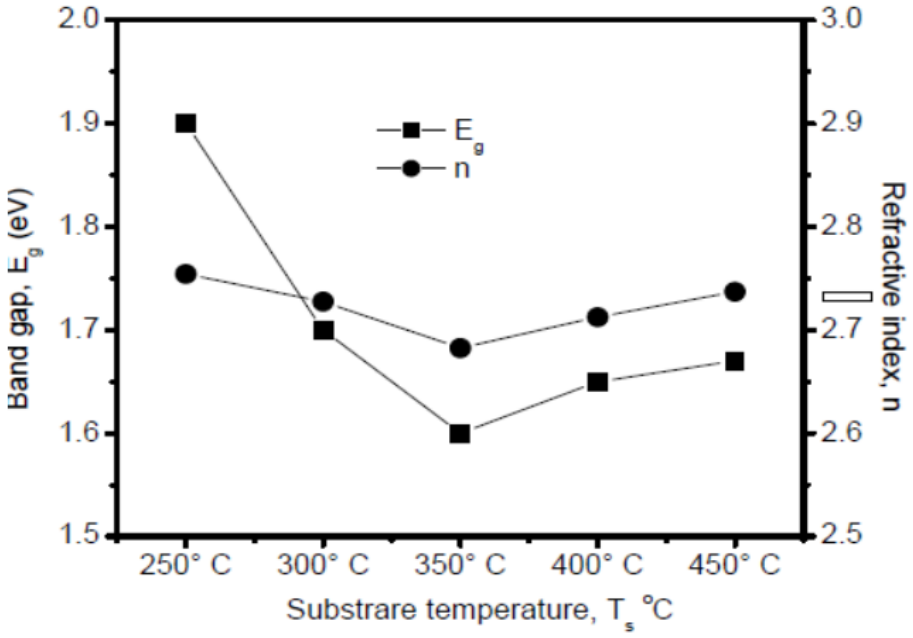

Figure 1. 10 Variation of band gap and refractive index as a function of substrate temperature.

c) Influence of doping: Doping with various elements modifies the band gap by introducing impurity states and modifying the electronic structure [67].

d) Influence of film thickness: This is the main subject of this dissertation and will be discussed in detail in Section 1.6.

1.5.4 Mechanical Properties

The mechanical properties of CuO thin films, although less studied than the electrical and optical properties, are important for their integration into devices. The main parameters include the hardness (HN), the elastic modulus (Er), the adhesion, and the fracture toughness [68].

The hardness of CuO is influenced by:

- The crystallite size (Hall–Petch effect): smaller crystallites lead to higher hardness due to grain boundaries that block dislocation motion.
- Doping with impurities such as Li, which increases hardness [69].
- The annealing temperature, which can reduce internal stresses [70].

1.6 Influence of Film Thickness on the Properties of CuO Films

Film thickness is a fundamental parameter that influences all the properties of CuO films. This section presents a detailed review of the effects of thickness on the structural, optical, and electrical properties.

1.6.1 Effect on Structural Properties

As the film thickness increases:

1. **Crystallite size generally increases** at first, due to the additional growth of crystallites with the addition of new layers. However, beyond a certain critical thickness, the size may decrease due to the formation of new defects [71].
2. **Crystallinity improves** to an optimal thickness, then can deteriorate due to the accumulation of stresses and defects [72].
3. **Microstrain and dislocation density** are minimal at intermediate thickness, reflecting the best crystallographic quality [73].
4. **Surface roughness** generally increases with thickness [74].

1.6.2 Effect on Optical Properties

The variation of optical properties with thickness is governed by several mechanisms:

1. **Decrease in transmittance:** According to the Beer–Lambert law, transmittance decreases exponentially with thickness [75].
2. **Decrease in optical band gap:** Several studies have reported a decrease in the band gap with increasing film thickness. Akaltun [76] observed a decrease from 2.03 eV to 1.79 eV when the thickness varied from 120 to 310 nm. This decrease is attributed to :
    - The reduction of quantum confinement effects in larger crystallites,
    - The increase in disorder reflected by an increase in Urbach energy,
    - The reduction of defects at grain boundaries [77].
3. **Increase in Urbach energy:** Indicating an increase in disorder in thicker films [78].
4. **Modification of the refractive index:** which depends on density and structure [79].

1.6.3 Effect on Electrical Properties

The thickness influences the electrical properties as follows:

1. **Decrease in resistivity** with increasing thickness, due to:
    - Larger crystallites and reduced grain boundaries,
    - Reduction of carrier scattering,
    - Increase in carrier mobility [80].
2. **Increase in carrier concentration** in some cases [81].
3. **Optimal thickness:** Many studies report an optimal thickness for electrical performance, beyond which the resistivity may increase due to the formation of new defects [82].

The work of Shariffudin et al. [83], Saâd et al. [84], and Kamli et al. [85] confirms these trends and emphasizes the importance of carefully optimizing the film thickness for each specific application.

1.7 Applications of CuO Thin Films

CuO thin films have a wide range of applications due to their unique combination of properties.

1.7.1 Solar Cells

CuO is an attractive material for thin film solar cells due to its appropriate band gap, high absorption coefficient, and abundance. Several heterojunction configurations have been studied [86] :

- **p-CuO/n-Si:** Achieves efficiencies up to 1.0% [87].
- **p-CuO/n-ZnO:** With an open-circuit voltage of 480 mV and an efficiency of 0.232% [88].
- **p-CuO/n-Cu_2O:** Efficiency of 0.02% [89].

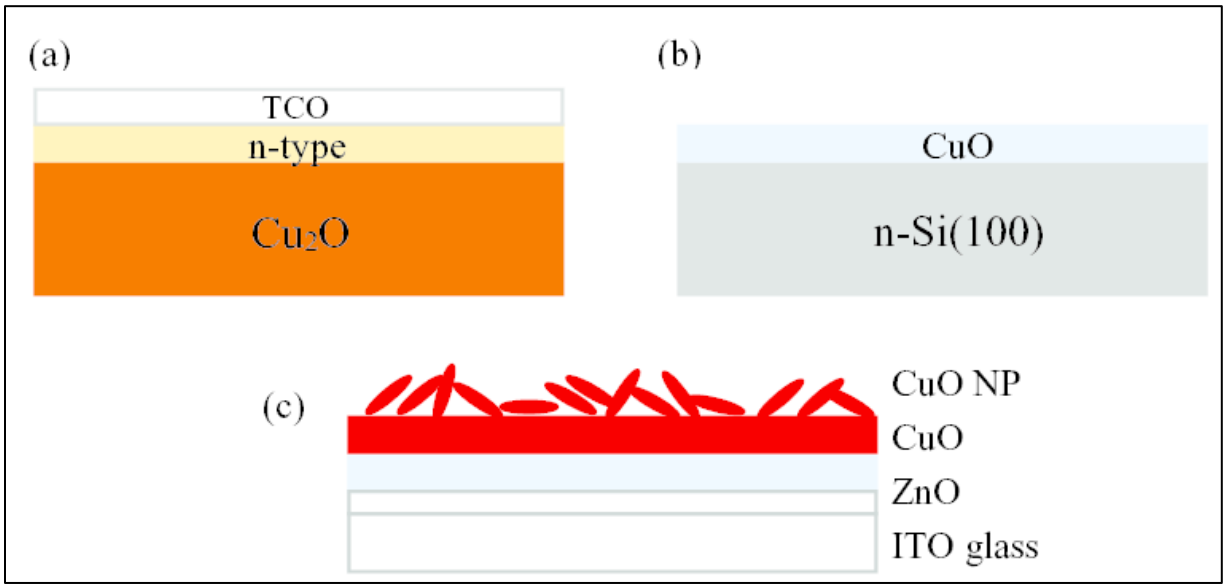

Figure 1. 11 Schematic structure of a p-CuO/n-Si solar cell and typical I-V characteristic.

Table 1. 4 Performance of different CuO-based solar cells [86-89].

Heterojunction	Voc (mV)	Isc (mA)	FF (%)	η (%)
CuO/Si	200	0.0073	24	9.7×10^{-3}
CuO/ZnO:Sn	480	1.82	0.63	0.232
CuO/C_{60}	0.24	0.067	0.25	2.3×10^{-4}
CuO/Cu_2O	210	0.310	0.26	0.02

1.7.2 Gas Sensors

CuO thin films are excellent gas sensors due to their large surface area and modulable conductivity. They have been used to detect [90] :

- **NO_2:** with sensitivities up to 5600% [91].
- **H_2S:** sensitivity of 119% with Pd doping [92].
- **CO and CO_2:** with sensitivities up to 1400% [93].
- **Ethanol and acetone:** with sensitivities up to 70% [94].

The mechanism of CuO gas sensors is based on the modification of the surface electrical conductivity due to interaction with target gas molecules [95].

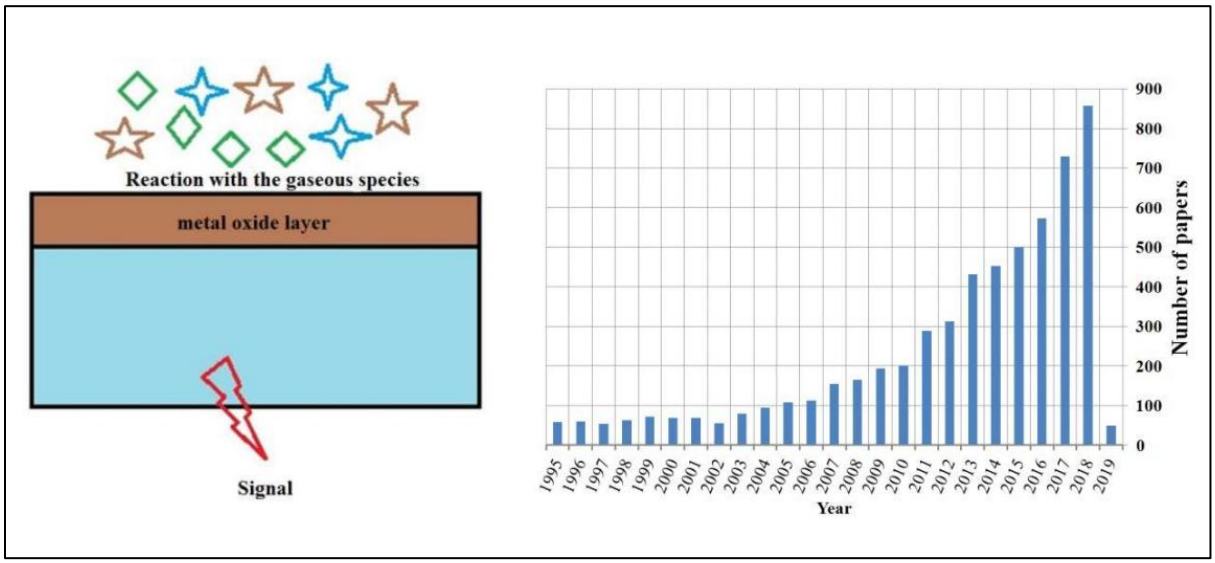

Figure 1. 12 Schematic of a metal oxide-based gas sensor and number of publications on CuO-based gas sensors from 1995 to 2019.

1.7.3 Photocatalysis

CuO is used as a photocatalyst for the degradation of organic pollutants in water. Its narrow band gap allows it to absorb a large fraction of visible light, generating electron-hole pairs that participate in oxidation/reduction reactions [96].

The photocatalytic mechanism involves [97] :

1. Absorption of a photon with energy ≥ Eg.
2. Generation of electron-hole pairs.
3. Migration of carriers to the surface.
4. Reaction with adsorbed species (H_2O, O_2) to form reactive radicals ($OH^{\bullet}$, $O_2^{\bullet -}$).
5. Degradation of organic pollutants by these radicals.

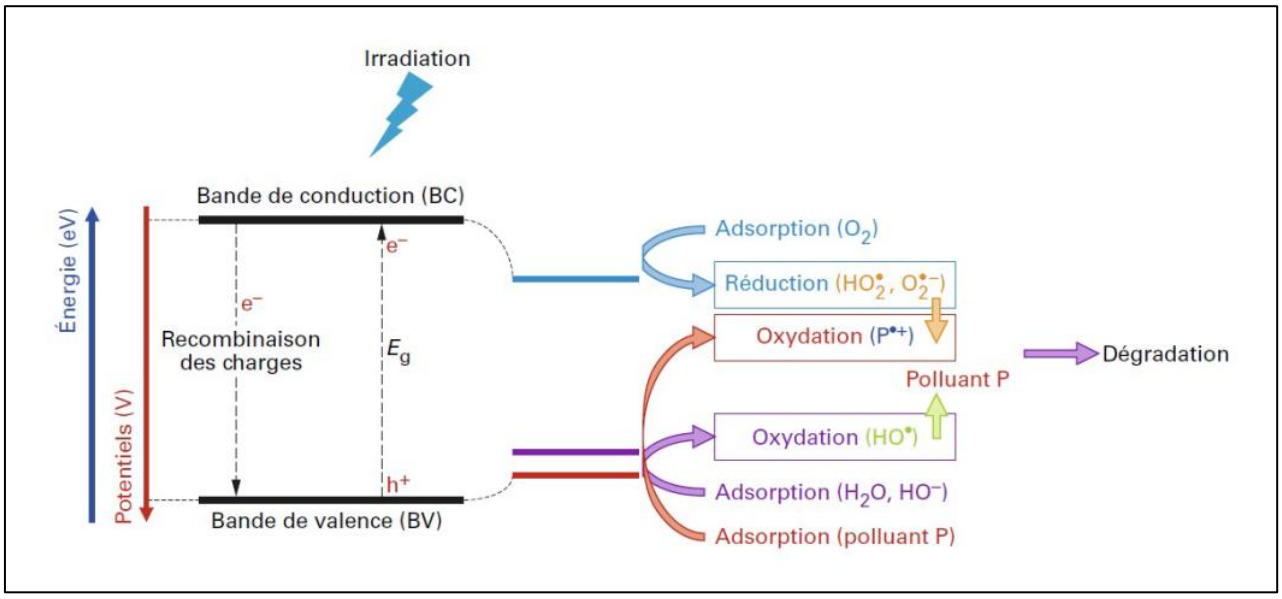

Figure 1. 13 Schematic illustration of the photocatalytic mechanism of CuO under visible illumination.

1.7.4 Lithium-Ion Batteries

CuO is a promising material as an anode for lithium-ion batteries due to its high theoretical capacity (~674 mAh/g), much higher than that of conventional graphite (372 mAh/g) [98]. However, problems related to volume expansion during cycling limit its practical use.

1.7.5 Thermoelectric Devices

CuO has recently attracted attention for thermoelectric applications, particularly for the recovery of waste heat. Studies have shown that doping CuO with elements such as Li can improve its thermoelectric performance [99].

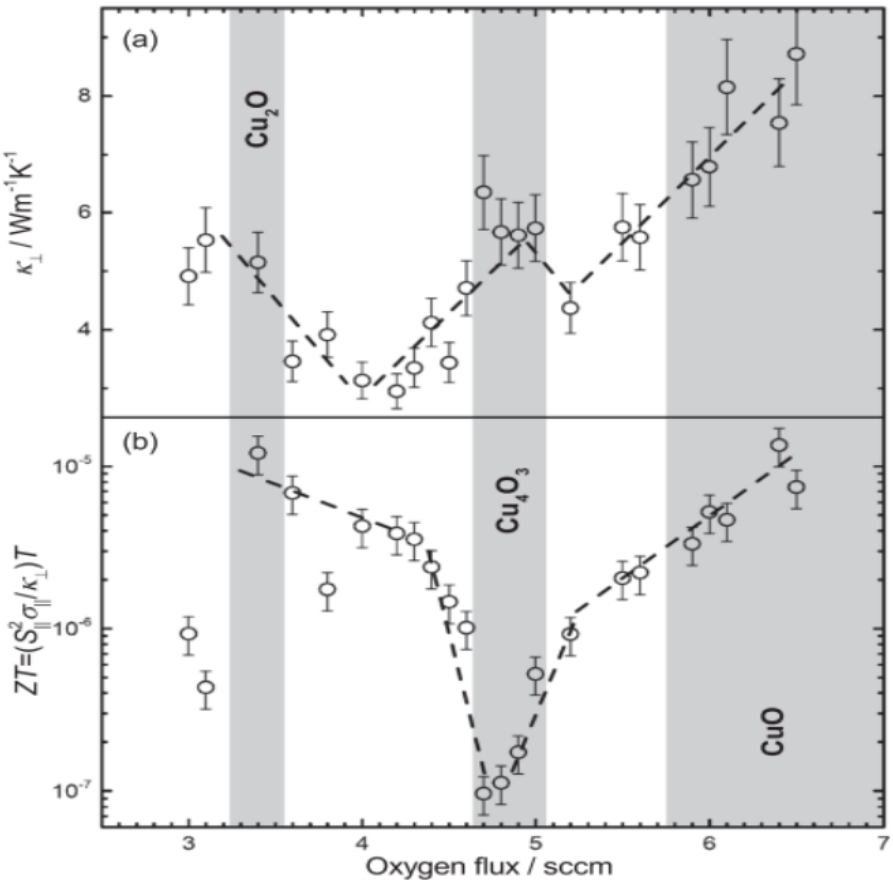

Figure 1. 14 Variation of thermal conductivity and thermoelectric figure of merit ZT of CuO as a function of oxygen flux during sputtering deposition.

1.8 Conclusion

This chapter has presented a comprehensive review of CuO thin films, covering their fundamental physical properties, monoclinic crystal structure, and structural, optical, and electrical characteristics. The main points to remember are:

- **CuO is a p-type semiconductor** with a direct band gap of 1.2–2.1 eV, abundant, non-toxic, and inexpensive.
- The properties of CuO films depend strongly on deposition conditions, particularly on annealing temperature, doping, and film thickness.
- The **film thickness** has a fundamental influence on crystallinity, optical band gap, optical transmittance, and electrical resistivity.

- CuO has many promising applications in solar cells, gas sensors, photocatalysis, batteries, and thermoelectric devices.

The fundamental concepts presented in this chapter form the theoretical basis for the experimental study to be described in the following chapters. **Chapter 2** will detail the experimental procedure for the preparation of CuO films by the sol-gel spin coating technique, as well as the characterization methods used. **Chapter 3** will present and discuss the experimental results obtained, with particular emphasis on the influence of film thickness on the optical band gap.

References

[1] G. Filipič and U. Cvelbar, "Copper oxide nanowires: a review of growth," Nanotechnology, vol. 23, p. 194001, 2012.

[2] A. Barhoum and M. L. García-Betancourt, "Physicochemical characterization of nanomaterials: Size, morphology, optical, magnetic, and electrical properties," in Emerging applications of nanoparticles and architecture nanostructures, ed: Elsevier, 2018, pp. 279-304.

[3] N. D. Hoa, N. Van Quy, H. Jung, D. Kim, H. Kim, and S.-K. Hong, "Synthesis of porous CuO nanowires and its application to hydrogen detection," Sensors and Actuators B: Chemical, vol. 146, pp. 266-272, 2010.

[4] B. Balamurugan and B. Mehta, "Optical and structural properties of nanocrystalline copper oxide thin films prepared by activated reactive evaporation," Thin solid films, vol. 396, pp. 90-96, 2001.

[5] Z. Chen, T. F. Jaramillo, T. G. Deutsch, A. Kleiman-Shwarsctein, A. J. Forman, N. Gaillard, R. Garland, K. Takanabe, C. Heske, and M. Sunkara, "Accelerating materials development for photoelectrochemical hydrogen production: Standards for methods, definitions, and reporting protocols," Journal of Materials Research, vol. 25, pp. 3-16, 2010.

[6] S. Saleem, A. H. Jabbar, M. H. Jameel, A. Rehman, Z. H. Kareem, A. H. Abbas, Z. Ghaffar, S. A. Razzaq, R. A. Pashameah, and E. Alzahrani, "Enhancement in structural, morphological, and optical properties of copper oxide for optoelectronic device applications," Nanotechnology Reviews, vol. 11, pp. 2827-2838, 2022.

[7] S. Norzaee, B. Djahed, R. Khaksefidi, and F. K. Mostafapour, "Photocatalytic degradation of aniline in water using CuO nanoparticles," Journal of Water Supply: Research and Technology—Aqua, vol. 66, pp. 178-185, 2017.

[8] M. Umar, M. Y. Swinkels, M. De Luca, C. Fasolato, L. Moser, G. Gadea, L. Marot, T. Glatzel, and I. Zardo, "Morphological and stoichiometric optimization of Cu2O thin films by deposition conditions and post-growth annealing," Thin Solid Films, vol. 732, p. 138763, 2021.

[9] K. Khojier and A. Behju, "Annealing temperature effect on nanostructure and phase transition of copper oxide thin films," 2012.

[10] L. Yuan, Y. Wang, R. Mema, and G. Zhou, "Driving force and growth mechanism for spontaneous oxide nanowire formation during the thermal oxidation of metals," Acta Materialia, vol. 59, pp. 2491-2500, 2011.

[11] I. Ezenwa, "Optical analysis of chemical bath fabricated CuO thin films," Res. J. Recent Sci, vol. 1, pp. 46-50, 2012.

[12] F. J. Arregui, Sensors based on nanostructured materials vol. 10: Springer, 2009.

[13] J. Hafner, C. Wolverton, and G. Ceder, "Toward computational materials design: the impact of density functional theory on materials research," MRS bulletin, vol. 31, pp. 659-668, 2006.

[14] T. Y. Hill, "Fabrication of zinc oxide thin films for renewable energy and sensor applications," 2010.

[15] N. Mukwakwa, "Desposition of zinc oxide thin films by spin coating and examination of their structural, electrical and optical characteristics for solar cell application," The University of Zambia, 2017.

[16] S. Waita, "Dye sensitized TiO2 solar cells," Department of Physics, University of Nairobi, Kenya (PhD Thesis), 2008.

[17] L. D. L. S. Valladares, D. H. Salinas, A. B. Dominguez, D. A. Najarro, S. Khondaker, T. Mitrelias, C. Barnes, J. A. Aguiar, and Y. Majima, "Crystallization and electrical resistivity of Cu2O and CuO obtained by thermal oxidation of Cu thin films on SiO2/Si substrates," Thin solid films, vol. 520, pp. 6368-6374, 2012.

[18] D. Bokov, A. Turki Jalil, S. Chupradit, W. Suksatan, M. Javed Ansari, I. H. Shewael, G. H. Valiev, and E. Kianfar, "Nanomaterial by sol-gel method: synthesis and application," Advances in Materials Science and Engineering, vol. 2021, pp. 1-21, 2021.

[19] L. Olsen, F. Addis, and W. Miller, "Experimental and theoretical studies of Cu2O solar cells," Solar cells, vol. 7, pp. 247-279, 1982.

[20] V. Avrutin, N. Izyumskaya, and H. Morkoç, "Semiconductor solar cells: Recent progress in terrestrial applications," Superlattices and Microstructures, vol. 49, pp. 337-364, 2011.

[21] D. Hartung, F. Gather, P. Hering, C. Kandzia, D. Reppin, A. Polity, B. Meyer, and P. Klar, "Assessing the thermoelectric properties of CuxO (x= 1 to 2) thin films as a function of composition," Applied Physics Letters, vol. 106, 2015.

[22] F. A. Akgul, G. Akgul, N. Yildirim, H. E. Unalan, and R. Turan, "Influence of thermal annealing on microstructural, morphological, optical properties and surface electronic structure of copper oxide thin films," Materials Chemistry and Physics, vol. 147, pp. 987-995, 2014.

[23] L. Huanga, S. Yanga, T. Lia, B. Gua, Y. Dua, Y. Lub, and S. Shi, "Preparation of large-scale cupric oxide nanowires by thermal evaporation," J. Cryst. Growth, vol. 260, pp. 130-135, 2004.

[24] G. Filipič and U. Cvelbar, "Copper oxide nanowires: a review of growth," Nanotechnology, vol. 23, p. 194001, 2012.

[25] A. Bhaduri and K. Kajal, "Facile synthesis and characterization of cupric oxide (CuO) nanoparticles: Inexpensive and abundant candidate for light harvesting," in AIP Conference Proceedings, 2019.

[26] M. R. Hoffmann, S. T. Martin, W. Choi, and D. W. Bahnemann, "Environmental applications of semiconductor photocatalysis," Chemical reviews, vol. 95, pp. 69-96, 1995.

[27] R. Gusain and O. P. Khatri, "Ultrasound assisted shape regulation of CuO nanorods in ionic liquids and their use as energy efficient lubricant additives," Journal of Materials Chemistry A, vol. 1, pp. 5612-5619, 2013.

[28] B. Meyer, A. Polity, D. Reppin, M. Becker, P. Hering, P. Klar, T. Sander, C. Reindl, J. Benz, and M. Eickhoff, "Binary copper oxide semiconductors: From materials towards devices," physica status solidi (b), vol. 249, pp. 1487-1509, 2012.

[29] F. Gao, X.-J. Liu, J.-S. Zhang, M.-Z. Song, and N. Li, "Photovoltaic properties of the p-CuO/n-Si heterojunction prepared through reactive magnetron sputtering," Journal of applied physics, vol. 111, 2012.

[30] S. Åsbrink and L.-J. Norrby, "A refinement of the crystal structure of copper (II) oxide with a discussion of some exceptional esd's," Acta Crystallographica Section B: Structural Crystallography and Crystal Chemistry, vol. 26, pp. 8-15, 1970.

[31] G. Tunell, E. Posnjak, and C. Ksanda, "Geometrical and optical properties, and crystal structure of tenorite," Zeitschrift für Kristallographie-Crystalline Materials, vol. 90, pp. 120-142, 1935.

[32] D. Volanti, D. Keyson, L. Cavalcante, A. Z. Simões, M. Joya, E. Longo, J. A. Varela, P. Pizani, and A. Souza, "Synthesis and characterization of CuO flower-nanostructure processing by a domestic hydrothermal microwave," Journal of Alloys and Compounds, vol. 459, pp. 537-542, 2008.

[33] M. Boumezrag, K. Almi, S. Lakel, and H. Touhami, "Alkali Metals Doped Cu0. 94A0. 06O (A= Li, Na and K) Thin Films: Facile Synthesis, Structural, Optical and Thermoelectric Properties," Russian Journal of Physical Chemistry B, vol. 18, pp. 895-906, 2024.

[34] G. Pezzotti, "Raman spectroscopy of piezoelectrics," Journal of Applied Physics, vol. 113, p. 8_1, 2013.

[35] B. Balamurugan, B. Mehta, D. Avasthi, F. Singh, A. K. Arora, M. Rajalakshmi, G. Raghavan, A. Tyagi, and S. Shivaprasad, "Modifying the nanocrystalline characteristics—structure, size, and surface states of copper oxide thin films by high-energy heavy-ion irradiation," Journal of applied physics, vol. 92, pp. 3304-3310, 2002.

[36] N. Touka, D. Tabli, and K. Badari, "Effect of annealing temperature on structural and optical properties of copper oxide thin films deposited by sol-gel spin coating method," Journal of Optoelectronics and Advanced Materials, vol. 21, pp. 698-701, 2019.

[37] R. D. Prabu, S. Valanarasu, V. Ganesh, M. Shkir, S. AlFaify, A. Kathalingam, S. Srikumar, and R. Chandramohan, "An effect of temperature on structural, optical, photoluminescence and

electrical properties of copper oxide thin films deposited by nebulizer spray pyrolysis technique," Materials Science in Semiconductor Processing, vol. 74, pp. 129-135, 2018.

[38] X. Zhang, Z. Li, and J. Fan, "An effect of rapid post-annealing temperature on the properties of cupric oxide thin films deposited by a remote plasma sputtering technique," Materials Science in Semiconductor Processing, vol. 137, p. 106227, 2022.

[39] T. Çayir Taşdemirci, "Copper oxide thin films synthesized by SILAR: role of varying annealing temperature," Electronic Materials Letters, vol. 16, pp. 239-246, 2020.

[40] A. A. Baqer, K. A. Matori, N. M. Al-Hada, H. M. Kamari, A. H. Shaari, E. Saion, and J. L. Y. Chyi, "Copper oxide nanoparticles synthesized by a heat treatment approach with structural, morphological and optical characteristics," Journal of Materials Science: Materials in Electronics, vol. 29, pp. 1025-1033, 2018.

[41] L. Attou, B. Jaber, and H. Ez-Zahraouy, "Effect of annealing temperature on structural, optical and photocatalytic properties of CuO nanoparticles," Mediterranean Journal of Chemistry, vol. 7, pp. 308-316, 2018.

[42] I. Singh and R. Bedi, "Studies and correlation among the structural, electrical and gas response properties of aerosol spray deposited self-assembled nanocrystalline CuO," Applied surface science, vol. 257, pp. 7592-7599, 2011.

[43] P. Ooi, S. Ng, M. Abdullah, H. A. Hassan, and Z. Hassan, "Effects of oxygen percentage on the growth of copper oxide thin films by reactive radio frequency sputtering," Materials Chemistry and Physics, vol. 140, pp. 243-248, 2013.

[44] N. Serin, T. Serin, Ş. Horzum, and Y. Celik, "Annealing effects on the properties of copper oxide thin films prepared by chemical deposition," Semiconductor science and technology, vol. 20, p. 398, 2005.

[45] C. Abdelmounaïm, Z. Amara, A. Maha, and D. Mustapha, "Effects of molarity on structural, optical, morphological and CO2 gas sensing properties of nanostructured copper oxide films

deposited by spray pyrolysis," Materials Science in Semiconductor Processing, vol. 43, pp. 214-221, 2016.

[46] F. Bayansal, Y. Gülen, B. Şahin, S. Kahraman, and H. Çetinkara, "CuO nanostructures grown by the SILAR method: influence of Pb-doping on the morphological, structural and optical properties," Journal of Alloys and Compounds, vol. 619, pp. 378-382, 2015.

[47] B. Meyer, A. Polity, D. Reppin, M. Becker, P. Hering, P. Klar, T. Sander, C. Reindl, J. Benz, and M. Eickhoff, "Binary copper oxide semiconductors: From materials towards devices," physica status solidi (b), vol. 249, pp. 1487-1509, 2012.

[48] Y. Gong, C. Lee, and C. Yang, "Atomic force microscopy and Raman spectroscopy studies on the oxidation of Cu thin films," Journal of Applied Physics, vol. 77, pp. 5422-5425, 1995.

[49] J.-H. Lee, B.-W. Yeo, and B.-O. Park, "Effects of the annealing treatment on electrical and optical properties of ZnO transparent conduction films by ultrasonic spraying pyrolysis," Thin Solid Films, vol. 457, pp. 333-337, 2004.

[50] F. M. Li, R. Waddingham, W. I. Milne, A. J. Flewitt, S. Speakman, J. Dutson, S. Wakeham, and M. Thwaites, "Low temperature (< 100 C) deposited P-type cuprous oxide thin films: Importance of controlled oxygen and deposition energy," Thin Solid Films, vol. 520, pp. 1278-1284, 2011.

[51] S. Kose, F. Atay, V. Bilgin, and I. Akyuz, "Some physical properties of copper oxide films: The effect of substrate temperature," Materials Chemistry and Physics, vol. 111, pp. 351-358, 2008.

[52] D. Ozaslan, O. Erken, M. Gunes, and C. Gumus, "The effect of annealing temperature on the physical properties of Cu2O thin film deposited by SILAR method," Physica B: Condensed Matter, vol. 580, p. 411922, 2020.

[53] H. B. Saâd, M. Ajili, S. Dabbabi, and N. T. Kamoun, "Investigation on thickness and annealing effects on physical properties and electrical circuit model of CuO sprayed thin films," Superlattices and Microstructures, vol. 142, p. 106508, 2020.

[54] H. Siddiqui, M. Qureshi, and F. Z. Haque, "Alkali metals doped Cu0. 95X0. 05O (X= Li, Na and K) nanoparticles: Facile synthesis, structural, optical properties and solar cell application," Materials letters, vol. 275, p. 128090, 2020.

[55] M. L. Zeggar, M. Aida, and N. Attaf, "Copper oxide thin films deposition by spray pyrolysis," Journal of New Technology and Materials, vol. 277, pp. 1-3, 2014.

[56] A. Ogwu, T. Darma, and E. Bouquerel, "Electrical resistivity of copper oxide thin films prepared by reactive magnetron sputtering," Journal of achievements in materials and manufacturing engineering, vol. 24, pp. 172-177, 2007.

[57] M. Dhaouadi, M. Jlassi, I. Sta, I. B. Miled, G. Mousdis, M. Kompitsas, and W. Dimassi, "Physical properties of copper oxide thin films prepared by sol–gel spin–coating method," Am. J. Phys. Appl, vol. 6, pp. 43-50, 2018.

[58] S. Roy, A. Bhuiyan, and J. Podder, "Optical and electrical properties of copper oxide thin films synthesized by spray pyrolysis technique," Sensors & Transducers, vol. 191, p. 21, 2015.

[59] J. Tauc, "Optical properties and electronic structure of amorphous Ge and Si," Materials Research Bulletin, vol. 3, pp. 37-46, 1968.

[60] L. Ozawa, Cathodoluminescence and photoluminescence: theories and practical applications vol. 2: CRC Press, 2018.

[61] P. Chand and P. Kumar, "Effect of precursors medium on structural, optical and dielectric properties of CuO nanostructures," Optik, vol. 156, pp. 743-753, 2018.

[62] V. Saravanakannan and T. Radhakrishnan, "Structural, electrical and optical characterization of CuO thin films prepared by spray pyrolysis technique," International Journal of ChemTech Research, vol. 6, pp. 306-310, 2014.

[63] F. Urbach, "The Long-Wavelength Edge of Photographic Sensitivity and of the Electronic Absorption of Solids," Physical Review, vol. 92, p. 1324, 1953.

[64] N. Sharma, K. Prabakar, S. Ilango, S. Dash, and A. Tyagi, "Optical band-gap and associated Urbach energy tails in defected AlN thin films grown by ion beam sputter deposition: Effect of assisted ion energy," Advanced Materials Proceedings, vol. 2, pp. 342-346, 2017.

[65] R. Shabu, A. M. E. Raj, C. Sanjeeviraja, and C. Ravidhas, "Assessment of CuO thin films for its suitablity as window absorbing layer in solar cell fabrications," Materials Research Bulletin, vol. 68, pp. 1-8, 2015.

[66] D. Gopalakrishna, K. Vijayalakshmi, and C. Ravidhas, "Effect of annealing on the properties of nanostructured CuO thin films for enhanced ethanol sensitivity," Ceramics International, vol. 39, pp. 7685-7691, 2013.

[67] H. Touhami, K. Almi, and S. Lakel, "Experimental and theoretical investigation of the effect of alkali (Li, Na and K) doping on the properties of nickel oxide thin films: Comparative study," Main Group Chemistry, pp. 1-15.

[68] G.-D. Sim, J.-H. Park, M. D. Uchic, P. A. Shade, S.-B. Lee, and J. J. Vlassak, "An apparatus for performing microtensile tests at elevated temperatures inside a scanning electron microscope," Acta materialia, vol. 61, pp. 7500-7510, 2013.

[69] F. Bayansal, O. Şahin, and H. Çetinkara, "Mechanical and structural properties of Li-doped CuO thin films deposited by the successive ionic layer adsorption and reaction method," Thin Solid Films, vol. 697, p. 137839, 2020.

[70] A. S. Kumar, K. Perumal, and P. Thirunavukkarasu, "Structural and optical properties of chemically sprayed CuO thin films," Optoelec. Advan. Mater. –Rapid Commun, vol. 4, pp. 831-833, 2010.

[71] S. Shariffudin, S. Khalid, N. Sahat, M. Sarah, and H. Hashim, "Preparation and characterization of nanostructured CuO thin films using sol-gel dip coating," in IOP Conference Series: Materials Science and Engineering, 2015, p. 012007.

[72] N. Raship, M. Sahdan, F. Adriyanto, M. Nurfazliana, and A. Bakri, "Effect of annealing temperature on the properties of copper oxide films prepared by dip coating technique," in AIP Conference Proceedings, 2017.

[73] H. B. Saâd, M. Ajili, S. Dabbabi, and N. T. Kamoun, "Investigation on thickness and annealing effects on physical properties and electrical circuit model of CuO sprayed thin films," Superlattices and Microstructures, vol. 142, p. 106508, 2020.

[74] M. Imran, G. Asghar, G. H. Tariq, A. W. Faridi, S. Bano, M. S. Shifa, and S. Ullah, "Investigation of annealing effects on physical properties of chemically prepared copper oxide thin films," Results in Optics, vol. 10, p. 100331, 2023.

[75] A. López-Suárez and D. R. Acosta, "The Influence of Different Solvents on the Physical Properties of ZnO Thin Films," Journal of Composites Science, vol. 8, p. 332, 2024.

[76] Y. Akaltun, "Effect of thickness on the structural and optical properties of CuO thin films grown by successive ionic layer adsorption and reaction," Thin Solid Films, vol. 594, pp. 30-34, 2015.

[77] S. A. M. H. M. Ali and S. Makki, "The thickness effects characterization properties of copper oxide thin films prepared by thermal evaporation technique," J. Mult. Eng. Sci. Stud., vol. 2, p. 532, 2016.

[78] T. Çayir Taşdemirci, "Copper oxide thin films synthesized by SILAR: role of varying annealing temperature," Electronic Materials Letters, vol. 16, pp. 239-246, 2020.

[79] R. Bekkari, B. Jaber, H. Labrim, M. Ouafi, N. Zayyoun, and L. Laânab, "Effect of Solvents and Stabilizer Molar Ratio on the Growth Orientation of Sol-Gel-Derived ZnO Thin Films," International Journal of Photoenergy, vol. 2019, p. 3164043, 2019.

[80] V. Dhanasekaran and T. Mahalingam, "Physical properties evaluation of various substrates coated cupric oxide thin films by dip method," Journal of alloys and compounds, vol. 539, pp. 50-56, 2012.

[81] K. Khojier, H. Savaloni, and Z. Sadeghi, "A comparative investigation on growth, nanostructure and electrical properties of copper oxide thin films as a function of annealing conditions," Journal of Theoretical and Applied Physics, vol. 8, pp. 1-8, 2014.

[82] M. L. Zeggar, F. Bourfaa, A. Adjimi, F. Boutbakh, M. Aida, and N. Attaf, "CuO thin films deposition by spray pyrolysis: influence of precursor solution properties," International Journal of Mathematical, Computational, Physical, Electrical and Computer Engineering, vol. 9, pp. 610-13, 2015.

[83] S. Shariffudin, S. Khalid, N. Sahat, M. Sarah, and H. Hashim, "Preparation and characterization of nanostructured CuO thin films using sol-gel dip coating," in IOP Conference Series: Materials Science and Engineering, 2015, p. 012007.

[84] H. B. Saâd, M. Ajili, S. Dabbabi, and N. T. Kamoun, "Investigation on thickness and annealing effects on physical properties and electrical circuit model of CuO sprayed thin films," Superlattices and Microstructures, vol. 142, p. 106508, 2020.

[85] K. Kamli, Z. Hadef, B. Chouial, and B. Hadjoudja, "Thickness effect on electrical properties of copper oxide thin films," Surface Engineering, vol. 35, pp. 86-90, 2019.

[86] R. P. Wijesundera, M. Hidaka, K. Koga, J.-Y. Choi, and N. E. Sung, "Structural and electronic properties of electrodeposited heterojunction of CuO/Cu 2 O," Ceramics-silikàty, vol. 54, pp. 19-25, 2010.

[87] S. Masudy-Panah, G. K. Dalapati, K. Radhakrishnan, A. Kumar, H. R. Tan, E. Naveen Kumar, C. Vijila, C. C. Tan, and D. Chi, "p-CuO/n-Si heterojunction solar cells with high open circuit voltage and photocurrent through interfacial engineering," Progress in Photovoltaics: Research and Applications, vol. 23, pp. 637-645, 2015.

[88] E. Omayio, P. Karimi, W. Njoroge, and F. Mugwanga, "Current-voltage characteristics of p-CuO/n-ZnO: Sn Solar cell," Int. J. Thin Film Sci. Tec, vol. 2, pp. 25-28, 2013.

[89] T. Oku, R. Motoyoshi, K. Fujimoto, T. Akiyama, B. Jeyadevan, and J. Cuya, "Structures and photovoltaic properties of copper oxides/fullerene solar cells," Journal of Physics and Chemistry of Solids, vol. 72, pp. 1206-1211, 2011.

[90] A. Rydosz, "The use of copper oxide thin films in gas-sensing applications," Coatings, vol. 8, p. 425, 2018.

[91] D. N. Oosthuizen, D. E. Motaung, and H. Swart, "In depth study on the notable room-temperature NO2 gas sensor based on CuO nanoplatelets prepared by sonochemical method: Comparison of various bases," Sensors and Actuators B: Chemical, vol. 266, pp. 761-772, 2018.

[92] X. Hu, Z. Zhu, C. Chen, T. Wen, X. Zhao, and L. Xie, "Highly sensitive H2S gas sensors based on Pd-doped CuO nanoflowers with low operating temperature," Sensors and Actuators B: Chemical, vol. 253, pp. 809-817, 2017.

[93] J.-H. Lee, J.-H. Kim, and S. S. Kim, "CuO–TiO2 p–n core–shell nanowires: Sensing mechanism and p/n sensing-type transition," Applied Surface Science, vol. 448, pp. 489-497, 2018.

[94] A. Umar, J.-H. Lee, R. Kumar, O. Al-Dossary, A. A. Ibrahim, and S. Baskoutas, "Development of highly sensitive and selective ethanol sensor based on lance-shaped CuO nanostructures," Materials & Design, vol. 105, pp. 16-24, 2016.

[95] D. Ju, H. Xu, Z. Qiu, J. Guo, J. Zhang, and B. Cao, "Highly sensitive and selective triethylamine-sensing properties of nanosheets directly grown on ceramic tube by forming NiO/ZnO PN heterojunction," Sensors and Actuators B: Chemical, vol. 200, pp. 288-296, 2014.

[96] M. R. Hoffmann, S. T. Martin, W. Choi, and D. W. Bahnemann, "Environmental applications of semiconductor photocatalysis," Chemical reviews, vol. 95, pp. 69-96, 1995.

[97] C. Guillard, B. Kartheuser, and S. Lacombe, "La photocatalyse : dépollution de l'eau ou de l'air et matériaux autonettoyants," Tech. Ing. Génie Procédés Prot. Environ, 2011.

[98] T. V. Thi, A. K. Rai, J. Gim, and J. Kim, "Potassium-doped copper oxide nanoparticles synthesized by a solvothermal method as an anode material for high-performance lithium-ion secondary battery," Applied surface science, vol. 305, pp. 617-625, 2014.

[99] V. Andrei, K. Bethke, and K. Rademann, "Adjusting the thermoelectric properties of copper (i) oxide–graphite–polymer pastes and the applications of such flexible composites," Physical Chemistry Chemical Physics, vol. 18, pp. 10700-10707, 2016.

Chapter 2. Experimental Procedure and Characterization Methods

2.1 Introduction

The success of any experimental investigation in materials science depends critically on the careful selection and execution of the deposition method, as well as the appropriate use of characterization techniques. The properties of thin films, particularly their structural, optical, and electrical characteristics, are highly sensitive to the experimental conditions during synthesis [1].

This chapter describes in detail the experimental methodology adopted for the preparation of copper oxide (CuO) thin films of different thicknesses, as well as the characterization techniques used to investigate their structural, optical, and electrical properties. The CuO thin films were prepared using the sol-gel spin coating technique, which has been chosen for its simplicity, low cost, excellent thickness control, and the high homogeneity of the produced films [2, 3].

The chapter is organized as follows:

- **Section 2.2** introduces the fundamental principles of the sol-gel process.
- **Section 2.3** describes the spin coating technique and the parameters that influence film deposition.
- **Section 2.4** details the experimental procedure used in this work, including substrate preparation, solution preparation, and film deposition.
- **Section 2.5** presents the characterization techniques: thickness measurement, X-ray diffraction (XRD), UV-Visible spectroscopy, and the four-point probe method.
- **Section 2.6** concludes the chapter.

2.2 The Sol-Gel Process

2.2.1 Definition and Principles

The sol-gel process is a wet chemistry method widely used for the synthesis of inorganic materials, including oxides, glasses, and ceramics. It involves the transition of a liquid solution (the sol) into a solid network (the gel) through hydrolysis and polycondensation reactions [4].

A **sol** is a colloidal suspension of solid particles (typically 1 to 100 nm in size) dispersed in a liquid. A **gel** is a three-dimensional solid network formed from the sol, containing trapped solvent in its pores [5].

The sol-gel method has been used since the mid-19th century, but it gained significant importance in the second half of the 20th century due to its versatility for the synthesis of a wide variety of materials at low temperatures [6].

2.2.2 Advantages of the Sol-Gel Process

The sol-gel process offers many advantages compared to other synthesis methods [7]:

1. **Simplicity:** does not require complex or expensive equipment.
2. **Low cost:** uses inexpensive precursors and operates at low temperatures.
3. **High homogeneity:** allows mixing at the molecular level.
4. **Composition control:** allows the synthesis of complex compounds with precise stoichiometry.
5. **Easy doping:** the addition of dopants is simple and uniform.
6. **Versatility of forms:** allows obtaining films, fibers, powders, monoliths, and aerogels.
7. **Low processing temperatures:** generally, less than 1000 °C.
8. **Coating of complex shapes:** suitable for substrates of various geometries [8].

2.2.3 Stages of the Sol-Gel Process

The sol-gel process generally proceeds in four main stages:

a) Hydrolysis

The metal alkoxide precursor $M(OR)_n$ reacts with water to form hydroxyl groups (M-OH) [9]:

$$\text{M-(OR)}_n + \text{H}_2\text{O} \rightarrow \text{HO-M-(OR)}_{n-1} + \text{R-OH}$$

This is a nucleophilic substitution reaction that introduces -OH groups into the precursor.

b) Condensation

The -OH groups formed during hydrolysis can react in two ways:

Alcoxolation:

$$(\mathrm{RO})_{n-1}\text{-M-OH} + \text{RO-M-}(\mathrm{OR})_{n-1} \rightarrow (\mathrm{RO})_{n-1}\text{-M-O-M-}(\mathrm{OR})_{n-1} + \text{R-OH}$$

Oxolation:

$$(\mathrm{RO})_{n-1}\text{-M-OH} + \text{HO-M-}(\mathrm{OR})_{n-1} \rightarrow (\mathrm{RO})_{n-1}\text{-M-O-M-}(\mathrm{OR})_{n-1} + \mathrm{H_2O}$$

These reactions form M-O-M bonds, leading to the formation of an inorganic three-dimensional network [10].

c) Aging

During aging, the polycondensation reactions continue, the sol becomes more viscous, and the gel structure is gradually reinforced. Phenomena such as syneresis (expulsion of solvent) and Ostwald ripening can also occur [11].

d) Drying and Annealing

The final stage involves removing the solvent (drying) and crystallizing the material (annealing). The annealing temperature determines the crystalline phase obtained and influences the microstructure of the final material [12].

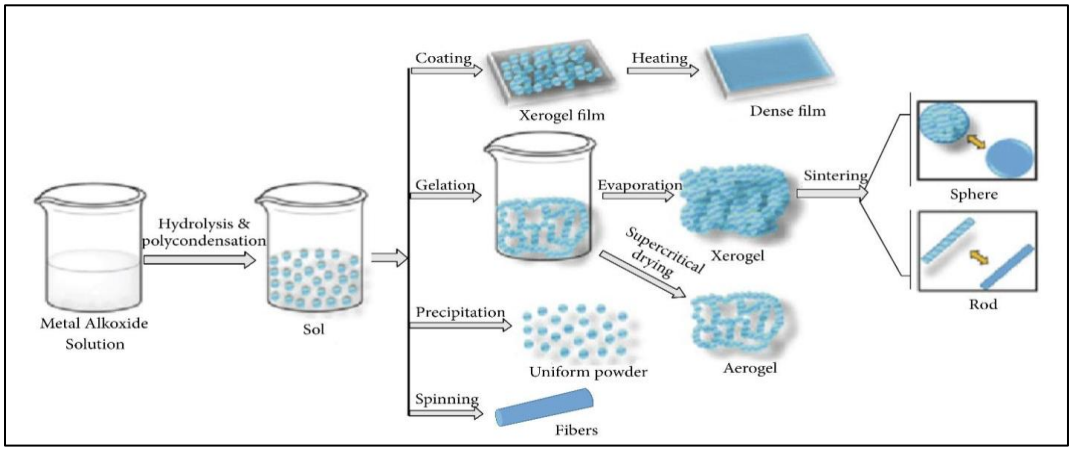

Figure 2. 1 Schematic overview of the sol-gel process and the various products that can be obtained.

2.2.4 Parameters Influencing the Sol-Gel Process

Several parameters influence the kinetics and final result of the sol-gel process:

1. **Nature and concentration of the precursor:** Determines the chemical reactivity and final composition.
2. **Type of solvent:** Affects the viscosity, evaporation rate, and reaction rate.
3. **Water content (hydrolysis ratio):** Controls the rate of hydrolysis and condensation.
4. **pH and use of catalysts:** Acidic catalysts favor hydrolysis, basic catalysts favor condensation.
5. **Temperature:** Affects the reaction rate and stability of the sol.
6. **Aging time:** Influences the structure of the final gel [13, 14].

2.2.5 Use of Stabilizers and Additives

To prevent precipitation and stabilize the sol, stabilizing agents are often added. The most commonly used stabilizers for the synthesis of CuO are:

- **Monoethanolamine (MEA, $HOCH_2CH_2NH_2$):** the most common, used in this work.
- **Diethanolamine (DEA):** $((HOCH_2CH_2)_2NH)$.
- **Triethanolamine (TEA):** $((HOCH_2CH_2)_3N)$.
- **Acetic acid (CH_3COOH):** used as an acidic catalyst.
- **Lactic acid ($CH_3CHOHCOOH$):** to control viscosity [15, 16].

These additives play a crucial role in the formation of stable solutions and in obtaining high-quality films.

2.3 The Spin Coating Technique

2.3.1 Principle

Spin coating is one of the most widely used techniques for depositing thin films from a solution. It consists of depositing a few drops of solution at the center of a substrate that is then rotated at high speed. The centrifugal force spreads the solution uniformly over the surface, while the volatile solvent evaporates, leaving a thin film [17].

This technique is particularly suitable for flat substrates of small size (a few cm^2) and allows the deposition of films with thicknesses ranging from a few nanometers to several micrometers [18].

2.3.2 The Four Stages of Spin Coating

The spin coating process can be divided into four well-defined stages [19]:

1. **Deposition:** A controlled volume of solution (typically 0.1 to 1 mL) is dispensed at the center of the substrate, either before or during the start of rotation.
2. **Spin-up (acceleration):** The substrate is accelerated to the desired rotation speed. Centrifugal force begins to spread the liquid radially outward from the center.
3. **Spin-off (steady state):** The substrate rotates at a constant angular velocity. Excess liquid is ejected from the edges of the substrate in the form of droplets. The film thickness decreases due to the centrifugal effect.
4. **Evaporation:** The solvent evaporates progressively, increasing the viscosity of the film and stabilizing its final thickness.

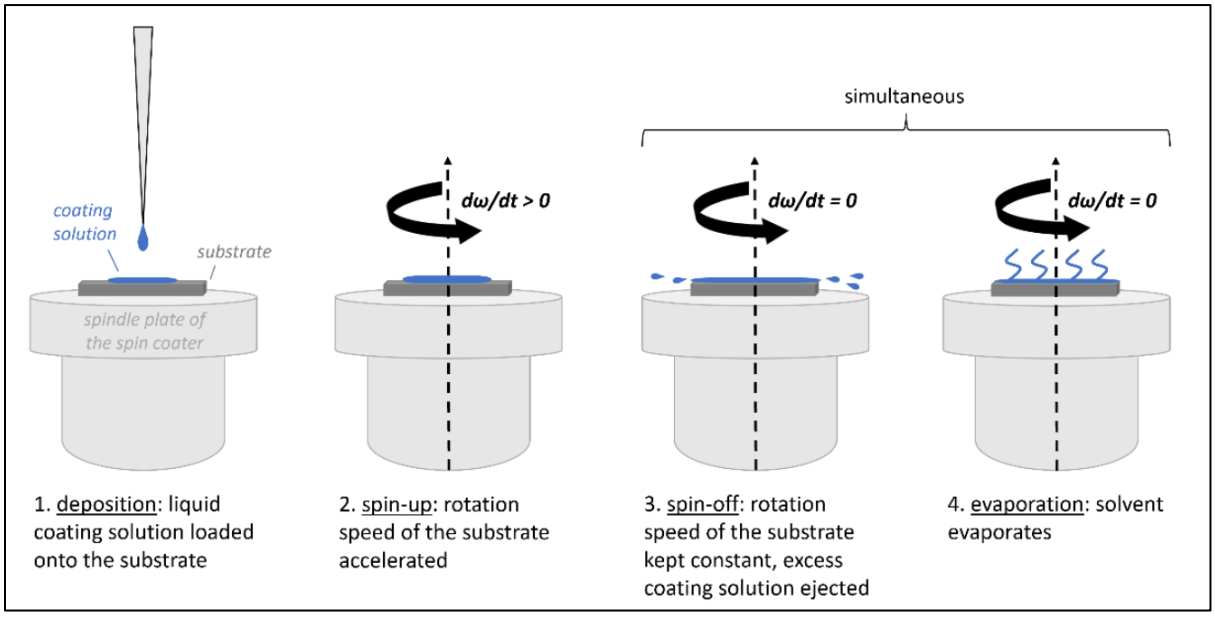

Figure 2. 2 The four stages of the spin coating procedure: deposition, spin-up, spin-off, and evaporation.

2.3.3 Parameters Influencing the Spin Coating Process

a) Rotation Speed

The rotation speed is the most important parameter that controls the final film thickness. According to Meyerhofer's theory, the film thickness h is given by [20]:

$$h \propto \omega^{-1/2}$$

where ω is the angular velocity. Therefore, increasing the rotation speed leads to thinner films. However, an excessively high speed can cause defects such as cracks and irregularities [21].

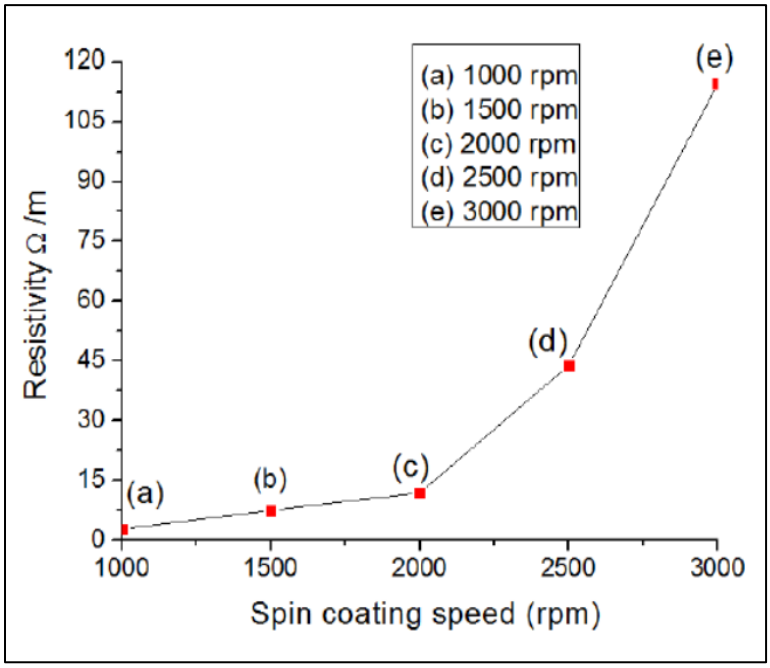

Figure 2. 3 Variation of the resistivity of CuO films as a function of spin coating speed.

b) Rotation Time

The rotation time must be sufficient to allow the spin-off phase and partial evaporation of the solvent. Generally, durations of 20 to 60 seconds are sufficient. Beyond a critical time, the influence of duration becomes negligible [22].

c) Solution Viscosity

The viscosity of the solution influences the kinetics of spreading and the final thickness. More viscous solutions produce thicker films because they resist centrifugal force more effectively. However, very high viscosity can lead to non-uniform films [23].

d) Solvent Volatility

The evaporation rate of the solvent influences the kinetics of film formation. More volatile solvents produce films faster, but can lead to more porous structures. Less volatile solvents allow better organization of the molecules, leading to better crystallinity [24].

e) Solute Concentration

A **higher concentration** generally leads to thicker films. The relationship between concentration and thickness is approximately linear in the dilute regime [25].

f) Substrate Temperature

Substrate preheating can influence the evaporation rate and adhesion of the film. A moderately heated substrate (50–100 °C) reduces the drying time and improves uniformity [26].

2.3.4 Advantages and Disadvantages of Spin Coating

Advantages :

- Simple and inexpensive technique.
- Excellent reproducibility.
- Excellent thickness control.
- Films of high uniformity.
- Suitable for organic, inorganic, and hybrid solutions.

Disadvantages :

- Limited to flat substrates of small size.
- Significant material waste (more than 90% of the solution is ejected).
- Less suitable for large-scale industrial production [27, 28].

2.4 Experimental Procedure for the Preparation of CuO Films

This section describes in detail the experimental procedure followed for the preparation of CuO thin films of different thicknesses, prepared by the sol-gel spin coating method.

2.4.1 Materials and Reagents Used

The reagents used in this work are listed in Table 2.1.

Table 2. 1 Reagents used for the preparation of CuO thin films.

Reagent	Chemical formula	Role	Purity
Copper acetate monohydrate	$Cu(CH_3COO)_2 \cdot H_2O$	Precursor of Cu^{2+}	≥ 99%
Ethanol	C_2H_5OH	Solvent	≥ 99.5%
Monoethanolamine (MEA)	$HOCH_2CH_2NH_2$	Stabilizer	≥ 99%
Distilled water	H_2O	Cleaning	—
Methanol	CH_3OH	Cleaning	≥ 99%

2.4.2 Substrate Preparation

The substrates used are standard glass slides with dimensions 75 × 25 × 1 mm^3. The cleaning procedure for the substrates is critical to ensure good adhesion and uniformity of the films. The procedure adopted is as follows:

1. **First cleaning in methanol:** The slides are immersed in methanol and ultrasonically cleaned for 10 minutes. This step is repeated three times to remove organic contamination (greases, oils, fingerprints).
2. **Second cleaning in distilled water:** The slides are then immersed in distilled water and ultrasonically cleaned for 10 minutes. This step is also repeated three times to remove residues of methanol and inorganic impurities.
3. **Drying:** The substrates are dried with a hot air dryer or under a flow of dry nitrogen.
4. **Storage:** The cleaned substrates are stored in a closed Petri dish until use.

The cleanliness of the substrate has a major impact on film adhesion and uniformity. Any contamination can cause defects such as bubbles, holes, or dewetting [29].

2.4.3 Solution Preparation

The CuO precursor solution was prepared according to the following procedure:

1. **Weighing the precursor:** A precise quantity of copper acetate monohydrate ($Cu(CH_3COO)_2 \cdot H_2O$) is weighed using a precision balance to obtain a final concentration of **0.5 M** in ethanol.
2. **Dissolution:** The copper acetate is dissolved in 50 mL of absolute ethanol under continuous magnetic stirring at room temperature.
3. **Addition of the stabilizer:** Monoethanolamine (MEA) is added drop by drop with a molar ratio of MEA/Cu = 1. MEA acts as both a stabilizer and a complexing agent, preventing the precipitation of copper hydroxide and forming a stable complex with Cu^{2+} ions.
4. **Stirring and heating:** The solution is stirred at 60 °C for 2 hours to ensure complete dissolution and the formation of a homogeneous complex. The color of the solution changes from light blue to deep blue, indicating the formation of the Cu-MEA complex.
5. **Aging:** After stirring, the solution is left to age at room temperature for 24 hours to allow the polycondensation reactions to stabilize.

The reaction mechanism of formation of CuO from copper acetate and ethanol can be schematized as follows [30]:

$$Cu(CH_3COO)_2 \cdot H_2O + C_2H_5OH \rightarrow CuO + CH_3COCH_3 + CO_2 \uparrow + H_2O \uparrow + CH_3CHO \uparrow$$

This thermal decomposition reaction occurs during the annealing of the films.

2.4.4 Film Deposition by Spin Coating

The deposition of CuO films was carried out according to the following procedure:

1. **Mounting the substrate:** The clean substrate is placed at the center of the spin coater chuck and held by vacuum suction.
2. **Deposition of the solution:** Approximately 0.5 mL of the prepared solution is dispensed at the center of the substrate using a micropipette.

3. **Spin coating:** The substrate is rotated at 3000 rpm for 30 seconds. This speed was chosen to obtain a film of optimal uniform thickness.
4. **Preheating:** After deposition of each layer, the film is preheated in a furnace at 250 °C for 15 minutes to evaporate the solvent and remove organic residues. This step is essential to obtain a stable layer before depositing the next layer.
5. **Repetition for thickness variation:** Steps 2 to 4 are repeated to vary the number of layers and consequently the film thickness:
    - **Sample S1 :** 6 layers
    - **Sample S2 :** 9 layers
    - **Sample S3 :** 12 layers
6. **Final annealing:** After deposition of all layers, the films are annealed at 500 °C for 2 hours in air to obtain the final crystalline CuO phase.

Table 2. 2 Deposition parameters of the prepared CuO thin films.

Parameter	Value
Substrate	Glass (75 × 25 × 1 mm^3)
Precursor	Copper acetate monohydrate
Solvent	Ethanol
Stabilizer	Monoethanolamine (MEA)
Concentration	0.5 M
MEA/Cu molar ratio	1
Stirring temperature	60 °C
Stirring time	2 hours
Aging time	24 hours
Volume per layer	0.5 mL
Spin speed	3000 rpm
Spin time	30 s
Preheating temperature	250 °C
Preheating time	15 min
Final annealing temperature	500 °C
Final annealing time	2 hours

Number of layers	6, 9, and 12

Table 2. 3 Identification of the prepared samples.

Sample	Number of layers	Estimated thickness	Description
S1	6	~200 nm	Thin film
S2	9	~420 nm	Medium film
S3	12	~940 nm	Thick film

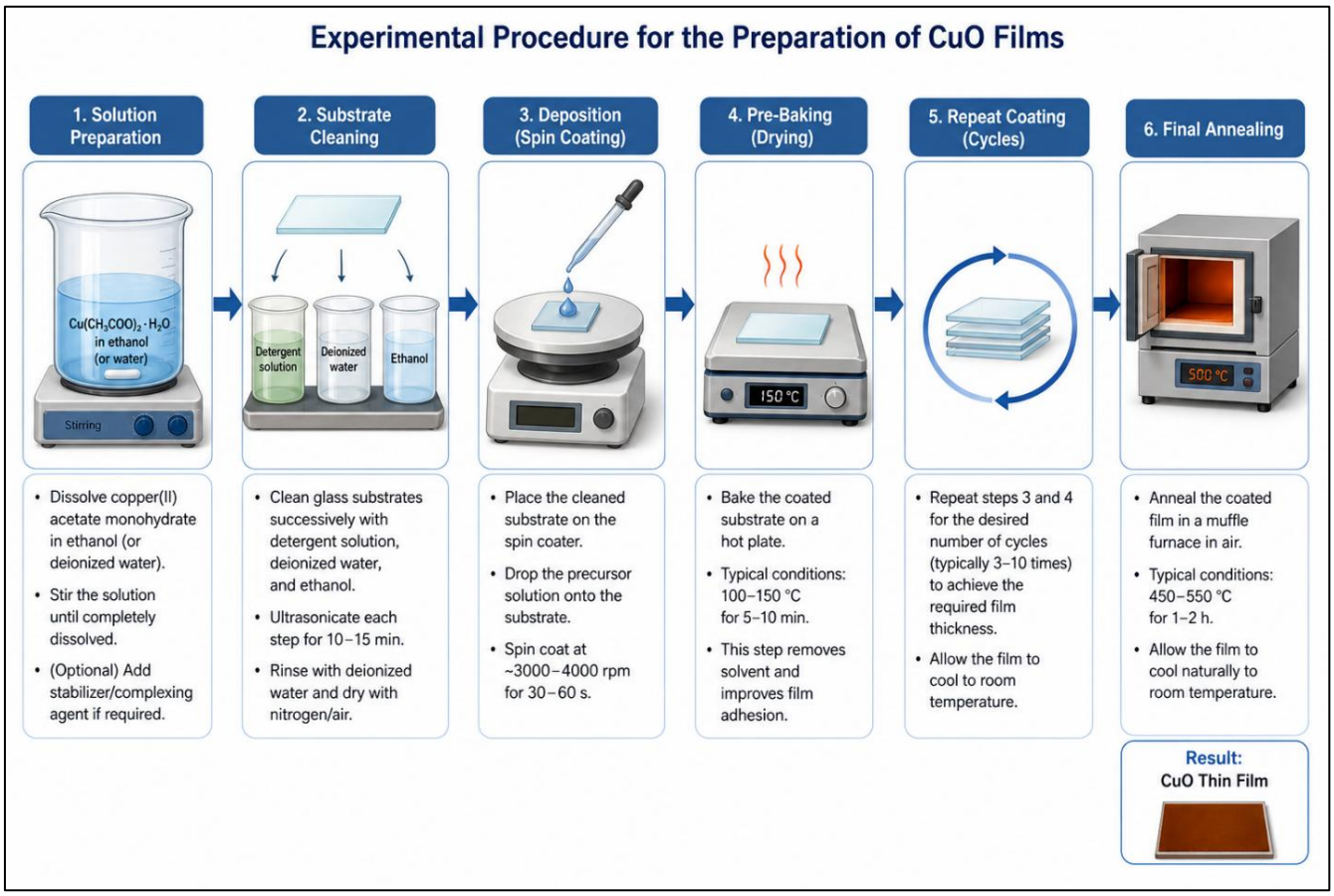

Figure 2. 4 Schematic flowchart of the experimental procedure for the preparation of CuO films, from solution preparation to final annealing.

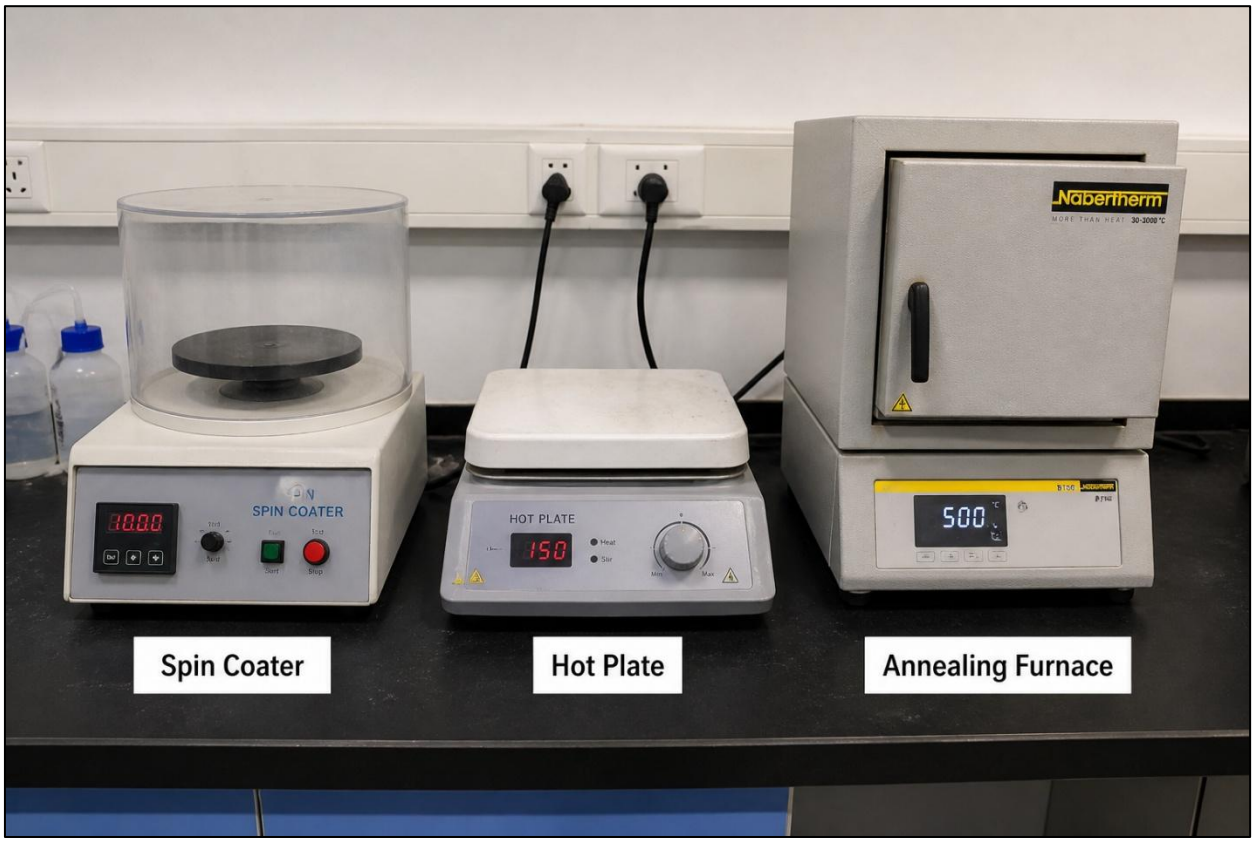

Figure 2. 5 Photo of the experimental setup including the spin coater, hot plate, and annealing furnace.

2.5 Characterization Methods

After deposition, the films were characterized using several complementary techniques to study their thickness, structure, optical properties, and electrical properties.

2.5.1 Thickness Measurement

The thickness of the films is a critical parameter, particularly in this study which focuses on the effect of thickness. Several methods exist for measuring film thickness:

- **Mechanical profilometry**
- **Scanning electron microscopy (SEM) cross-section**
- **Spectroscopic ellipsometry**
- **Mass difference method**

In this work, we used the mass difference method, which is simple and accurate enough for our needs [31]. The procedure is as follows:

1. The mass of the bare substrate is measured (m_1) using a precision balance (precision ± 0.1 mg).
2. After film deposition and final annealing, the total mass (m_2) is measured.
3. The mass of the deposited film is calculated as $\Delta m = m_2 - m_1$.
4. The film thickness t is calculated using:

$$t = \frac{\Delta m}{\rho \cdot A}$$

where:

- ρ is the density of CuO (6.32 g/cm³) [32]
- A is the area of the deposited film (typically 75 × 25 = 1875 mm² = 18.75 cm²)

This method assumes that the film has a uniform density equal to that of bulk CuO, which is a reasonable approximation for well-crystallized films [33].

2.5.2 X-Ray Diffraction (XRD)

2.5.2.1. Principle

X-ray diffraction (XRD) is a non-destructive characterization technique that allows the determination of the crystalline structure, phase identification, lattice parameters, crystallite size, and lattice strains in materials [34].

When an X-ray beam encounters a crystal, the X-rays are diffracted by the crystallographic planes according to Bragg's law:

$$2d_{hkl}\sin\,\theta = n\lambda$$

where:

- d_hkl is the interplanar distance for the (hkl) planes

- θ is the angle of incidence (Bragg angle)
- n is the order of diffraction (usually 1)
- λ is the wavelength of the X-rays

When this condition is satisfied, constructive interference occurs and gives rise to a peak in the diffraction pattern [35].

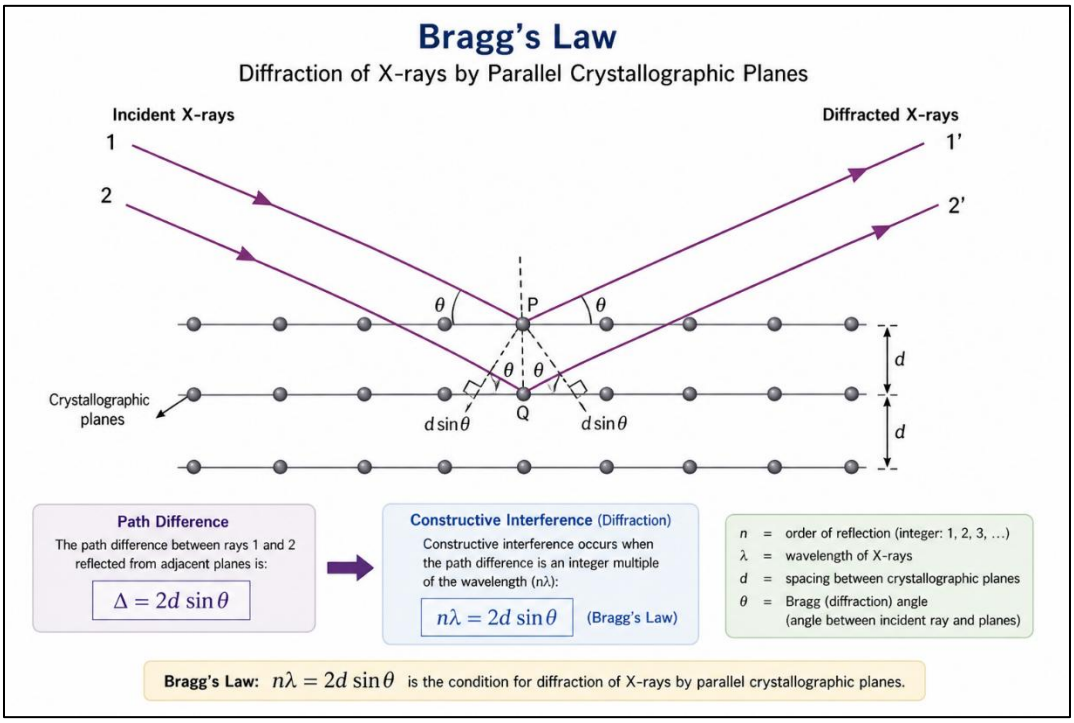

Figure 2. 6 Schematic illustration of Bragg's law showing the diffraction of X-rays by parallel crystallographic planes.

2.5.2.2. Diffractometer Used

The XRD measurements were carried out using a Bruker D8 Advance diffractometer with the following parameters:

- **X-ray source:** Cu-Kα anticathode (λ = 0.154 nm)
- **Voltage and current:** 40 kV and 40 mA
- **Geometry:** Bragg-Brentano θ-2θ
- **Scan range :** $30° \leq 2\theta \leq 80°$
- **Step size :** 0.02°

- **Counting time :** 1 s/step

The diffractometer is controlled by the Diffrac Plus XRD Commander software. Data analysis is performed with the EVA software, which allows phase identification by comparison with the JCPDS (Joint Committee on Powder Diffraction Standards) database [36].

2.5.2.3. Information Extracted from XRD Patterns

Several types of information can be extracted from XRD patterns:

a) Phase identification: The position (2θ) and relative intensity of the peaks are compared with reference patterns (JCPDS cards) to identify the present crystalline phases. For CuO, the reference is JCPDS card No. 98-004-3179.

b) Crystallite size (D): Calculated from the Scherrer formula [37]:

$$D = \frac{0.9 \cdot \lambda}{\beta \cos\ \theta}$$

where β is the full width at half maximum (FWHM) of the peak in radians, after correction for instrumental broadening.

c) Lattice parameters: For the monoclinic structure of CuO, the lattice parameters a, b, c, and β are calculated using the relation:

$$\frac{1}{d_{hkl}^2} = \frac{1}{\sin^2 \beta}\left(\frac{h^2}{a^2} + \frac{k^2 \sin^2 \beta}{b^2} + \frac{l^2}{c^2} - \frac{2hl\cos\ \beta}{ac}\right)$$

d) Lattice strain (ε): Calculated from [38]:

$$\varepsilon = \frac{\beta}{4\tan\ \theta}$$

e) Dislocation density (δ): Calculated by the Williamson-Smallman method [39]:

$$\delta = \frac{1}{D^2}$$

This parameter represents the number of dislocation lines per unit area and is a measure of the crystalline defects in the film.

Figure 2. 7 Photo of the Bruker D8 Advance diffractometer used in this work.

2.5.3 UV-Visible Spectroscopy

2.5.3.1. Principle

UV-Visible spectroscopy is a non-destructive optical characterization technique that measures the transmittance, reflectance, and absorbance of materials in the ultraviolet (200-400 nm), visible (400-800 nm), and near-infrared (800-2500 nm) regions of the electromagnetic spectrum [40].

When light of intensity I_0 is incident on a thin film of thickness d, part of it is absorbed by the material, part is reflected, and part is transmitted. The transmittance is defined as :

$$T = \frac{I_t}{I_0}$$

where It is the intensity of the transmitted light.

UV-Visible spectroscopy provides essential information on :

- The optical band gap (Eg)
- The Urbach energy (Eu)
- The absorption coefficient (α)
- The refractive index (n)
- The film thickness (in some cases)
- Defects and impurities [41].

2.5.3.2. Spectrophotometer Used

The optical measurements were performed using a dual-beam UV-Vis-NIR spectrophotometer in the wavelength range of 300 to 1100 nm. The instrument consists of :

- Two light sources: a deuterium lamp for UV and a tungsten-halogen lamp for the visible/NIR.
- A monochromator (diffraction grating) to select specific wavelengths.
- A sample compartment with a sample channel and a reference channel.
- Detectors (typically photomultipliers and photodiodes).

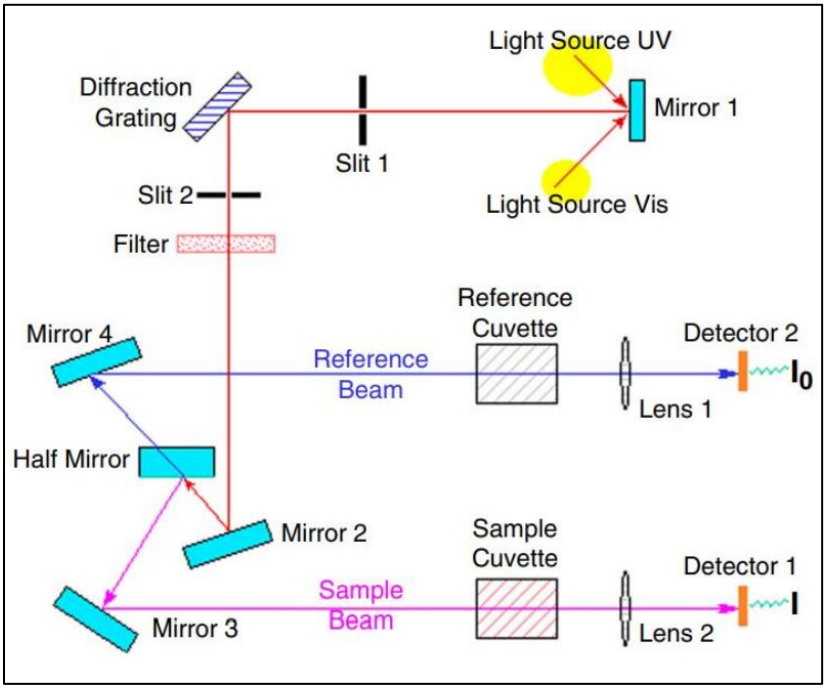

Figure 2. 8 Schematic diagram of a dual-beam UV-Visible spectrophotometer.

2.5.3.3. Calculation of Optical Parameters

a) Absorption coefficient (α):

The absorption coefficient is calculated from the transmittance using the Beer-Lambert law [42]:

$$T = e^{-\alpha d}$$

$$\alpha = \frac{1}{d}\ln\left(\frac{1}{T}\right) = \frac{2.303A}{d}$$

where A is the absorbance and d are the film thickness.

b) Extinction coefficient (k) :

$$k = \frac{\alpha\lambda}{4\pi}$$

where λ is the wavelength.

c) Optical band gap (Eg):

The optical band gap is determined using the Tauc relation [43]:

$$(\alpha h\nu)^n = A(h\nu - E_g)$$

The exponent n depends on the type of optical transition:

- n = 2 for direct allowed transitions
- n = 1/2 for indirect allowed transitions
- n = 2/3 for direct forbidden transitions
- n = 1/3 for indirect forbidden transitions

For CuO, which has a direct band gap, n = 2. The band gap is determined by plotting $(\alpha h\nu)^2$ vs. hν and extrapolating the linear part of the curve to the energy axis.

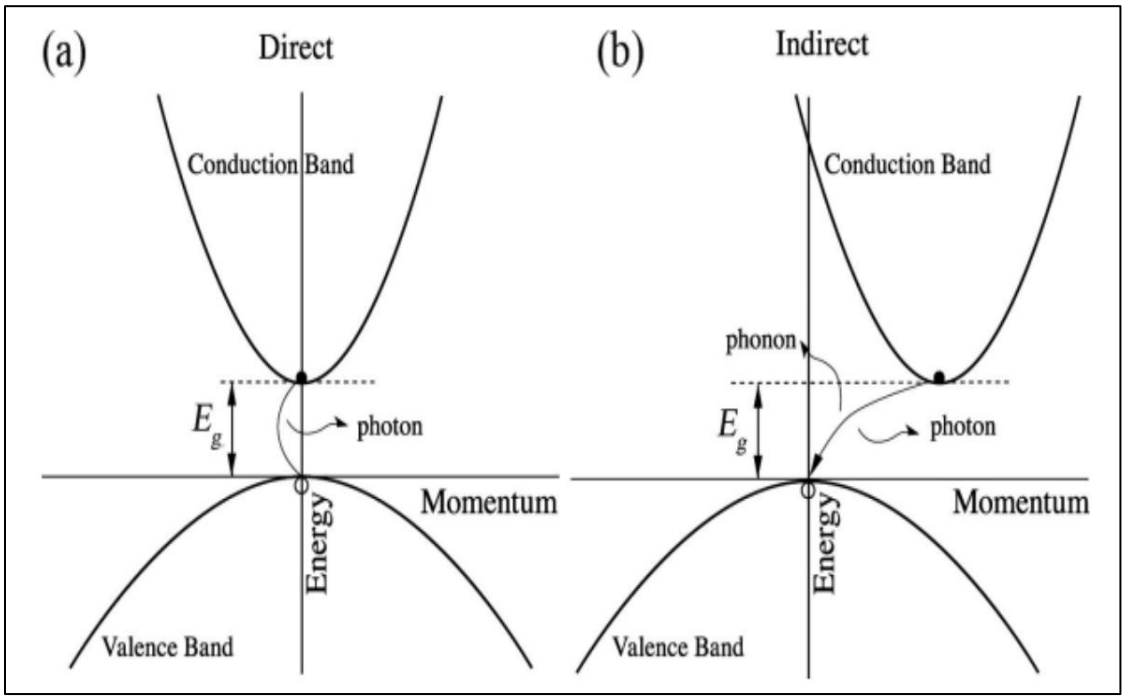

Figure 2. 9 E-K diagram showing direct band and indirect band transitions.

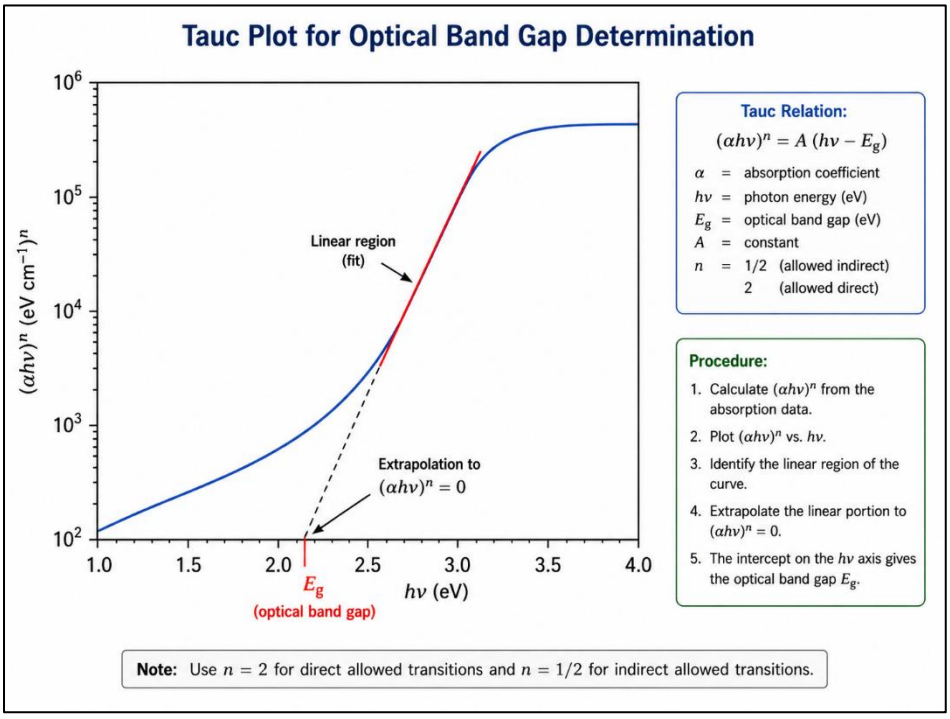

Figure 2. 10 Typical Tauc plot used to determine the optical band gap, with extrapolation of the linear part.

d) Urbach energy (Eu):

The Urbach energy characterizes the disorder in the film and is defined by the Urbach law [44]:

$$\alpha = \alpha_0 \exp\left(\frac{h\nu}{E_u}\right)$$

By plotting ln(α) as a function of hν, a straight line is obtained whose slope is 1/Eu:

$$E_u = \left[\frac{d(\ln\ \alpha)}{d(h\nu)}\right]^{-1}$$

A higher Urbach energy indicates a higher density of defects and disorder in the film, leading to a more pronounced absorption tail near the band edges.

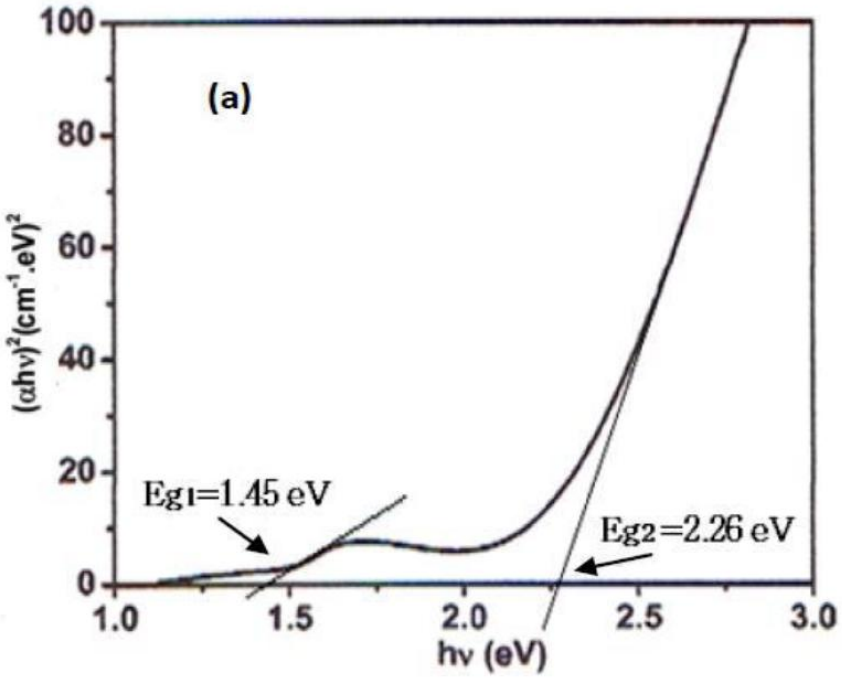

Figure 2. 11 Schematic representation of optical transitions: Tauc region (band-to-band transitions), Urbach region (transitions involving localized states), and weak absorption tail.

2.5.4 Four-Point Probe Method

2.5.4.1. Principle

The four-point probe method is the standard technique for measuring the electrical resistivity of thin films. It uses four equally spaced metal probes aligned and pressed against the film surface. A current I is applied between the two outer probes, while the voltage V is measured between the two inner probes [45].

The advantage of this method over the simpler two-point measurement is that it eliminates the contribution of the contact resistance between the probes and the film, providing an accurate measurement of the resistivity of the film itself [46].

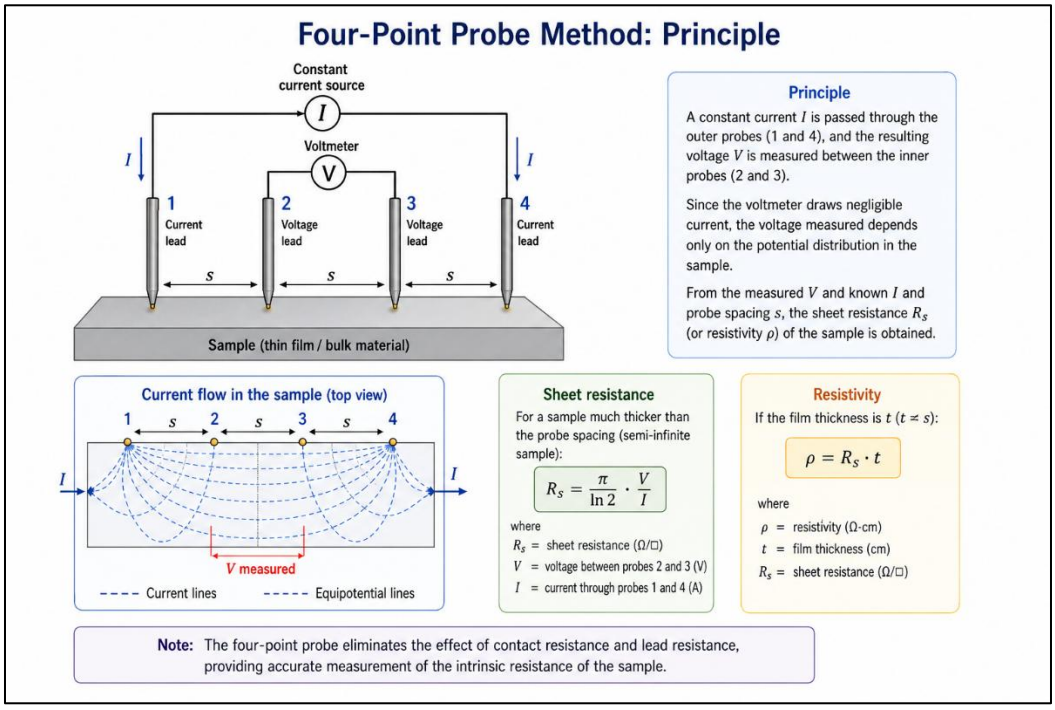

Figure 2. 12 Schematic diagram of the principle of the four-point probe method.

2.5.4.2. Calculation of Resistivity

For a thin film deposited on an insulating substrate, where the film thickness d is much smaller than the spacing between the probes (d << s), the sheet resistance Rs is given by [47]:

$$R_s = \frac{\pi}{\ln 2} \cdot \frac{V}{I} = 4.532 \cdot \frac{V}{I}$$

The electrical resistivity ρ is then calculated by:

$$\rho = R_s \cdot d$$

The electrical conductivity σ is the inverse of the resistivity:

$$\sigma = \frac{1}{\rho}$$

2.5.4.3. Equipment Used

The electrical measurements were performed using a Keysight B1500A semiconductor device analyzer with a four-point probe at room temperature. The applied voltage was varied to obtain the I-V characteristic, from which the resistance and consequently the resistivity were calculated.

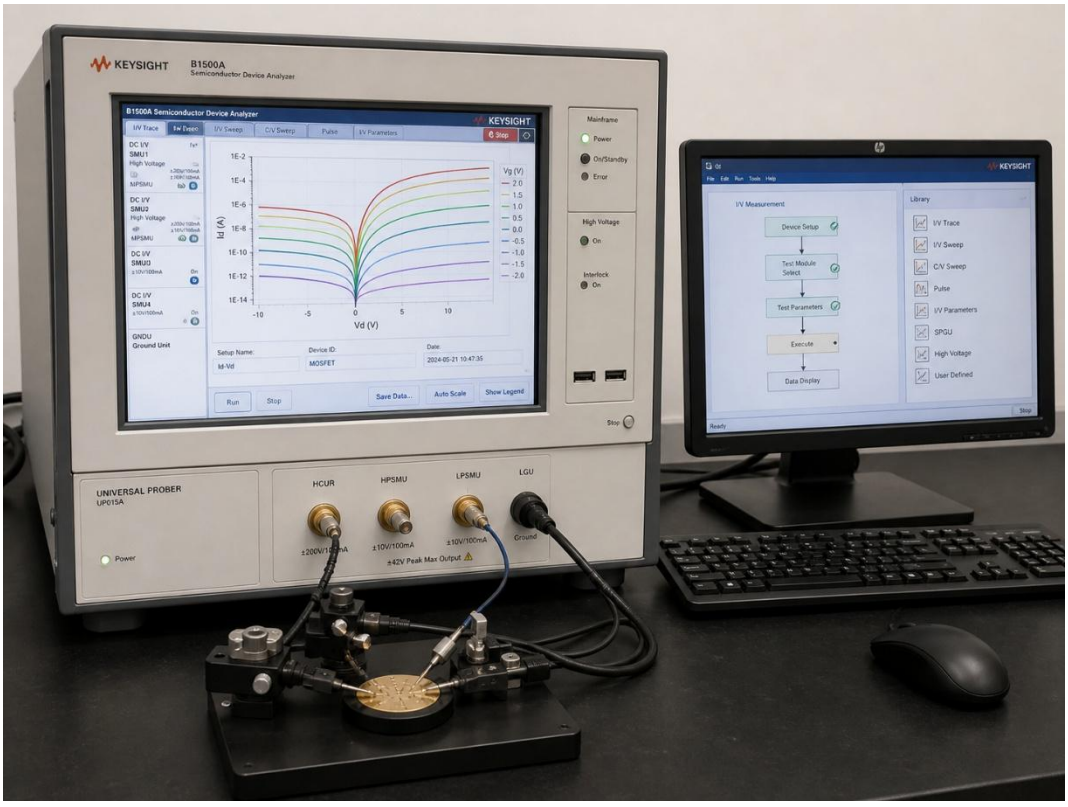

Figure 2. 13 Photo of the Keysight B1500A semiconductor analyzer used for electrical measurements.

2.5.4.4. Sources of Error and Precautions

To obtain accurate measurements, several precautions must be taken [48]:

1. **Probe contact:** Ensure good contact between the probes and the film without damaging the surface.
2. **Geometry:** Verify that the film dimensions are large enough relative to the probe spacing to avoid edge effects.
3. **Temperature:** Perform measurements at a controlled temperature (room temperature in this case).
4. **Repeatability:** Make several measurements at different positions and calculate the average.
5. **Substrate:** Verify that the substrate is sufficiently insulating to not influence the measurement.

2.6 Summary of the Experimental Workflow

To summarize, the experimental workflow used in this study can be schematized as follows:

Glass substrate cleaning

↓

Solution preparation (Cu acetate + EtOH + MEA)

↓

Aging (24 h)

↓

Spin coating (3000 rpm, 30 s)

↓

Preheating (250 °C, 15 min)

↓

Repeat for desired number of layers (6, 9, or 12)

↓

Final annealing (500 °C, 2 h)

↓

Characterization

├──→ *Thickness (mass difference)*

├──→ *Structural (XRD)*

├──→ *Optical (UV-Vis)*

└──→ *Electrical (4-point probe)*

Experimental Procedure Flowchart

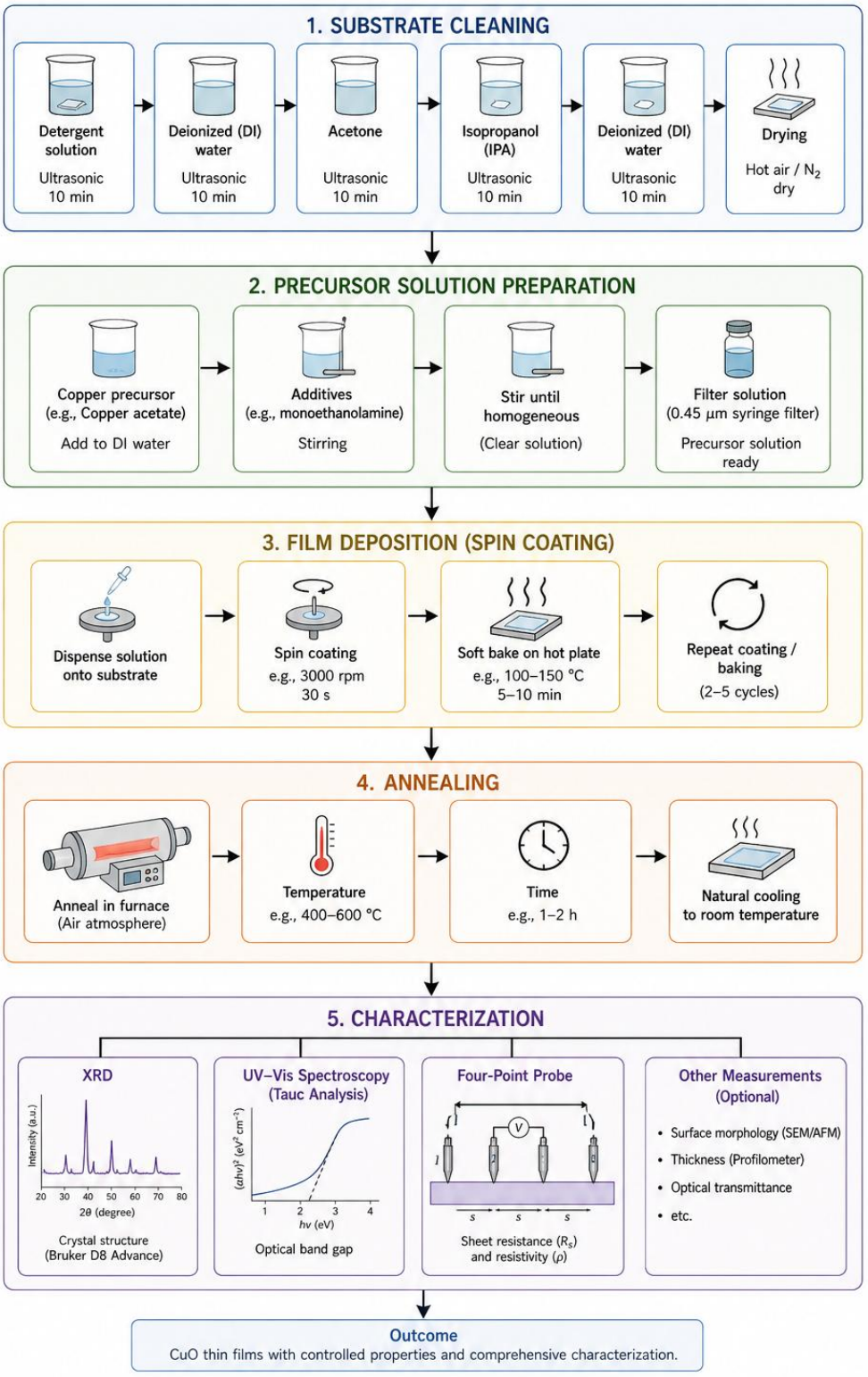

Figure 2. 14 Schematic flowchart of the complete experimental procedure, from substrate cleaning to characterization.

2.7 Conclusion

This chapter has presented in detail the experimental procedure adopted for the preparation of CuO thin films of different thicknesses by the sol-gel spin coating method, as well as the characterization techniques used to investigate the obtained films.

The main points to remember are:

1. The sol-gel process is a wet chemistry method offering many advantages: simplicity, low cost, excellent thickness control, and homogeneity of the films.
2. The spin coating technique allows the deposition of uniform films on flat substrates with precise thickness control by varying parameters such as rotation speed, solution concentration, and number of deposited layers.
3. The films were prepared using copper acetate monohydrate as the precursor, ethanol as the solvent, and monoethanolamine as the stabilizer. Three series of samples (S1, S2, S3) with respectively 6, 9, and 12 layers were prepared to study the effect of thickness.
4. The films were characterized using complementary techniques:
    - **Thickness:** by the mass difference method.
    - **Structural properties:** by XRD on a Bruker D8 Advance diffractometer.
    - **Optical properties:** by UV-Visible spectroscopy in the range 300-1100 nm.
    - **Electrical properties:** by the four-point probe method using a Keysight B1500A analyzer.
5. The data analysis methods (Scherrer formula for crystallite size, Tauc relation for the optical band gap, Urbach law for disorder energy, etc.) were detailed.

The experimental and analytical methodology presented in this chapter forms the basis of the experimental study to be presented in **Chapter 3**, where the results obtained for the three CuO samples of different thicknesses will be discussed in detail, with particular emphasis on the influence of thickness on the optical band gap.

References

[1] D. Bokov, A. Turki Jalil, S. Chupradit, W. Suksatan, M. Javed Ansari, I. H. Shewael, G. H. Valiev, and E. Kianfar, "Nanomaterial by sol-gel method: synthesis and application," Advances in Materials Science and Engineering, vol. 2021, pp. 1-21, 2021.

[2] L. Znaidi, "Sol–gel-deposited ZnO thin films: A review," Materials Science and Engineering: B, vol. 174, pp. 18-30, 2010.

[3] M. Tyona, "A theoritical study on spin coating technique," Advances in materials Research, vol. 2, p. 195, 2013.

[4] M. Abdelhafid, "Etude des couches minces d'Oxyde de Zinc dopé Aluminium et Cobalt élaborées par le technique sol gel-spin coating. Application à la photodétection et au photocourant," Universite Freres Mentouri-Constantine, 2015.

[5] D. Bokov, A. Turki Jalil, S. Chupradit, W. Suksatan, M. Javed Ansari, I. H. Shewael, G. H. Valiev, and E. Kianfar, "Nanomaterial by sol-gel method: synthesis and application," Advances in Materials Science and Engineering, vol. 2021, pp. 1-21, 2021.

[6] E. Benrezgua, B. Deghfel, Z. Abdelhalim, W. J. Basirun, R. Amari, A. Boukhari, M. K. Yaakob, S. Kheawhom, and A. A. Mohamad, "Synthesis and properties of copper doped zinc oxide thin films by sol-gel, spin coating and dipping: A characterization review," Journal of Molecular Structure, p. 133639, 2022.

[7] L. Znaidi, "Sol–gel-deposited ZnO thin films: A review," Materials Science and Engineering: B, vol. 174, pp. 18-30, 2010.

[8] D. Halin, I. Talib, A. Daud, and M. Hamid, "Characterizations of cuprous oxide thin films prepared by sol-gel spin coating technique with different additives for the photoelectrochemical solar cell," International Journal of Photoenergy, vol. 2014, 2014.

[9] P. Samarasekara and N. Premasiri, "Optical properties of spin coated and sol-gel dip coated cupric oxide thin films," arXiv preprint arXiv:1806.03976, 2018.

[10] T. Jiang, Y. Wang, D. Meng, X. Wu, J. Wang, and J. Chen, "Controllable fabrication of CuO nanostructure by hydrothermal method and its properties," Applied Surface Science, vol. 311, pp. 602-608, 2014.

[11] S. Chaurasiya, J. Udaya Bhanu, and P. Thangadurai, "Precursor dependent structural phase evolution in hydrothermally prepared Cu2O octahedrons and cu micro-flakes and their structural and optical properties," Transactions of the Indian Institute of Metals, vol. 71, pp. 1185-1191, 2018.

[12] O. Reyes, D. Maldonado, J. Escorcia-García, and P. Sebastian, "Effect of temperature and pH on direct chemical bath deposition of cuprous oxide thin films," Journal of Materials Science: Materials in Electronics, vol. 29, pp. 15535-15545, 2018.

[13] G. Sığırcık and T. Tüken, "ZnO/CuO hybrid films synthesized by sequential application of electrochemical and spin coating technique," Journal of Materials Science: Materials in Electronics, vol. 31, pp. 17855-17871, 2020.

[14] Z. N. Kayani, W. Chaudhry, R. Sagheer, S. Riaz, and S. Naseem, "Effect of Ce doping on crystallite size, band gap, dielectric and antibacterial properties of photocatalyst copper oxide Nano-structured thin films," Materials Science and Engineering: B, vol. 283, p. 115799, 2022.

[15] A. Maini and M. Shah, "Sol-Gel Fabricated CuO Thin Film: Characterization for Device Application," 2021.

[16] Q. Zhu, Y. Zhang, J. Wang, F. Zhou, and P. K. Chu, "Microwave synthesis of cuprous oxide micro-/nanocrystals with different morphologies and photocatalytic activities," Journal of Materials Science & Technology, vol. 27, pp. 289-295, 2011.

[17] S. Moschetto, "Functional engineering of hybrid heterostructures for application in electronic, optical and optoelectronic nanostructured devices," 2023.

[18] H. Hashim, S. Shariffudin, P. Saad, and H. Ridah, "Electrical and optical properties of copper oxide thin films by sol-gel technique," in IOP Conference Series: Materials Science and Engineering, 2015, p. 012032.

[19] B. Shivaraj, H. N. Murthy, M. Krishna, and S. Sharma, "Investigation of influence of spin coating parameters on the morphology of ZnO thin films by taguchi method," Int. j. thin film sci. tec, vol. 2, pp. 143-154, 2013.

[20] D. Meyerhofer, "Characteristics of resist films produced by spinning," Journal of Applied Physics, vol. 49, pp. 3993-3997, 1978.

[21] P. Burmann, B. Zornoza, C. Téllez, and J. Coronas, "Mixed matrix membranes comprising MOFs and porous silicate fillers prepared via spin coating for gas separation," Chemical Engineering Science, vol. 107, pp. 66-75, 2014.

[22] M. Dhaouadi, M. Jlassi, I. Sta, I. B. Miled, G. Mousdis, M. Kompitsas, and W. Dimassi, "Physical properties of copper oxide thin films prepared by sol–gel spin–coating method," Am. J. Phys. Appl, vol. 6, pp. 43-50, 2018.

[23] H. Hashim, S. Shariffudin, M. Sarah, and N. Nasir, "The characterization of copper oxide with different molar concentration using sol-gel spin coating," in 2016 IEEE International Conference on Semiconductor Electronics (ICSE), 2016, pp. 224-227.

[24] V. Solyanikov and L. Petrov, "The Rate of the Oxygen Absorption by the Styrene Epoxide–p-Toluene Sulfonic Acid Double System Depending on the Structure of the Aliphatic Tail of the Alcohol Solvent," Russian Journal of Physical Chemistry B, vol. 17, pp. 1259-1264, 2023.

[25] T. Munekata, T. Suzuki, S. Yamakawa, and R. Asahi, "Effects of viscosity, surface tension, and evaporation rate of solvent on dry colloidal structures: A lattice Boltzmann study," Physical Review E—Statistical, Nonlinear, and Soft Matter Physics, vol. 88, p. 052314, 2013.

[26] K. Iimura, Y. Ishikawa, T. Kikuchi, T. Takai, H. Satone, and M. Suzuki, "Preparation of yttrium barium copper oxide superconductive fibers via electrospinning through a lactic-acid gel route," Journal of the Ceramic Society of Japan, vol. 125, pp. 634-637, 2017.

[27] T. Fujiwara, T. Nakaue, and M. Yoshimura, "Direct fabrication and patterning of Cu2O film by local electrodeposition method," Solid State Ionics, vol. 175, pp. 541-544, 2004.

[28] S. Farhad, S. Majumder, M. A. Hossain, N. Tanvir, R. Akter, and M. A. Patwary, "Effect of solution pH and post-annealing temperatures on the optical bandgap of the copper oxide thin films grown by modified SILAR method," MRS Advances, vol. 4, pp. 937-944, 2019.

[29] N. Beji, M. Souli, M. Ajili, S. Azzaza, S. Alleg, and N. K. Turki, "Effect of iron doping on structural, optical and electrical properties of sprayed In2O3 thin films," Superlattices and Microstructures, vol. 81, pp. 114-128, 2015.

[30] M. Boumezrag, K. Almi, S. Lakel, and H. Touhami, "Alkali Metals Doped Cu0. 94A0. 06O (A= Li, Na and K) Thin Films: Facile Synthesis, Structural, Optical and Thermoelectric Properties," Russian Journal of Physical Chemistry B, vol. 18, pp. 895-906, 2024.

[31] M. Imran, G. Asghar, G. H. Tariq, A. W. Faridi, S. Bano, M. S. Shifa, and S. Ullah, "Investigation of annealing effects on physical properties of chemically prepared copper oxide thin films," Results in Optics, vol. 10, p. 100331, 2023.

[32] G. C. Wang, The utilization of slag in civil infrastructure construction: Woodhead Publishing, 2016.

[33] N. Munir, M. Hanif, D. A. Dias, and Z. Abideen, "The role of halophytic nanoparticles towards the remediation of degraded and saline agricultural lands," Environmental Science and Pollution Research, vol. 28, pp. 60383-60405, 2021.

[34] A. Barhoum and M. L. García-Betancourt, "Physicochemical characterization of nanomaterials: Size, morphology, optical, magnetic, and electrical properties," in Emerging applications of nanoparticles and architecture nanostructures, ed: Elsevier, 2018, pp. 279-304.

[35] C. Kittel, "Introduction to Solid State Physics," 8th edition, John Wiley & Sons Inc, New York, 2005.

[36] S. Benhamida, "Caractérisation Des Couches Minces D'oxyde De Nickel (NiO) Elaboré Par Spray Pyrolyse," Université Mohamed Khider-BISKRA, 2018.

[37] B. D. Cullity and S. R. Stock, Elements of X-Ray Diffraction, 3rd edition, Prentice Hall, 2001.

[38] G. K. Williamson and R. E. Smallman, "Dislocation densities in some annealed and cold-worked metals from measurements on the X-ray Debye-Scherrer spectrum," Philosophical Magazine, vol. 1, pp. 34-46, 1956.

[39] M. D. Jawad, "Senior Year Project: Fabrication and Optimization of Quantum Dots based Photonic devices," 2022.

[40] R. A. Vasudev, "Synthesis and characterization of nanocrystalline ZnO Gas Sensor," 2015.

[41] M. C. BENACHOUR, "Elaboration et caractérisation des couches minces de matériau CZTS (Cu2ZnSnS4) obtenues par voie sol gel : Applications a la photovoltaïque," ecole polytechnique, 2020.

[42] W. Allag, "Study of thin films for photovoltaic solar cells," 2023.

[43] J. Tauc, "Optical properties and electronic structure of amorphous Ge and Si," Materials Research Bulletin, vol. 3, pp. 37-46, 1968.

[44] F. Urbach, "The Long-Wavelength Edge of Photographic Sensitivity and of the Electronic Absorption of Solids," Physical Review, vol. 92, p. 1324, 1953.

[45] S. Amara, "Caractérisation optique et structurale des couches minces d'oxydes complexes pour applications photoniques," 2018.

[46] F. Khediri, "Etude expérimental des propriétés physiques des couches minces de ZnO," Université Echahid Cheikh Larbi-Tebessi-Tébessa, 2022.

[47] L. J. van der Pauw, "A method of measuring specific resistivity and Hall effect of discs of arbitrary shape," Philips Research Reports, vol. 13, pp. 1-9, 1958.

[48] A. Hafdallah and N. Attaf, "Étude du dopage des couches minces de ZnO élaborées par spray ultrasonique," 2007.

Chapter 3. Results and Discussion — Influence of Film Thickness on the Optical Band Gap of CuO Thin Films

3.1 Introduction

This chapter presents and discusses the experimental results obtained for CuO thin films deposited by the sol-gel spin coating technique with varying numbers of layers (6, 9, and 12 layers). The primary objective is to investigate how film thickness influences the structural, optical, and electrical properties of the films, with particular emphasis on the variation of the optical band gap.

The results are organized into four main sections: thickness measurement (Section 3.2), structural characterization by XRD (Section 3.3), optical characterization by UV-Visible spectroscopy (Section 3.4), and electrical characterization by the four-point probe method (Section 3.5). Each section includes a detailed discussion of the observed trends and their physical interpretation, supported by comparisons with literature data. Section 3.6 provides a comprehensive discussion correlating the different properties, and Section 3.7 summarizes the key findings.

3.2 Film Thickness Measurement

3.2.1 Results

The thickness of each CuO thin film was determined using the gravimetric (mass difference) method described in Chapter 2. The results are presented in Table 3.1 and illustrated in Figure 3.1.

Table 3. 1 Measured thickness of CuO thin films as a function of the number of deposited layers.

Sample	Number of layers	Thickness (nm)
S1	6	201.06
S2	9	421.75
S3	12	943.23

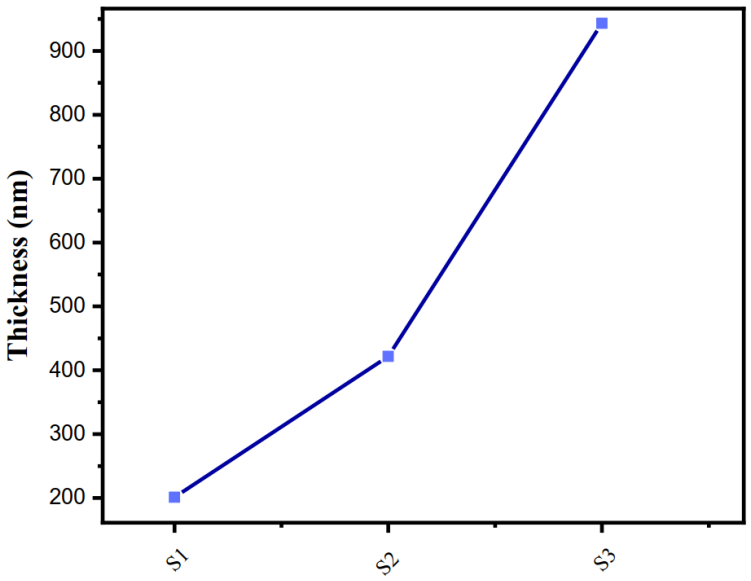

Figure 3. 1 Bar graph or line plot showing the variation of CuO thin film thickness as a function of the number of deposited layers.

3.2.2 Discussion

The results show a clear increase in film thickness with the number of deposited layers. The relationship is approximately linear for the first two data points (S1 and S2), with each layer contributing approximately 33–47 nm to the total thickness. However, a significant increase is observed for S3 (12 layers), where the thickness reaches 943 nm.

This behavior can be explained as follows:

1. **Linear accumulation:** In the spin coating process, each coating cycle deposits a relatively uniform layer of material. When multiple layers are deposited sequentially, the total thickness increases approximately proportionally to the number of layers.
2. **Surface roughness effects:** As more layers are deposited, the surface roughness of the underlying layers can increase, which may cause subsequent layers to be deposited less uniformly. This can lead to localized thickening.
3. **Solution retention:** As the film becomes thicker, its surface may retain more solution during subsequent coating cycles due to changes in wettability and surface energy.

The approximately linear relationship between thickness and number of layers confirms that the spin coating technique provides reasonable control over film thickness. This approach allows us to systematically investigate the influence of thickness on the properties of CuO films.

3.3 Structural Properties (XRD Analysis)

3.3.1 Phase Identification

Figure 3.2 shows the XRD patterns of the three CuO samples with different thicknesses. All patterns were analyzed by comparison with the standard JCPDS reference data for CuO (Card No. 98-004-3179).

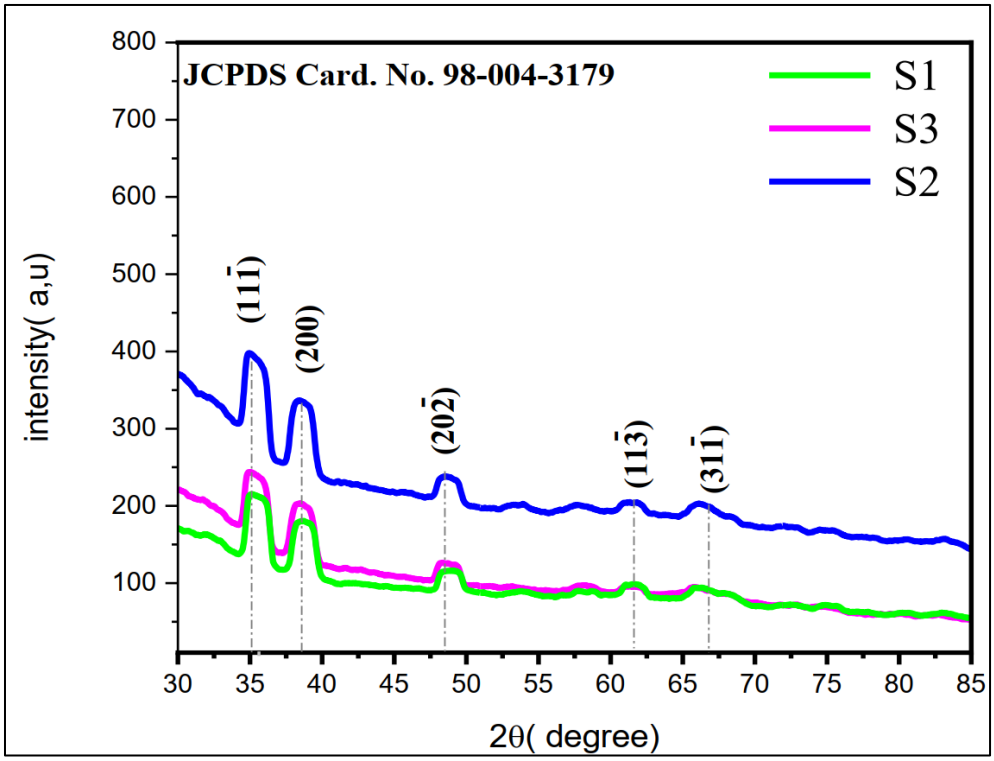

Figure 3. 2 XRD patterns of all three CuO samples (S1, S2, S3) plotted together for comparison, with peak indexing.

The XRD analysis reveals the following key observations:

a) Polycrystalline nature: All three films exhibit multiple diffraction peaks, confirming their polycrystalline nature. The peaks are located at positions consistent with the monoclinic CuO structure (tenorite phase).

b) Main diffraction peaks: The two most prominent peaks appear at approximately $2\theta = 35.5°$ and 38.6°, corresponding to the (-111) and (111) crystallographic planes, respectively. Additional peaks corresponding to the (-202), (-113), and (-311) planes are also observed, though with lower intensity.

c) Phase purity: No diffraction peaks corresponding to Cu_2O (cuprite), metallic Cu, or $Cu(OH)_2$ were detected in any of the samples. This confirms the formation of pure, single-phase CuO in all films, validating the effectiveness of the annealing conditions (500°C for 2 hours in air).

d) Variation of peak intensity with thickness: The peak intensities change significantly with film thickness. The peaks are most intense for sample S2 (9 layers, 421.75 nm), indicating that this thickness yields the best crystallinity. In contrast, S1 (6 layers) shows lower intensities due to the smaller amount of diffracting material, while S3 (12 layers) also shows reduced intensities compared to S2.

3.3.2 Effect of Thickness on Peak Intensity

The variation of peak intensity with thickness deserves detailed discussion:

For thin films (S1, 6 layers, 201 nm): The relatively low peak intensity is primarily due to the small quantity of CuO material available for diffraction. With only 6 layers, the film is thin and contains fewer crystallites, resulting in a weaker diffraction signal.

For intermediate films (S2, 9 layers, 422 nm): The highest peak intensity is observed, indicating optimal crystallinity. At this thickness, the crystallites are well-ordered and the film has sufficient material to produce a strong diffraction signal. The preheating and annealing conditions are most effective at this thickness for promoting grain growth and reducing defects.

For thick films (S3, 12 layers, 943 nm): The peak intensity decreases compared to S2. This unexpected decrease can be attributed to several factors:

- **X-ray absorption:** In thicker films, the X-rays are partially absorbed before reaching the deeper layers, reducing the effective volume contributing to diffraction.
- **Accumulated defects:** The deposition of many layers introduces cumulative stresses and defects at the interlayer interfaces.
- **Reduced crystallinity:** Beyond an optimal thickness, the crystallization quality may deteriorate due to the competition between grain growth and defect formation during successive preheating and annealing cycles.

3.3.3 Crystallite Size

The average crystallite size was calculated from the most intense peaks using the Scherrer formula. The results are presented in Table 3.2.

Table 3. 2 Crystallite size of CuO thin films calculated from different diffraction peaks.

Sample	2θ (°)	(hkl)	D (nm)	Average D (nm)
S1 (6 layers)	35.46	(-111)	10.94	**10.29**
	38.58	(111)	9.63	
S2 (9 layers)	35.40	(-111)	15.77	**15.12**
	38.56	(111)	14.46	
S3 (12 layers)	35.16	(-111)	11.55	**11.04**
	38.48	(111)	10.53	

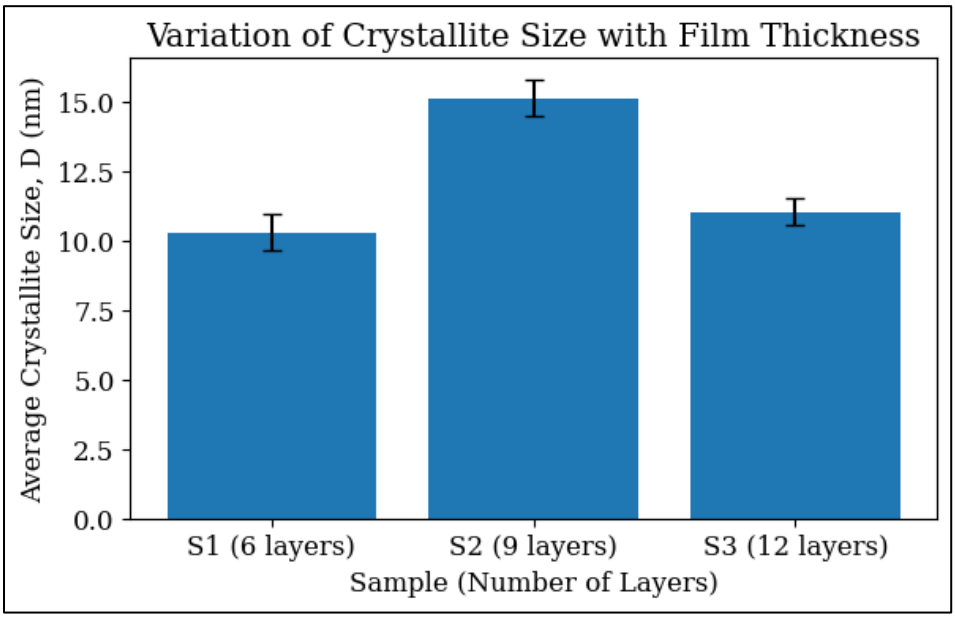

Figure 3. 3 Bar chart showing the variation of average crystallite size as a function of film thickness (or number of layers), with error bars.

The crystallite size shows a clear non-monotonic variation with film thickness:

- **S1 (201 nm):** Average crystallite size = 10.29 nm
- **S2 (422 nm):** Average crystallite size = 15.12 nm (maximum)
- **S3 (943 nm):** Average crystallite size = 11.04 nm

Physical interpretation:

The increase in crystallite size from S1 to S2 is attributed to grain growth during the annealing process. As the film thickens from 201 to 422 nm, additional layers provide more material for crystallite coalescence and growth. The annealing at 500°C provides sufficient thermal energy for atoms to migrate and crystallites to merge.

The decrease from S2 to S3 is more complex and can be explained by:

1. **Nucleation of new grains:** In thicker films with many layers, each new layer introduces fresh nucleation sites that compete with the growth of existing grains.
2. **Interlayer strain:** The repeated cycles of deposition and preheating create interfaces between successive layers that impede grain growth.

3. **Thermal gradient effects:** In thicker films, the heat distribution during annealing may be less uniform, affecting crystallization.

These observations are consistent with previous reports in the literature. Saâd et al. observed similar behavior in spray-deposited CuO films, where optimal crystallinity was achieved at intermediate thicknesses.

3.3.4 Lattice Strain and Dislocation Density

The lattice strain (ε) and dislocation density (δ) were calculated using the standard equations described in Chapter 2. These parameters provide insight into the defect concentration within the films.

Table 3. 3 Lattice strain and dislocation density of CuO thin films as a function of thickness.

Sample	Thickness (nm)	Strain ε ($\times 10^{-4}$)	Dislocation density δ ($\times 10^{14}$ lines/m^2)
S1 (6 layers)	201.06	33.06	9.56
S2 (9 layers)	421.75	23.01	4.41
S3 (12 layers)	943.23	31.45	8.98

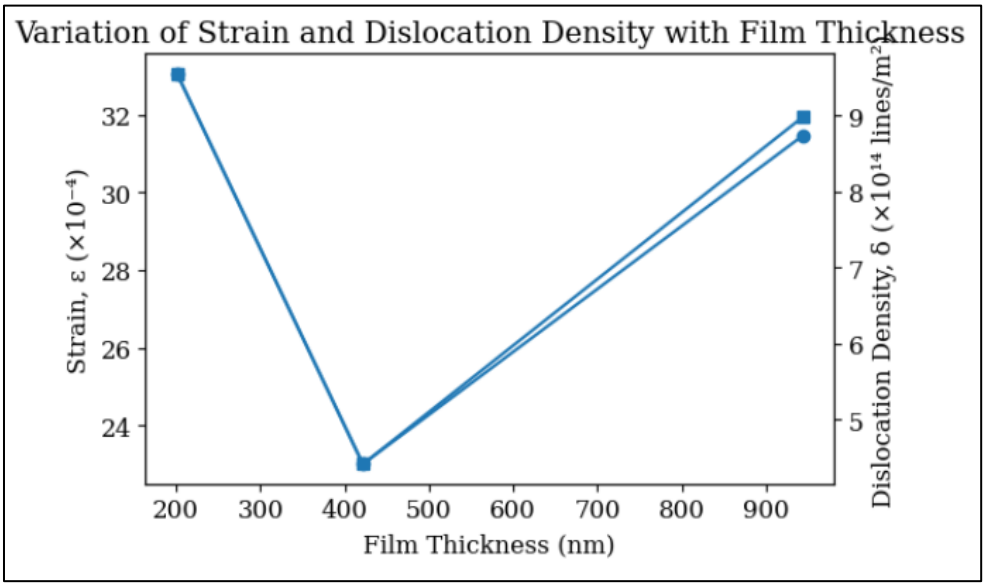

Figure 3. 4 Combined bar chart or dual-axis plot showing the variation of strain and dislocation density as a function of film thickness, demonstrating the inverse relationship with crystallite size.

Discussion:

The strain and dislocation density both follow a similar trend: they are highest for S1, minimum for S2, and increase again for S3. This behavior is directly correlated with the crystallite size, as predicted by the inverse relationship:

$$\delta = \frac{1}{D^2}$$

For S1 (thin film): The high strain and dislocation density reflect the incomplete crystallization and the presence of many small crystallites with abundant grain boundaries.

For S2 (intermediate thickness): The minimum values of strain (23.01×10^{-4}) and dislocation density (4.41×10^{14} lines/m^2) indicate the best crystallographic quality. At this thickness, the thermal treatment effectively promotes grain growth and relieves internal stresses.

For S3 (thick film): The increased strain and dislocation density suggest that the additional layers introduce new defects that partially offset the benefits of thermal treatment. The accumulation of interlayer stresses and the formation of new grain boundaries at layer interfaces contribute to the degradation of crystalline quality.

Key finding: Sample S2 (9 layers, ~422 nm) represents the **optimal thickness** for achieving the best crystallographic quality in spin-coated CuO thin films under the conditions used in this work.

3.4 Optical Properties

3.4.1 Optical Transmittance

The optical transmittance spectra of the three CuO samples, measured in the wavelength range of 300 to 1100 nm, are shown in Figure 3.5.

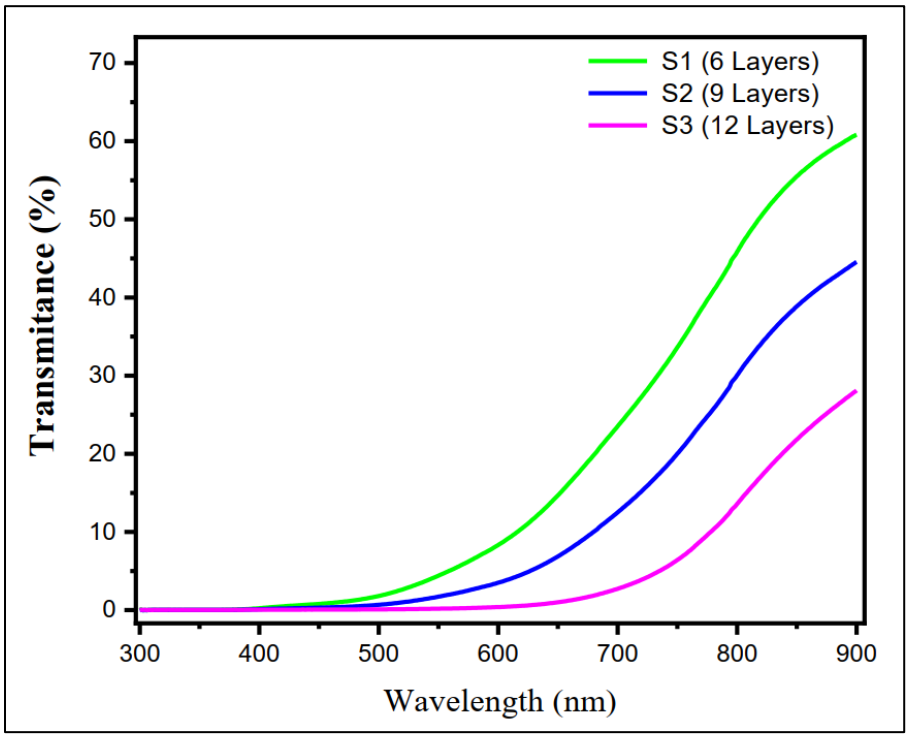

Figure 3. 5 Optical transmittance spectra of the three CuO samples plotted together, with wavelength on the x-axis and transmittance (%) on the y-axis.

Observations :

1. **General shape:** All samples exhibit low transmittance in the UV and visible regions (300–700 nm) and gradually increasing transmittance in the near-infrared region (700–1100 nm). This absorption profile is characteristic of CuO, which has strong absorption across the visible spectrum due to its narrow band gap.
2. **Effect of thickness:** The transmittance decreases significantly with increasing film thickness:
    - S1 (201 nm): Maximum transmittance ~65–70% at 1100 nm
    - S2 (422 nm): Maximum transmittance ~45–50% at 1100 nm
    - S3 (943 nm): Maximum transmittance ~25–30% at 1100 nm
3. **Absorption edge:** The absorption edge (the wavelength region where transmittance drops sharply) shifts slightly toward longer wavelengths (lower energies) with increasing thickness.

4. **No interference fringes:** None of the samples exhibit interference fringes (oscillations in the transmittance spectrum). Interference fringes would be expected from multiple reflections at smooth film/substrate interfaces. Their absence indicates that all films have a relatively rough surface that suppresses specular reflection.

Physical interpretation:

The decrease in transmittance with increasing film thickness is a direct consequence of the **Beer-Lambert law**:

$$T = e^{-\alpha d}$$

As the film thickness d increases, the optical path through the absorbing material increases, leading to greater absorption and lower transmission. This exponential dependence means that even small increases in thickness can lead to significant decreases in transmittance.

Additionally, surface roughness increases with the number of deposited layers, contributing to light scattering and further reducing the measured transmittance.

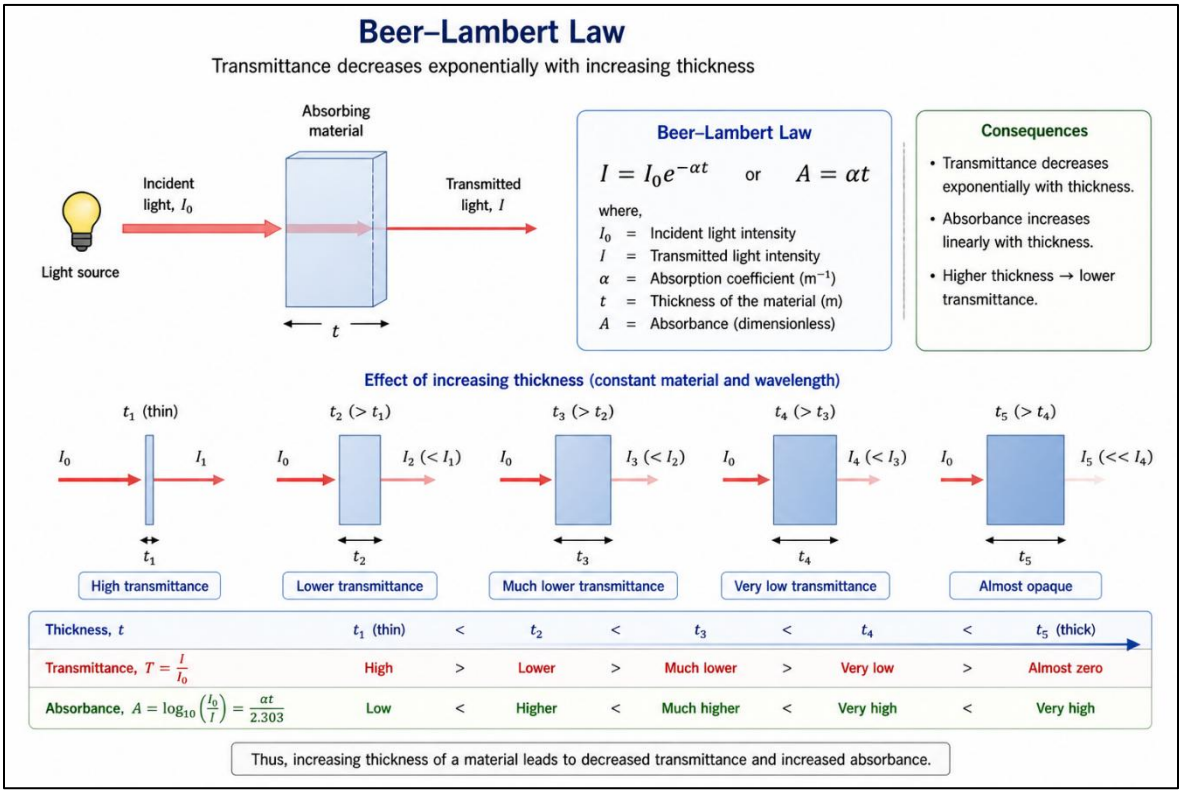

Figure 3. 6 Schematic diagram illustrating the Beer-Lambert law and how increasing thickness leads to decreased transmittance.

3.4.2 Optical Band Gap (Eg) — Main Result

The optical band gap is the central result of this dissertation. It was determined using the Tauc plot method, plotting $(\alpha h\nu)^2$ versus photon energy $h\nu$ and extrapolating the linear region to the energy axis.

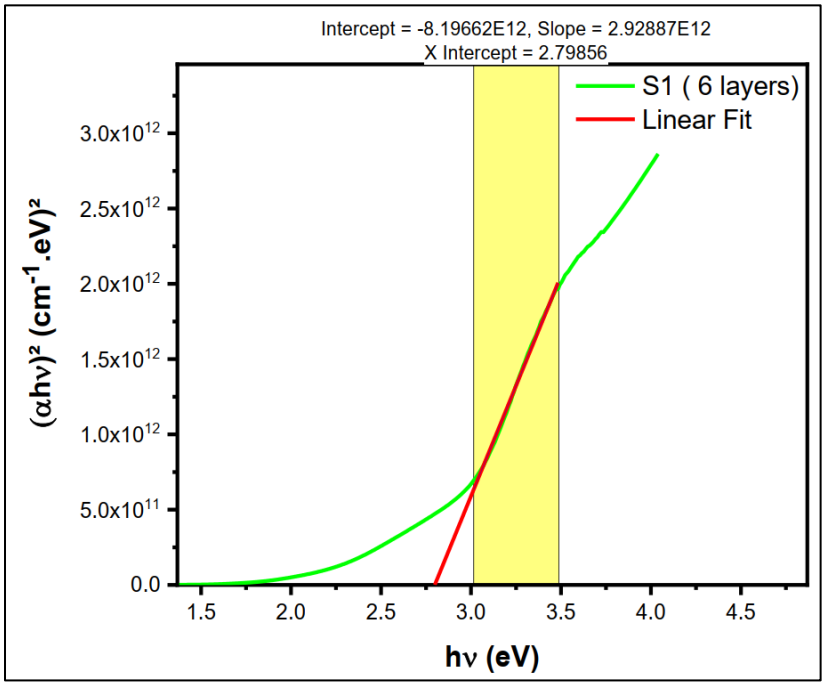

Figure 3. 7 Tauc plot for Sample S1 (6 layers) showing $(\alpha h\nu)^2$ versus $h\nu$ with linear extrapolation to determine Eg.

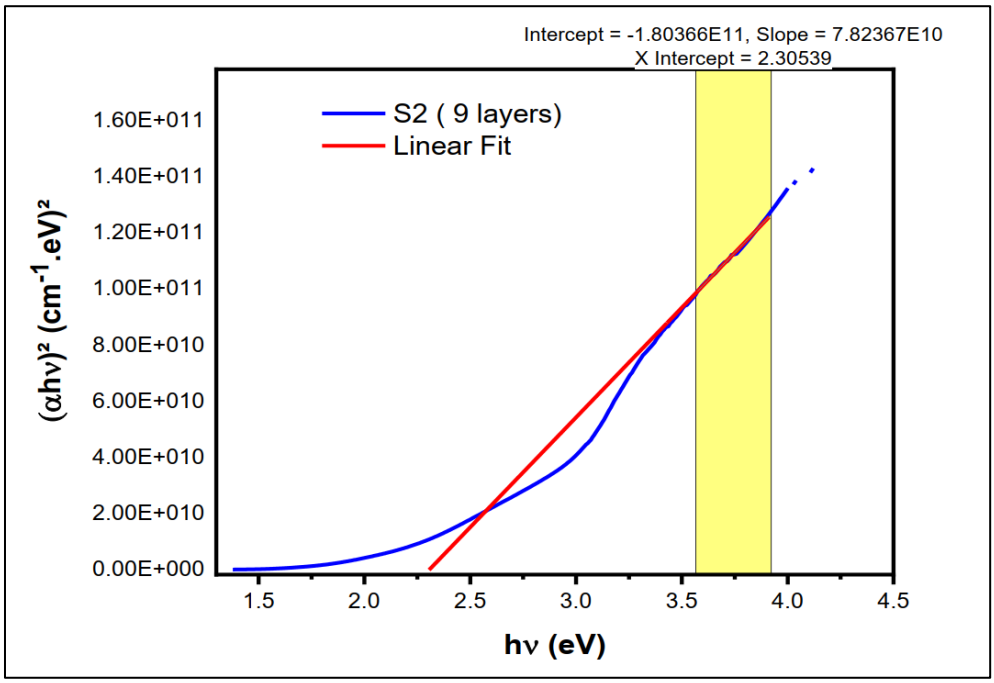

Figure 3. 8 Tauc plot for Sample S2 (9 layers) showing (αhν) ² versus hν with linear extrapolation.

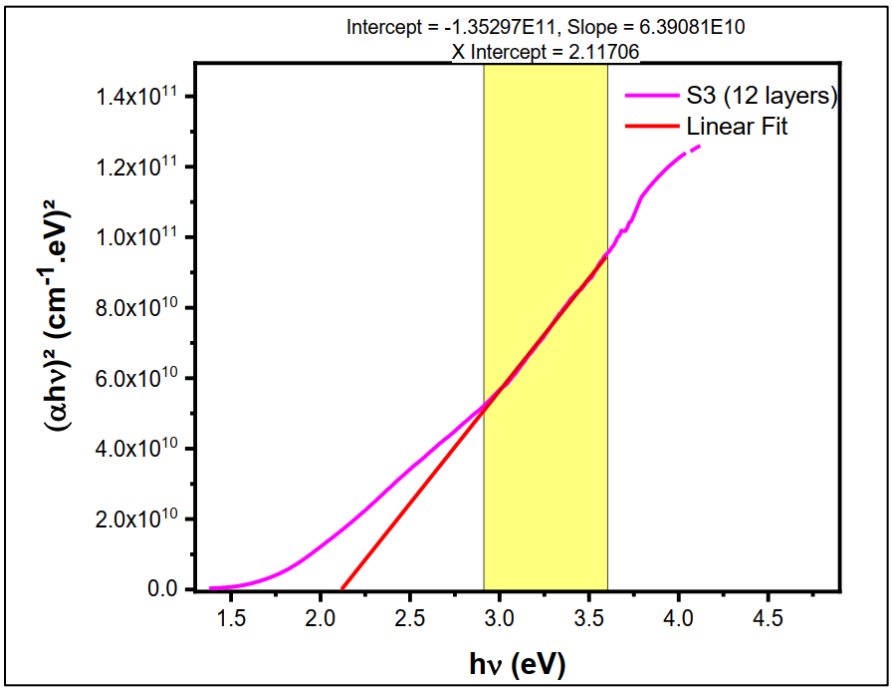

Figure 3. 9 Tauc plot for Sample S3 (12 layers) showing (αhν)² versus hν with linear extrapolation.

The extracted optical band gap values are summarized in Table 3.4.

Table 3. 4 Optical band gap of CuO thin films as a function of thickness.

Sample	Thickness (nm)	Optical band gap Eg (eV)
S1 (6 layers)	201.06	2.79
S2 (9 layers)	421.75	2.30
S3 (12 layers)	943.23	2.11

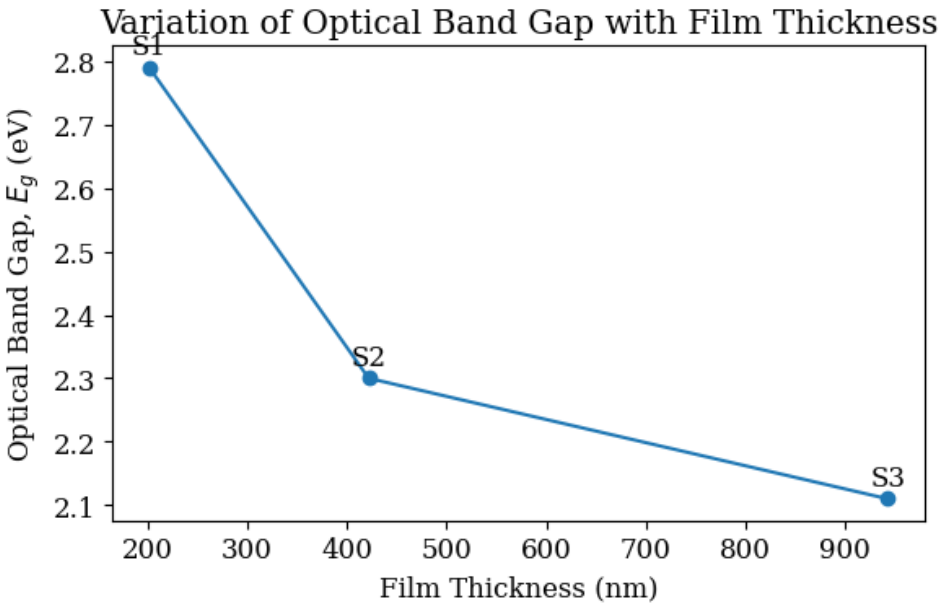

Figure 3. 10 Plot of optical band gap Eg versus film thickness, clearly showing the decreasing trend.

3.4.3 Detailed Discussion of the Band Gap Variation

The results reveal a clear and systematic decrease in the optical band gap with increasing film thickness, from 2.79 eV (201 nm) to 2.11 eV (943 nm). This decrease of approximately 0.68 eV represents a significant variation that has important implications for the optical and electronic applications of CuO thin films.

This behavior can be explained by several interconnected physical mechanisms:

Mechanism 1: Quantum Confinement Effect

When the crystallite size is comparable to or smaller than the exciton Bohr radius of the material, quantum confinement effects become significant. In confined systems, the energy levels become discrete rather than continuous, and the effective band gap increases relative to the bulk value.

For CuO, the exciton Bohr radius is estimated to be approximately 6.6 nm. In sample S1, the average crystallite size is 10.29 nm, which is close to this value. Therefore, weak quantum confinement effects may contribute to the widening of the band gap in the thinnest film.

As the film thickness and crystallite size increase (from S1 to S3), the confinement is reduced, and the band gap approaches the bulk value (~1.2 eV). This partially explains the decrease in Eg with increasing thickness.

However, the quantum confinement effect alone cannot fully account for the observed variation, since the crystallite sizes in all three samples (10–15 nm) are significantly larger than the Bohr radius.

Mechanism 2: Structural Disorder and Defects

The variation of the band gap is closely related to the structural quality of the films. As discussed in Section 3.3, sample S2 has the largest crystallite size, lowest strain, and lowest dislocation density, while S1 and S3 have more defects.

Structural disorder affects the band gap through the formation of **band tail states** (Urbach tails) near the edges of the valence and conduction bands. These tail states extend into the forbidden gap, effectively reducing the apparent optical band gap.

In thicker films (S3), despite the increase in structural disorder (as reflected by the higher Urbach energy), the band gap continues to decrease. This suggests that the dominant mechanism is the relaxation of quantum confinement effects rather than the introduction of disorder-related states.

Mechanism 3: Increase in Grain Size and Reduction of Grain Boundary Effects

In thinner films with smaller crystallites, the high density of grain boundaries creates additional energy barriers and scattering centers for electrons. These grain boundaries can modify the electronic band structure by introducing localized states that effectively widen the apparent band gap.

As the film becomes thicker and crystallites grow larger, the grain boundary density decreases, and its influence on the band gap is reduced, leading to a decrease in Eg.

Mechanism 4: Stress and Strain Effects

Residual stress in thin films can modify the band gap through the deformation of the crystal lattice. Compressive stress generally increases the band gap, while tensile stress decreases it. The variation of strain with thickness (Table 3.3) contributes to the observed band gap changes.

3.4.4 Comparison with Literature

Our observed decrease in band gap with increasing thickness is consistent with several previous reports on CuO thin films:

Table 3. 5 Comparison of the variation of optical band gap with thickness in CuO thin films from different studies.

Study	Technique	Thickness range (nm)	Eg range (eV)	Trend
This work	Sol-gel spin coating	201 – 943	2.79 – 2.11	Decreasing
Akaltun (2015)	SILAR	120 – 310	2.03 – 1.79	Decreasing
Saâd et al. (2020)	Spray pyrolysis	970 – 2900	Variable	Non-monotonic
Ali & Makki (2016)	Thermal evaporation	Variable	Variable	Decreasing

The absolute band gap values in our study (2.11–2.79 eV) are somewhat higher than the bulk CuO value of 1.2 eV. This difference can be attributed to the nanocrystalline nature of the films, quantum confinement effects, and the specific deposition conditions used.

3.4.5 Urbach Energy

The Urbach energy (Eu) was determined from the slope of the ln(α) versus hν plots. The results are presented in Figure 3.12 and Table 3.6.

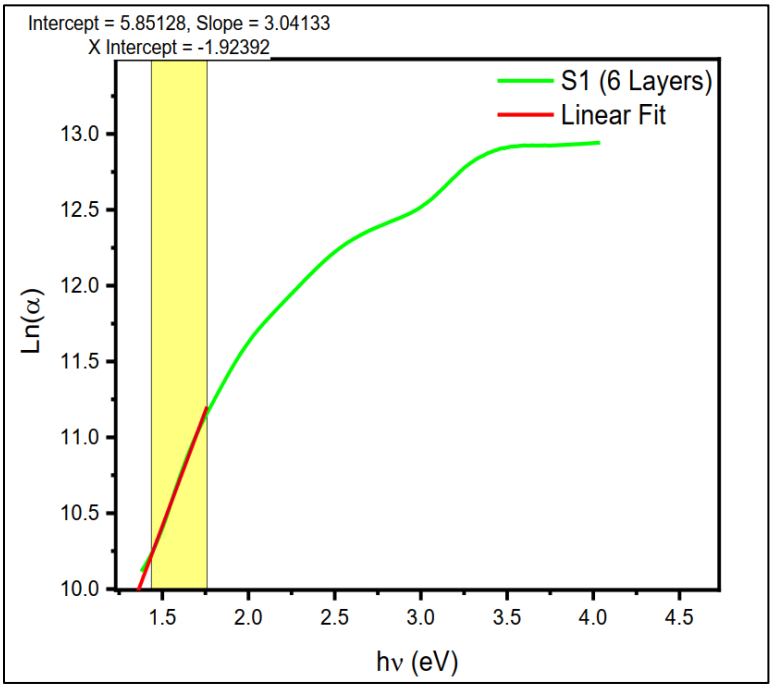

Figure 3. 11 Plots of ln(α) versus hν for sample S1, showing the linear fit in the Urbach tail region.

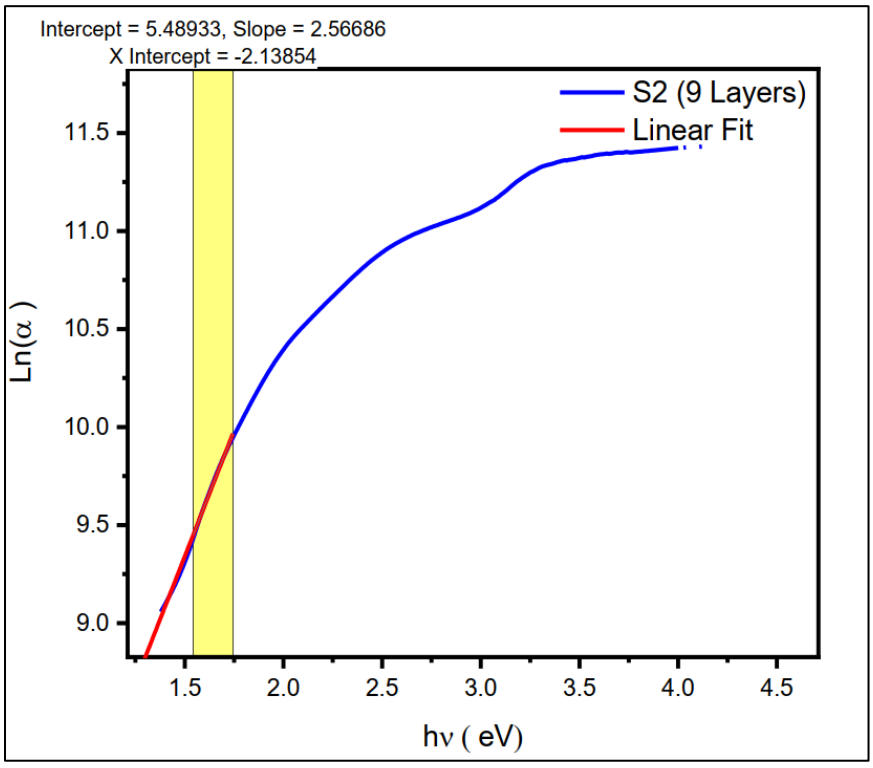

Figure 3. 12 Plots of ln(α) versus hν for sample S2.

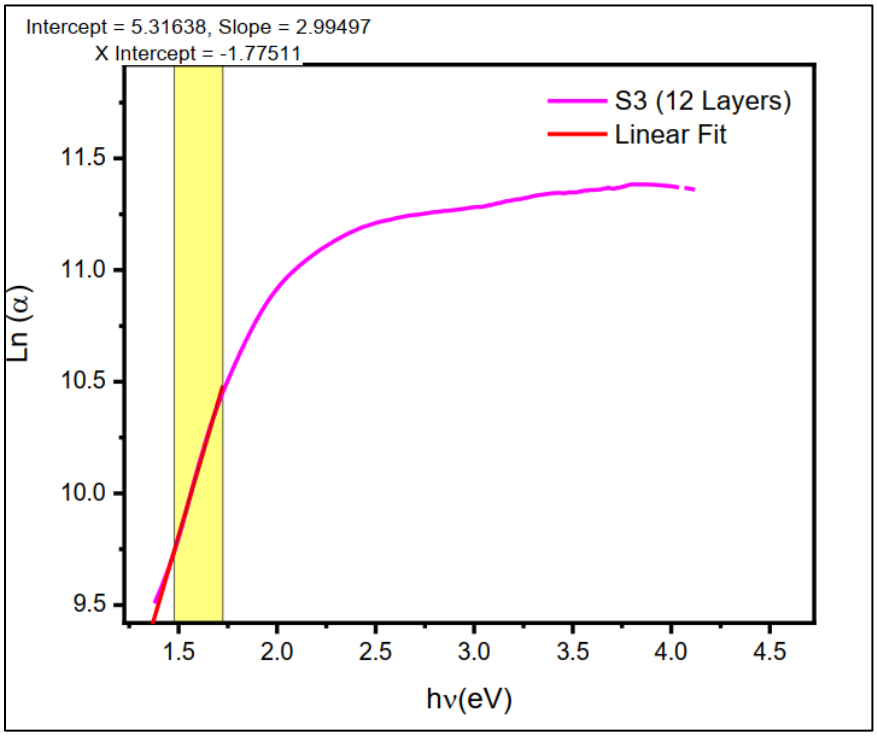

Figure 3. 13 Plots of ln(α) versus hν for sample S3.

Table 3. 6 Urbach energy of CuO thin films as a function of thickness.

Sample	Thickness (nm)	Urbach energy Eu (meV)
S1 (6 layers)	201.06	328.8
S2 (9 layers)	421.75	389.5
S3 (12 layers)	943.23	564.0

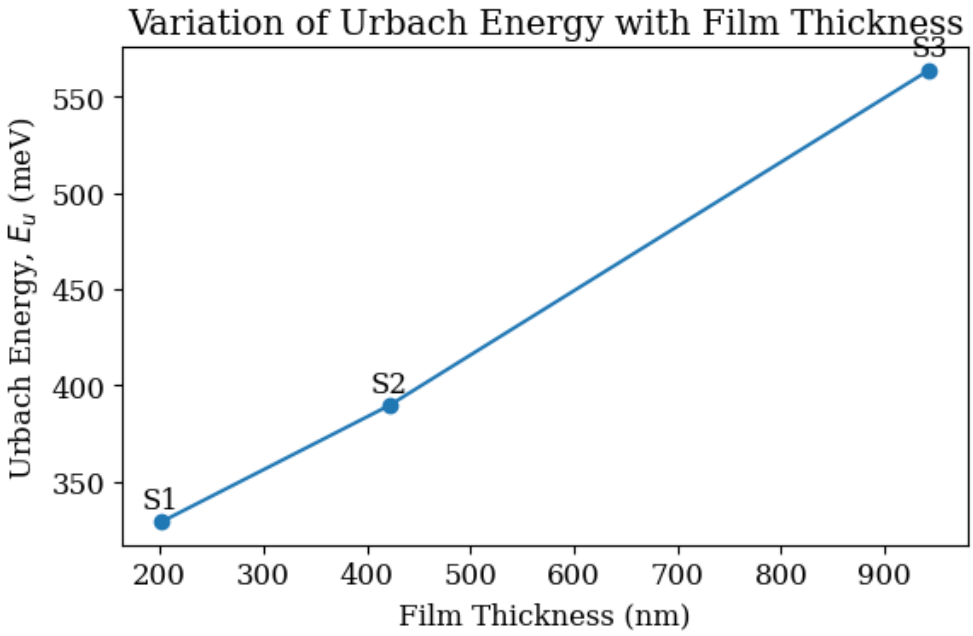

Figure 3. 14 Plot of Urbach energy Eu versus film thickness, showing the increasing trend.

Discussion:

The Urbach energy increases monotonically with film thickness, from 328.8 meV to 564.0 meV. This trend indicates that the degree of structural disorder increases in thicker films, which is consistent with the structural analysis results.

The increase in Urbach energy can be explained by:

1. **Accumulation of interlayer defects:** Each coating cycle introduces an interface between successive layers, creating boundary regions with increased disorder.

2. **Thermal cycling effects:** The repeated preheating at 250°C between layers can create thermal stresses and promote the formation of defects that are not fully healed during the final annealing.
3. **Increased grain boundary density:** Although individual crystallites may be larger in thicker films, the total number of grain boundaries increases with film volume.

3.4.6 Correlation Between Eg and Eu

One of the most important findings of this work is the inverse correlation between the optical band gap (Eg) and the Urbach energy (Eu). As Eu increases, Eg decreases.

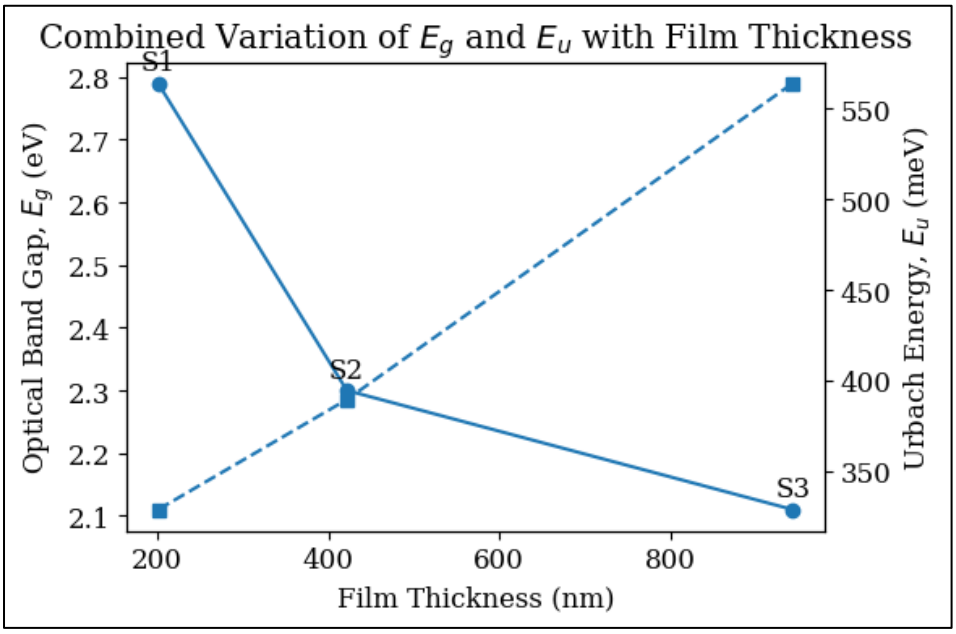

Figure 3. 15 Combined plot showing Eg and Eu as a function of thickness on the same graph with dual y-axes, clearly demonstrating the inverse correlation.

This inverse relationship is a well-documented phenomenon in semiconducting thin films. It indicates that the formation of band tail states (quantified by Eu) directly contributes to the narrowing of the apparent optical band gap. As disorder increases, the tail states extend further into the forbidden gap, shifting the absorption edge to lower energies and reducing the measured Eg.

This correlation is expressed quantitatively as:

$$E_g + E_u \approx \text{constant}$$

This approximate relationship, while not exact, provides a useful guideline for understanding how changes in film quality affect the optical properties.

3.5 Electrical Properties

3.5.1 Results

The electrical resistivity and conductivity of the CuO thin films were measured at room temperature using the four-point probe method. The results are presented in Table 3.7.

Table 3. 7 Electrical properties of CuO thin films as a function of thickness.

Sample	Thickness (nm)	Sheet resistance R_sq ($\times 10^5$ Ω/□)	Resistivity ρ ($\times 10^2$ Ω·cm)	Conductivity σ ($\times 10^{-2}$ $\Omega^{-1}\cdot cm^{-1}$)
S1 (6 layers)	201.06	136.4	2.74	0.365
S2 (9 layers)	421.75	17.5	0.74	1.355
S3 (12 layers)	943.23	22.1	2.08	0.480

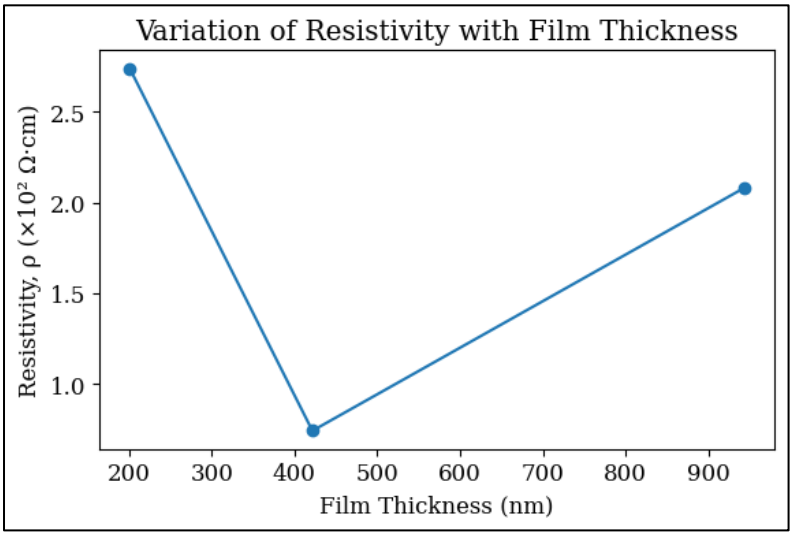

Figure 3. 16 plot showing the variation of resistivity as a function of film thickness.

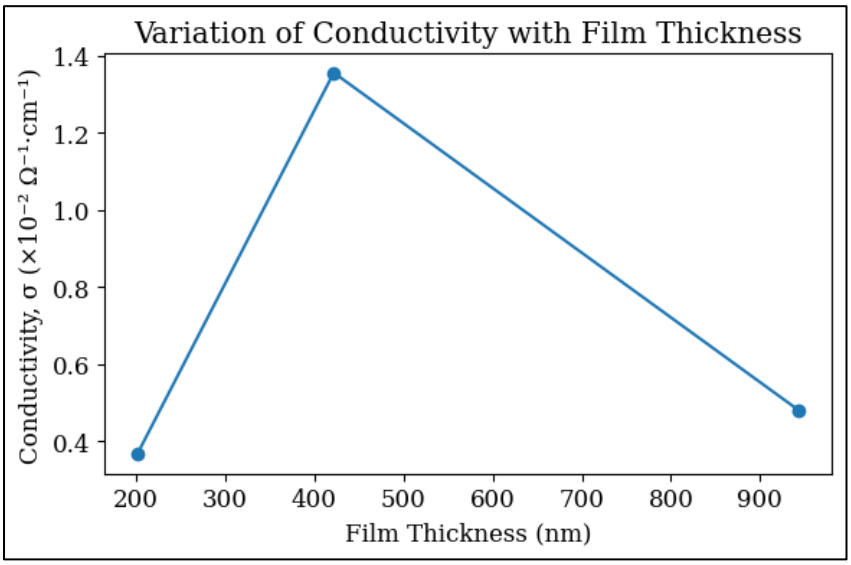

Figure 3. 17 Plot showing the variation of conductivity as a function of film thickness.

3.5.2 Discussion

The electrical properties show a non-monotonic variation with thickness, following the same trend as the structural properties:

S1 (thin film, 201 nm): High resistivity (274 Ω·cm) and low conductivity. The thin film has small crystallites with many grain boundaries that act as barriers to charge transport. Grain boundary scattering significantly reduces carrier mobility.

S2 (intermediate thickness, 422 nm): Minimum resistivity (74 Ω·cm) and maximum conductivity (1.355×10^{-2} $\Omega^{-1}\cdot cm^{-1}$). This sample has the largest crystallites and fewest defects, resulting in:

- Reduced grain boundary scattering
- Higher carrier mobility
- More efficient charge transport

S3 (thick film, 943 nm): The resistivity increases again to 208 Ω·cm. Despite the greater thickness (which provides more material for conduction), the deterioration of crystalline quality introduces additional scattering centers that impede charge carrier transport.

The electrical behavior can be understood through the relationship between crystallite size and grain boundary density. In polycrystalline films, grain boundaries act as potential barriers that trap free carriers and scatter mobile charges. The resistance associated with grain boundaries is:

$$R_{gb} \propto \frac{1}{D}$$

Therefore, larger crystallites (fewer grain boundaries per unit length) lead to lower resistance.

3.5.3 Correlation with Structural Properties

The strong correlation between the electrical and structural properties is summarized in Table 3.8.

Table 3. 8 Summary of the correlation between structural and electrical properties.

Sample	Crystallite size D (nm)	Dislocation density δ (×10¹⁴ m⁻²)	Resistivity ρ (Ω·cm)	Conductivity σ (Ω⁻¹·cm⁻¹)
S1	10.29	9.56	274	0.00365
S2	15.12	4.41	74	0.01355
S3	11.04	8.98	208	0.00480

The data clearly show that:

- The **largest crystallite size** correlates with the **lowest resistivity**
- The **lowest dislocation density** correlates with the **highest conductivity**
- Sample S2 exhibits optimal structural and electrical properties simultaneously

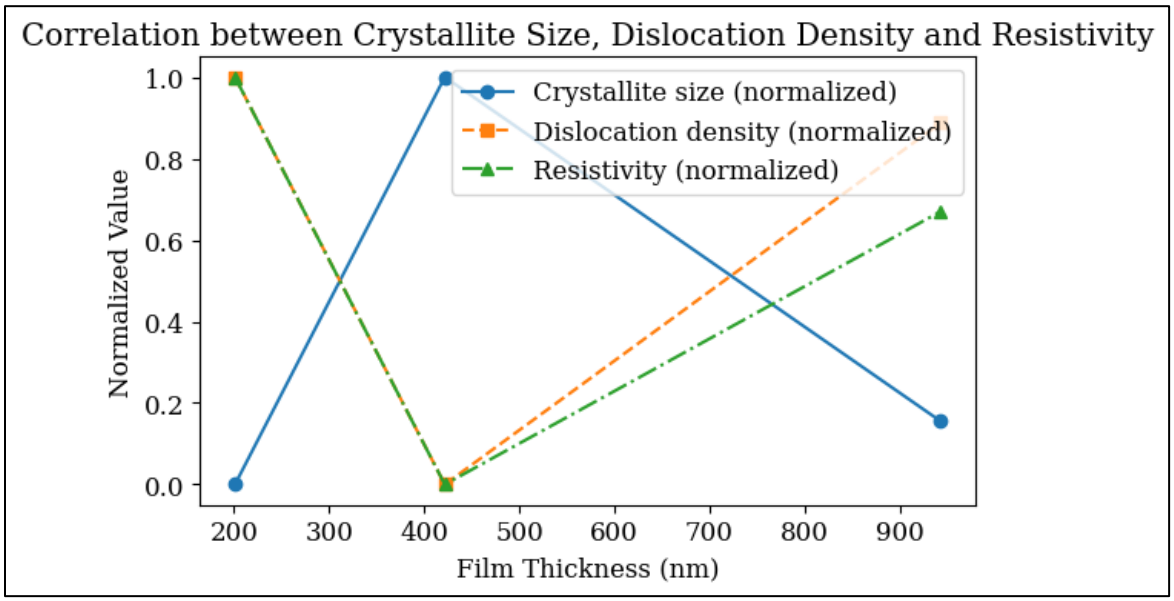

Figure 3. 18 Combined plot showing crystallite size, dislocation density, and resistivity as functions of thickness, demonstrating their correlation.

3.6 Comprehensive Discussion: Correlation of All Properties

3.6.1 Summary Table

All the key results are compiled in Table 3.9 for a comprehensive overview.

Table 3. 9 Complete summary of all measured properties of CuO thin films as a function of thickness.

Property	S1 (6 layers)	S2 (9 layers)	S3 (12 layers)	Trend
Thickness (nm)	201.06	421.75	943.23	Increasing
Crystallite size D (nm)	10.29	15.12	11.04	Non-monotonic (max at S2)
Strain ε ($\times 10^{-4}$)	33.06	23.01	31.45	Non-monotonic (min at S2)
Dislocation density δ ($\times 10^{14}$ m^{-2})	9.56	4.41	8.98	Non-monotonic (min at S2)
Max. transmittance (%)	~65–70	~45–50	~25–30	Decreasing

Optical band gap Eg (eV)	**2.79**	**2.30**	**2.11**	**Decreasing**
Urbach energy Eu (meV)	328.8	389.5	564.0	Increasing
Resistivity ρ (Ω·cm)	274	74	208	Non-monotonic (min at S2)
Conductivity σ ($\times 10^{-2}$ $\Omega^{-1}\cdot cm^{-1}$)	0.365	1.355	0.480	Non-monotonic (max at S2)

3.6.2 Key Correlations

Several important correlations emerge from the data:

a) Thickness vs. Band Gap (Main Finding):

The optical band gap decreases monotonically from 2.79 eV to 2.11 eV as thickness increases from 201 to 943 nm. This is the central result of this dissertation and demonstrates that the band gap of CuO thin films can be tuned over a range of approximately 0.7 eV simply by varying the film thickness.

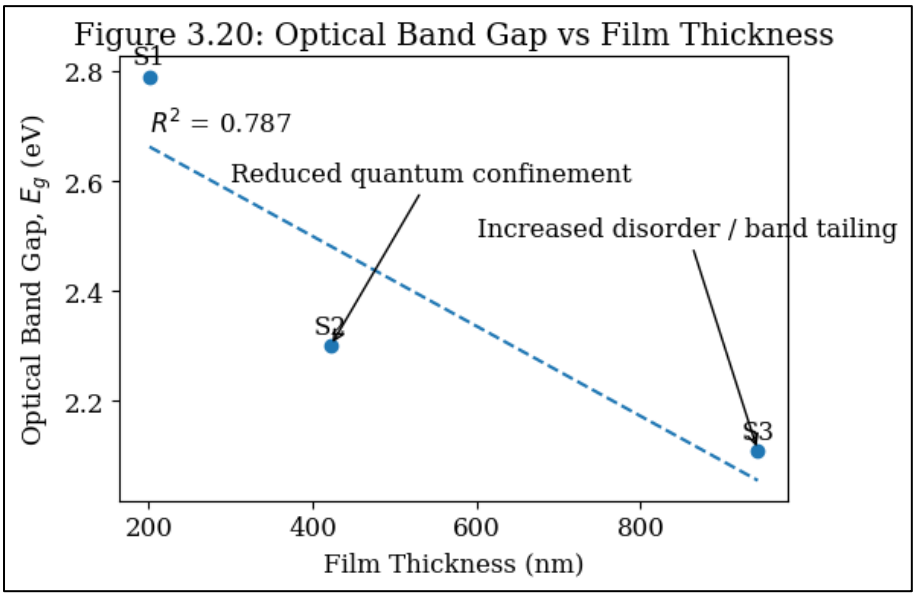

Figure 3. 19 Main result figure — Plot of Eg versus thickness with a clear trend line, annotated with physical mechanisms.

b) Eg vs. Eu (Inverse Correlation):

The optical band gap and Urbach energy are inversely correlated. This confirms that structural disorder plays a significant role in determining the optical properties.

c) Crystallite Size vs. Resistivity (Direct Correlation):

Larger crystallites result in lower resistivity due to reduced grain boundary scattering.

d) Structural Quality vs. Thickness (Non-monotonic):

The structural quality (measured by crystallite size, strain, and dislocation density) shows an optimal value at intermediate thickness (S2, 422 nm), while the optical band gap decreases monotonically. This indicates that the band gap is primarily controlled by quantum confinement and disorder effects rather than by crystallinity alone.

3.6.3 Implications for Applications

The ability to tune the optical band gap through thickness control has important implications for various applications:

a) Solar cells: For photovoltaic applications, the optimal band gap for single-junction solar cells is approximately 1.1–1.5 eV (Shockley-Queisser limit). Our thickest films (Eg = 2.11 eV) approach the range suitable for multi-junction or tandem solar cells.

b) Photodetectors: The spectral sensitivity of CuO-based photodetectors can be adjusted by selecting the appropriate film thickness.

c) Gas sensors: The optical and electrical properties at intermediate thickness (S2) may be optimal for sensor applications that require both good sensitivity and adequate conductivity.

d) Transparent electronics: The thinnest films (S1) with the widest band gap may be suitable for applications requiring some degree of optical transparency.

3.7 Conclusion

This chapter has presented a comprehensive study of the influence of film thickness on the structural, optical, and electrical properties of CuO thin films prepared by sol-gel spin coating. The principal findings are:

1. **Film thickness** increases approximately linearly with the number of deposited layers, from 201 nm (6 layers) to 943 nm (12 layers).
2. **Structural properties** show optimal crystallinity at intermediate thickness (~422 nm, 9 layers), with the largest crystallite size (15.12 nm), minimum strain (23.01×10^{-4}), and minimum dislocation density (4.41×10^{14} lines/m^2).
3. **The optical band gap decreases from 2.79 eV to 2.11 eV** with increasing thickness. This is the central finding of this work and is attributed primarily to the relaxation of quantum confinement effects and the increase in structural disorder.
4. **The Urbach energy increases from 328.8 meV to 564.0 meV** with increasing thickness, reflecting greater structural disorder in thicker films.
5. **An inverse correlation between Eg and Eu** is demonstrated, confirming that structural disorder plays a key role in determining the optical band gap.
6. **Electrical resistivity** is minimized at intermediate thickness (74 Ω·cm for S2), correlating with the best structural quality.
7. **Sample S2 (9 layers, ~422 nm)** provides the best overall combination of structural quality and electrical performance, making it the optimal choice for most applications.

These results demonstrate that **film thickness is a powerful parameter for tuning the optical band gap and other properties of CuO thin films**, enabling their optimization for specific applications in optoelectronics, photovoltaics, and sensing.

References

[1] H. Hashim, S. Shariffudin, P. Saad, and H. Ridah, "Electrical and optical properties of copper oxide thin films by sol-gel technique," in IOP Conference Series: Materials Science and Engineering, vol. 99, 2015, p. 012032.

[2] M. Boumezrag, K. Almi, S. Lakel, and H. Touhami, "Alkali Metals Doped Cu0. 94A0. 06O (A= Li, Na and K) Thin Films: Facile Synthesis, Structural, Optical and Thermoelectric Properties," Russian Journal of Physical Chemistry B, vol. 18, pp. 895-906, 2024.

[3] O. Daoudi, Y. Qachaou, A. Raidou, K. Nouneh, M. Lharch, and M. Fahoume, "Study of the physical properties of CuO thin films grown by modified SILAR method for solar cells applications," Superlattices and microstructures, vol. 127, pp. 93-99, 2019.

[4] H. B. Saâd, M. Ajili, S. Dabbabi, and N. T. Kamoun, "Investigation on thickness and annealing effects on physical properties and electrical circuit model of CuO sprayed thin films," Superlattices and Microstructures, vol. 142, p. 106508, 2020.

[5] M. Dhaouadi, M. Jlassi, I. Sta, I. B. Miled, G. Mousdis, M. Kompitsas, and W. Dimassi, "Physical properties of copper oxide thin films prepared by sol–gel spin–coating method," Am. J. Phys. Appl, vol. 6, pp. 43-50, 2018.

[6] R. Shabu, A. M. E. Raj, C. Sanjeeviraja, and C. Ravidhas, "Assessment of CuO thin films for its suitablity as window absorbing layer in solar cell fabrications," Materials Research Bulletin, vol. 68, pp. 1-8, 2015.

[7] N. Sharma, K. Prabakar, S. Ilango, S. Dash, and A. Tyagi, "Optical band-gap and associated Urbach energy tails in defected AlN thin films grown by ion beam sputter deposition: Effect of assisted ion energy," Advanced Materials Proceedings, vol. 2, pp. 342-346, 2017.

[8] F. A. Akgul, G. Akgul, N. Yildirim, H. E. Unalan, and R. Turan, "Influence of thermal annealing on microstructural, morphological, optical properties and surface electronic structure of copper oxide thin films," Materials Chemistry and Physics, vol. 147, pp. 987-995, 2014.

[9] Y. Akaltun, "Effect of thickness on the structural and optical properties of CuO thin films grown by successive ionic layer adsorption and reaction," Thin Solid Films, vol. 594, pp. 30-34, 2015.

[10] S. A. M. H. M. Ali and S. Makki, "The thickness effects characterization properties of copper oxide thin films prepared by thermal evaporation technique," J. Mult. Eng. Sci. Stud., vol. 2, p. 532, 2016.

[11] N. Touka, D. Tabli, and K. Badari, "Effect of annealing temperature on structural and optical properties of copper oxide thin films deposited by sol-gel spin coating method," Journal of Optoelectronics and Advanced Materials, vol. 21, pp. 698-701, 2019.

[12] H. Touhami, K. Almi, and S. Lakel, "Experimental and theoretical investigation of the effect of alkali (Li, Na and K) doping on the properties of nickel oxide thin films: Comparative study," Main Group Chemistry, pp. 1-15, 2023.

[13] N. Raship, M. Sahdan, F. Adriyanto, M. Nurfazliana, and A. Bakri, "Effect of annealing temperature on the properties of copper oxide films prepared by dip coating technique," in AIP Conference Proceedings, 2017.

[14] K. Kamli, Z. Hadef, B. Chouial, and B. Hadjoudja, "Thickness effect on electrical properties of copper oxide thin films," Surface Engineering, vol. 35, pp. 86-90, 2019.

[15] B. Balamurugan and B. Mehta, "Optical and structural properties of nanocrystalline copper oxide thin films prepared by activated reactive evaporation," Thin solid films, vol. 396, pp. 90-96, 2001.

GENERAL CONCLUSION

This master's dissertation has been devoted to a systematic and comprehensive investigation of the influence of film thickness on the optical band gap of copper oxide (CuO) thin films prepared by the sol-gel spin coating technique. The motivation for this study stems from the growing interest in CuO as a low-cost, abundant, non-toxic, and environmentally friendly p-type semiconductor with a suitable band gap for various optoelectronic and energy conversion applications. Understanding how to control and tune the optical band gap through simple process parameters such as film thickness is essential for optimizing CuO thin films for specific technological applications.

Three sets of CuO thin film samples were fabricated on glass substrates by varying the number of deposited layers: 6 layers (Sample S1), 9 layers (Sample S2), and 12 layers (Sample S3), corresponding to measured thicknesses of approximately 201 nm, 422 nm, and 943 nm, respectively. The precursor solution was prepared by dissolving copper acetate monohydrate in ethanol with monoethanolamine as a stabilizing agent. The films were deposited at 3000 rpm for 30 seconds per layer, preheated at 250°C for 15 minutes between successive layers, and finally annealed at 500°C for 2 hours in air to obtain the crystalline CuO phase. The structural, optical, and electrical properties of the resulting films were thoroughly characterized using X-ray diffraction (XRD), UV-Visible spectroscopy, and the four-point probe technique.

Principal Findings

Regarding Structural Properties

X-ray diffraction analysis confirmed that all three films possess a pure polycrystalline monoclinic CuO structure corresponding to the tenorite phase, in excellent agreement with the standard JCPDS reference card No. 98-004-3179. No secondary phases such as Cu_2O (cuprite), metallic copper, or copper hydroxide were detected in any of the samples, which validates the effectiveness of the chosen annealing conditions for achieving complete oxidation and crystallization.

The structural quality of the films was found to depend significantly on thickness. The crystallite size varied non-monotonically with thickness, reaching a maximum value of 15.12 nm at the

intermediate thickness of 422 nm (9 layers). This maximum was accompanied by the minimum values of lattice strain (23.01×10^{-4}) and dislocation density (4.41×10^{14} lines/m^2), indicating that the film with 9 layers exhibits the best crystallographic quality among the three samples studied. For the thinnest film (S1, 201 nm), the smaller crystallite size (10.29 nm) reflects incomplete grain growth due to insufficient material, while for the thickest film (S3, 943 nm), the reduced crystallite size (11.04 nm) is attributed to the accumulation of interlayer defects and stresses introduced by the repeated coating cycles.

Regarding Optical Properties — The Central Finding

The optical transmittance measurements revealed that all CuO films exhibit strong absorption across the visible spectrum, consistent with the narrow band gap character of CuO. The transmittance decreases significantly with increasing film thickness, from approximately 65–70% (S1) to 25–30% (S3) at 1100 nm, in direct accordance with the Beer-Lambert law.

The most important finding of this dissertation is the systematic decrease of the optical band gap from 2.79 eV to 2.11 eV as the film thickness increases from 201 nm to 943 nm. This decrease of approximately 0.68 eV represents a substantial and highly reproducible variation that can be exploited for practical applications. The band gap narrowing with increasing thickness is attributed to a combination of interconnected physical mechanisms:

First, the relaxation of quantum confinement effects: in the thinnest films with the smallest crystallites, the spatial confinement of charge carriers leads to a widening of the effective band gap. As the film becomes thicker and the crystallites grow, this confinement effect diminishes and the band gap approaches the bulk value.

Second, the increase in structural disorder: the Urbach energy, which quantifies the width of the exponential absorption tail and reflects the degree of disorder in the film, increases monotonically from 328.8 meV (S1) to 564.0 meV (S3). This increasing disorder creates localized states (band tails) that extend into the forbidden gap, effectively shifting the absorption edge to lower energies and reducing the apparent optical band gap.

Third, the reduction of grain boundary effects: in thinner films with higher grain boundary density, the electronic band structure is modified by the potential barriers at grain boundaries, contributing to an apparent widening of the band gap.

The inverse correlation between the optical band gap (Eg) and the Urbach energy (Eu) observed in this work is an important result that confirms the dominant role of structural disorder in controlling the optical absorption properties of nanocrystalline CuO thin films. This correlation provides a practical guideline for predicting how changes in film quality will affect the band gap.

Regarding Electrical Properties

The electrical characterization revealed that the resistivity of CuO films shows a minimum value of 74 Ω·cm at the intermediate thickness of 422 nm (S2), corresponding to a maximum conductivity of 1.355×10^{-2} $\Omega^{-1} \cdot cm^{-1}$. This optimal electrical performance correlates directly with the best structural quality observed for the same sample. The correlation between crystallite size and resistivity confirms that grain boundary scattering is the dominant mechanism controlling charge carrier transport in polycrystalline CuO films.

For the thinnest film (S1), the high resistivity (274 Ω·cm) is attributed to the large number of grain boundaries that scatter charge carriers, while for the thickest film (S3), the increased resistivity (208 Ω·cm) results from the deterioration of crystalline quality despite the greater volume of conducting material.

Regarding the Optimal Thickness

The comprehensive analysis of all properties reveals that the film with 9 layers (approximately 422 nm thickness) provides the best overall combination of crystallographic quality and electrical conductivity. However, the "optimal" thickness depends on the intended application:

- For applications requiring maximum transparency and wide band gap (such as transparent conductors or UV photodetectors), thinner films around 200 nm may be preferred.
- For applications requiring strong visible light absorption and narrow band gap (such as solar cells or photocatalysis), thicker films around 900 nm offer better absorption characteristics.

- For applications requiring high electrical conductivity (such as electrodes or interconnects), the intermediate thickness of approximately 400 nm provides the best balance.

Significance of the Results

The results obtained in this work carry both fundamental and applied significance:

From a fundamental perspective, this study provides clear experimental evidence of the thickness-dependent optical band gap in sol-gel deposited CuO thin films and establishes quantitative correlations between structural parameters (crystallite size, strain, dislocation density, Urbach energy) and optical properties (band gap, transmittance). The identification of the physical mechanisms responsible for the band gap variation contributes to the general understanding of size-dependent optical properties in nanocrystalline semiconductor thin films.

From an applied perspective, the demonstration that the optical band gap of CuO can be tuned over a range of approximately 0.7 eV through simple thickness control — without the need for doping or compositional changes — provides a straightforward and cost-effective approach for optimizing CuO thin films for specific applications. This is particularly valuable because the sol-gel spin coating technique used in this work is simple, inexpensive, and readily scalable.

Furthermore, the obtained band gap values (2.11–2.79 eV) are in a range that is highly relevant for several applications, including photoelectrochemical water splitting (which requires a band gap of approximately 1.8–2.4 eV), visible-light photocatalysis (requiring band gaps below 3.0 eV), and as a component in multi-junction solar cell architectures.

Limitations of the Study

While the results of this work are clear and internally consistent, several limitations should be acknowledged:

1. **Thickness measurement**: The gravimetric method provides an average thickness but does not capture local variations in thickness across the substrate. More precise techniques such as profilometry or spectroscopic ellipsometry would provide better thickness data.

2. **Limited number of thickness values**: Only three thicknesses were studied. A larger number of data points would allow the construction of a more detailed and statistically robust Eg versus thickness curve.
3. **Lack of morphological data**: The absence of scanning electron microscopy (SEM) or atomic force microscopy (AFM) measurements means that direct information about grain size, surface roughness, and morphological evolution with thickness was not obtained.
4. **Room-temperature measurements only**: All measurements were performed at room temperature. Temperature-dependent studies would provide additional insight into the thermal stability and activation energy of the observed properties.

Future Perspectives

Based on the findings and limitations of this work, several promising directions for future research are suggested:

1. **Extension of the thickness range**: Preparing films with a wider range of thicknesses (from below 50 nm to above 1500 nm) would allow the complete mapping of the band gap versus thickness relationship, including the identification of any saturation or reversal effects at extreme thicknesses.
2. **Use of advanced characterization techniques**: Employing profilometry or spectroscopic ellipsometry for thickness measurement, SEM and AFM for morphological characterization, and photoluminescence spectroscopy for defect analysis would provide a more complete picture of the thickness-property relationships.
3. **Combined effect of thickness and doping**: Investigating how doping with alkali metals (Li, Na, K) or transition metals (Zn, Ni, Mn) modifies the thickness dependence of the band gap would enable even more precise tunability of the optical properties.
4. **Annealing temperature optimization for each thickness**: Studying whether the optimal annealing temperature varies with film thickness could further improve the crystalline quality and properties of the films.
5. **Device fabrication and testing**: The ultimate validation of this work would be the integration of thickness-optimized CuO thin films into functional devices such as p-CuO/n-ZnO heterojunction solar cells, CuO-based photodetectors, or gas sensors,

followed by systematic evaluation of device performance as a function of CuO layer thickness.

6. **Theoretical modeling**: First-principles density functional theory (DFT) calculations could provide theoretical predictions of the band gap variation with crystallite size, which could be compared with the experimental observations to validate the proposed mechanisms.
7. **Reproducibility and statistical analysis**: Repeating the experiments multiple times and performing statistical analysis would strengthen the quantitative conclusions and provide confidence intervals for the reported values.

In conclusion, this dissertation has demonstrated that **film thickness is a simple yet powerful parameter for controlling the optical band gap of CuO thin films**, opening the door to optimized material design for a wide range of optoelectronic and energy applications. The sol-gel spin coating approach used in this work provides an accessible, reproducible, and scalable pathway for the fabrication of CuO thin films with tailored properties, making it suitable for both laboratory research and potential industrial applications.